Mémoire

Auteur : Delaive, Célia
Promoteur(s) : Schlagheck, Peter
Faculté : Faculté des Sciences
Diplôme : Master en sciences physiques, à finalité approfondie
Année académique : 2023-2024
URI/URL : http://hdl.handle.net/2268.2/20244

Dynamical tunneling in time crystals

Delaive Célia

promoter : *Schlagheck Peter*

Faculty of Sciences
Physics department

Université de Liège | Academic year 2023-2024

Thesis is presented as part of the Master's degree in physical sciences

Acknowledgements

First of all, I would like to deeply thank my supervisor, Mr. P.Schlagheck, for his good advice, support and availability throughout this work.

I would also like to express my gratitude to Mr. B. Bastin, Mr. B. Dupé and Mr. S. Dorbolo, for accepting to be members of my reading committee.

Finally, I would like to thank my family and my roommates who have been a great support throughout this journey.

Contents

Introduction

The study of entanglement has generated significant interest in recent years due to its crucial importance in quantum information science [1]. NOON states represents a special and important class of entangled states, defined by a superposition $|N,0\rangle + e^{i\phi}|0,N\rangle$ involving N bosons distributed over two modes. These states exhibit a high degree of entanglement, making them of great interest for quantum information [1] and for quantum metrology particularly [2]. Indeed, using these entangled states to perform measurements increases precision beyond the standard quantum limit[1]. In other words, using such states allows for ultra-precise measurements.

In 2010 and 2018, two research groups successfully created NOON states experimentally with photons [3] and phonons [4] with a number of quanta $N \approx 10$. Whether the creation of these particular states would be possible with bosonic atoms forming a Bose-Einstein condensate or not seems then to be a good question. A Bose-Einstein condensate is a particular state of matter that appears at temperatures close to the absolute zero. It is a state in which the N particles of a bosonic gas find themselves in the same quantum state and thus behave coherently and collectively as a single macroscopic matter wave. Such NOON states formed by ultracold bosonic atoms would be particularly interesting for quantum metrology, compared to those formed with photons and phonons, because atoms can interact strongly with external forces and light fields, making them ideal for precise detection applications. However, the experimental realization of these specific NOON states has not yet been achieved despite numerous theoretical proposals [5, 6, 7, 8, 9].

In [9], a particularly interesting protocol is proposed. It relies on a collective tunneling process of a bosonic gas when it is in a specific regime called the quantum self-trapping regime [10, 11]. The phenomenon of tunneling is one of the most remarkable implications of quantum mechanics. It corresponds to the ability of a quantum particle to penetrate regions that are classically forbidden, for example, because it doesn't have enough energy to enter these specific regions. The particular process of collective tunneling occurs, then, when N bosonic atoms are prepared in one of the wells of a symmetric double-well potential. As the wells are symmetric, the particles should tunnel to the other well, however, interactions between particles prevent this phenomenon, and the particles can only tunnel to the other well collectively. At the halfway point of this phenomenon, the NOON superposition is achieved.

However, some problems arise. The first one is that this phenomenon is very slow and generally cannot be observed experimentally, and the second one is the maintenance of the perfect symmetry between the two potential wells, as a loss of this symmetry could lead to the suppression of the tunneling process. These two problems can be resolved by introducing a periodic driving to the configuration. Indeed, this periodic perturbation will induce the emergence of chaos in the system, drastically accelerating the collective tunneling phenomenon, giving rise

[1] which represents the best theoretically possible precision when measuring a physical quantity

to what is called chaos-assisted tunneling[2] [12, 13]. Then, if this perturbation is a resonant perturbation of a mode of the unperturbed movement of the atomic gas, the system can form what is called a discrete time crystal [14, 15, 16] instead of having a static double-well potential. Discrete time crystals are particular systems that exhibit specific periodicity in time and can be realized through this perturbation. Indeed, such excitation generates a ring of stable periodic orbits whose number is directly related to the order of the resonance. In particular, two perfectly symmetrical islands of regular periodic motion are generated by a 2:1 resonance, where two periods of the excitation correspond exaclty to one period of the unperturbed motion. These two islands can be seen as two wells of a double-well potential, and the protocol from [9] is applicable to this configuration, but in this case, the symmetry of the islands is an intrinsic characteristic that cannot be compromised.

Thus, the aim of this Master's thesis is to export this NOON state creation protocol into the framework of time crystals, so that the two wells between which the transition occurs correspond to the two resonance islands associated with the 2:1 resonance we have just introduced. More specifically, the objective is to study the collective tunneling between these two sites of the time crystal by employing Floquet theory and the two-site Bose-Hubbard model, to obtain a first prediction of the characteristic time of this phenomenon.

In the first chapter, we begin by discussing the implications of the introduction of the periodic modulation on the classical dynamics corresponding to our system. We will see that its introduction indeed leads to the emergence of chaos in the system as well as the formation of nonlinear resonances. We will also discuss how these changes in the classical dynamics of the system will affect the underlying quantum dynamics. To do so, we will introduce two theoretical tools, Husimi distributions and Floquet theory.
In Chapter 2, we will introduce the theory of Bose-Einstein condensates as well as the two-site Bose-Hubbard model. We will see how this model can be applied to our system and how it can allow us to calculate the desired collective tunneling time. We will also introduce in this chapter the notion of time crystal and discrete time crystal, justifying that our system indeed represents one.
In Chapter 3, we will study how the presence of chaos and of the resonances themselves can accelerate the tunneling phenomenon between the two sites of our time crystal. We will explain the mechanisms behind this acceleration. Furthermore, we will introduce the theory of random matrix ensembles as we will need it to describe these processes.
Finally, in Chapter 4, we will use all the concepts discussed in the previous chapters to calculate the desired collective tunneling time. All our results will be explained and discussed there.

[2] as already done in the protocol presented in [9]

Chapter 1

Nonlinear resonances in periodically driven systems

Let's start by explaining the general configuration under consideration in the following of this work. We study a gas consisting of N ultracold bosonic atoms forming a Bose-Einstein condensate. This condensate is prepared within one of the two sites of a particular lattice, which constitutes what we will call a discrete time crystal (see Section 2.5). To achieve this setup, the N atoms are confined in an inclined annular trap, the inclination of which varies over time with a certain frequency, resulting in a periodic modulation of the trap potential amplitude. This situation then corresponds to the framework of a quantum pendulum subjected to a periodic modulation described by the following time-dependent Hamiltonian

$$\hat{H}(t) = \frac{\hat{\mathbf{p}}^2}{2m} - V\cos\left(\frac{2\pi\hat{q}}{L}\right)(1 + \delta\cos(\omega_0 t)) \tag{1.1}$$

Where m is the mass of the atomic species used, V is induced by a potential gradient, L is the circumference of the ring, δ is the amplitude of the periodic modulation, and ω_0 is its frequency. Here $\hat{q}$ is the position operator and $\hat{\mathbf{p}}$ is the associated momentum operator.

Because of this modulation, the dynamics of the condensate within the ring, described by this time-dependent Hamiltonian, will then be chaotic. However, for certain frequencies ω_0, stable solutions emerge. We will focus on the 2:1 resonance where two of these stable solutions appear. These stable solutions are resonance islands and correspond to a regular and periodic motion of the condensate in the trap, which can be depicted as shown in Fig. 1.1. The rotation of the condensate in the ring can be clockwise or counterclockwise, but we consider only the clockwise direction without loss of generality, and the two stable solutions in one direction of rotation differ only by a delay $T = 2\pi/\omega_0$ in their temporal evolution in the ring.

Moreover, when the condensate is prepared on one of the stable solutions of the 2:1 resonance, a collective tunneling of the atoms constituting the condensate to the other stable solution will be observed as explained in the introduction. This phenomenon constitutes the subject of investigation of this work. To model this tunneling phenomenon, we must understand the dynamics of the condensate in our system.

We have just said that chaotic dynamics are present in stable solutions defined through specific values of ω_0. Therefore, in this first Chapter, we will begin by exploring in detail the

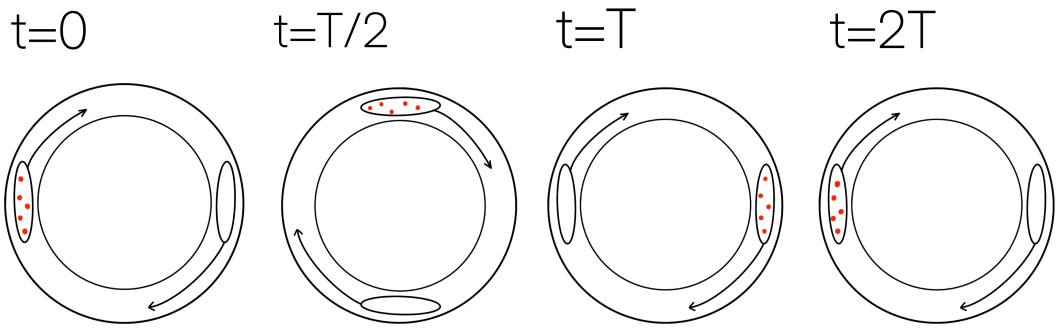

Figure 1.1: Representation of condensate motion in the ring trap. The drawn ellipses correspond to the two stable solutions of the dynamics described by the Hamiltonian $\hat{H}(t) = \hat{\mathbf{p}}^2/2m - V\cos(2\pi\hat{q}/L)(1+\delta\cos(\omega_0 t))$, which emerge when the frequency of the periodic modulation ω_0 is well chosen. The red dots represent the condensate atoms. Thus, when the condensate is prepared on one of these two stable solutions, it has a regular motion in the trap with a period $2T$ ($T = 2\pi/\omega_0$), as shown in the figure.

reasons behind the formation of these nonlinear resonances, as well as the emergence of chaos, and discuss the implications of their presence on our system.

While the formation of nonlinear resonances is a purely classical phenomenon, we will see that the implications of their presence at the quantum level are significant. Their presence will notably result in the confinement of the system's eigenstates to a certain region of phase space. Indeed, resonances are the stable solutions of our system, and thus, we will observe that a wave packet prepared on one of these stable solutions will remain confined near it. Thus, they play the role of dynamical barriers in our system and are crucial for the phenomenon of dynamical tunneling being investigated in this work.
In conclusion, nonlinear resonances provide the framework that enables the observation of all the processes we wish to study in this work.

Therefore, we begin by studying the impact of the introduction of a periodic modulation on the classical dynamics of the system, which will allow us to understand the process of the resonance island formation and the emergence of chaos in the system, before examining its impact on quantum dynamics. We will also theoretically introduce necessary tools for the quantum-classical correspondence such as Husimi distributions and Floquet theory.

1.1 The transition to chaos

Our system is a time-dependent system and the introduction of the time dependence occurs through a perturbation. More specifically, through a perturbation in the form of a periodic modulation. Then, we will observe later that the addition of such perturbation leads to the emergence of chaotic dynamics in the classical system. Understanding the emergence of this chaotic dynamic at the classical level is essential for our system's study and will occupy us throughout this section. Indeed, while the concept of classical chaos is now well established, we're going to see

that its manifestation at the quantum level is not straightforward. And, therefore, the description of quantum dynamics associated with classical chaos is done in parallel with the description of classical dynamics, justifying the importance of its study.

Indeed, the definition of chaos, as we conceive it, relies on a particular sensitivity to initial conditions [17]. In classical systems, chaotic behavior arises from nonlinearity, where a slight alterations in initial conditions lead to drastically different outcomes over time. However, the Schrödinger equation, being linear, implies that a small change in initial conditions only results in a weak and constant change in temporal evolution. Thus, chaos, in the classical sense, does not manifest at the quantum level due to this fundamental linearity, excluding the emergence of chaotic behaviors.
So, what exactly does "*quantum chaos*"[1] signify ? Well, in fact, quantum chaos is defined as the study of distinctive properties of quantum systems whose classical counterparts are chaotic. Three intrinsic characteristics of these quantum systems can be highlighted; the spectral fluctuations of energy levels, the ergodicity of the eigenvectors, and the thermalization of the expectation values of observables [19]. Ergodicity and thermalization of a system are two important properties of chaotic systems, which, in the quantum case, mean that the system's eigenvectors are uniformly distributed in phase space, and that, during the evolution of the system, the expected values of the observables tend towards predictions given by statistical physics and remain close to them [20]. Furthermore, in 1984, Bohigas, Giannoni, and Schmidt [21] proposed a conjecture suggesting that the energy level fluctuations of quantum systems, whose classical counterparts are entirely chaotic, correspond to the fluctuations predicted by the theory of random matrix ensembles. Initially, we will not employ this technique, but it will be necessary later to explain the process of chaos-assisted tunneling. Thus, the details of this method will be provided in the chapter dedicated to this subject.

Given this particular definition, it seems natural to adopt a semi-classical approach, meaning that we will analyze both the quantum mechanical elements of our system and its classical dynamics, thereby capturing quantum aspect while preserving the intuition provided by the classical aspect of the system. In order to carry out such a comparison, we must operate within the semi-classical limit $\hbar \to 0$. Indeed, the correspondence between classical and quantum dynamics is valid when a significant number of quantum levels are observed per unit Planck cell [22]. The notation $\hbar \to 0$ then takes on its full meaning.

With the importance of studying classical dynamics now clear, we will first define fundamental concepts essential for understanding this theory. Then, we will explain the emergence of chaos and its implications in classical systems.

1.1.1 Properties of classical chaos

As we just mentioned, we begin by citing some fundamental properties of classical chaos. In this section, we will introduce the concepts of Lyapunov exponents and ergodicity. Before that, we will also define Poincaré sections, a visualization tool of our system's dynamics.

The phase space of a system with N degrees of freedom is of dimension $2N$ [22]. One can quickly realize that for $N \geq 2$, it becomes difficult, if not impossible, to have a purely geometric

[1]The term "*quantum chaos*" is somewhat of a misnomer, and some meticulous researchers prefer the term "*quantum chaology*" [18]. However, as the former is more commonly used in the scientific domain, we will continue to employ it.

representation of this space. Indeed, even in the case of $N = 2$, the surface representing a given energy is a three-dimensional hyperplane. Visualization tools of three-dimensional phase space exist, as used in [23] and described in [24]. However, we introduce here another method to represent any N-dimensional system by a two-dimensional plane, known as Poincaré sections [22]. The construction principle is simple : we choose a plane in phase space and visualize each of the points where a trajectory intersects this plane. This technique is illustrated in Fig. 1.2.

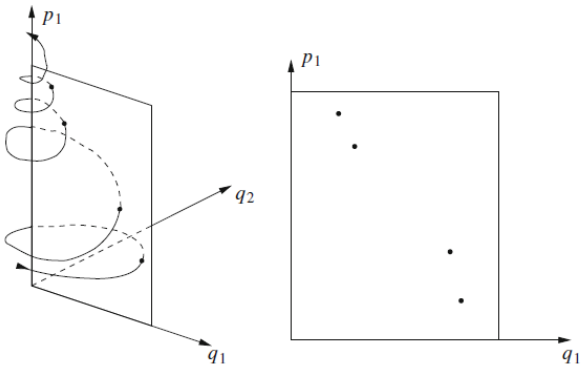

Figure 1.2: Representation of the construction of a Poincaré section on the plan defined by $q_2 = 0$, we visualize all the points at which the trajectory intersects that plane. The image on the right represents the resulting Poincaré section. This diagram comes from Ref.[22]

Since the time evolution of a Hamiltonian system is unique, we can assume the same is true for Poincaré sections. Therefore, much information about the system's dynamics can be found in theses maps. For example, if the system has a periodic orbit of order n for the initial postion and momentum (q_0, p_0), then the corresponding Poincaré section $\mathscr{P}$ has a fixed point of order n for the same initial condition. We have

$$\mathscr{P}^n(q_0, p_0) = (q_0, p_0)$$

Regular trajectories are represented by closed curves, while chaotic trajectories manifest as scattered points, allowing for a clear distinction between these two types of dynamics.

A simpler construction of the Poincaré section is possible when the Hamiltonian is periodic. This periodicity can be temporal. In this case, we simply trace the intersections with trajectories at all multiples of the period. This is called a stroboscopic Poincaré section [22], and a schematic representation of constructing such a map is given in Fig. 1.3.

Next, fundamentally, classical chaos is characterized by its sensitivity to initial conditions. Accordingly, we can define the Lyapunov exponents σ of a dynamical system, which provide a measure of how trajectories diverge when subjected to slight modifications in initial conditions [22]. More precisely, they gauge the mean rate of exponential separation of neighboring trajectories [17]. Consequently, if $\sigma > 0$, trajectories diverge exponentially, labeling the system as chaotic, whereas if $\sigma \leq 0$, trajectories separates only linearly in time and the system is considered stable. Lyapunov exponents are calculated by considering a generic trajectory of a system (non-periodic) which will be our reference trajectory, and assessing the evolution of deviation from this trajectory over time. To derive the expression of this exponent, we will follow the same reasoning as in [17].

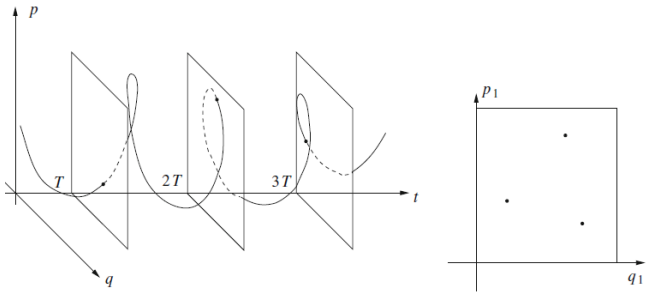

Figure 1.3: Representation of the construction of a stroboscopic Poincaré section, we visualize all the points at which the trajectory intersects a plane at each multiple of the period. The image on the right represents the resulting stroboscopic Poincaré section. This diagram comes from Ref.[22]

So, we consider any system governed by the general differential equations

$$\frac{dx_i}{dt} = F_i(x_1, ..., x_n) \; i = 1, ..., n \tag{1.2}$$

Linearizing these equations around any reference trajectories $\bar{\mathbf{x}} = (\bar{x}_1, ..., \bar{x}_n)$ yields what we call the tangent map

$$\frac{d\delta x_i}{dt} = \sum_{j=1}^{n} \delta x_j \left(\frac{\partial F_i}{\partial x_j}\right)_{\mathbf{x}=\bar{\mathbf{x}}(\mathbf{t})} \tag{1.3}$$

This map provides the tangent to the system's trajectory at each point in phase space. Then the norm defined as

$$d(t) = \sqrt{\sum_{i=1}^{n} \delta x_i^2(t)} \tag{1.4}$$

measures the divergence of neighboring trajectories, that is, the reference trajectory $\bar{\mathbf{x}}$ and its neighbor with initial conditions $\bar{\mathbf{x}}(0) + \delta\mathbf{x}(0)$. And then, the mean rate of exponential divergence is defined as

$$\sigma = \lim_{t\to\infty} \lim_{d(0)\to 0} \left(\frac{1}{t}\right) \ln\left(\frac{d(t)}{d(0)}\right) \tag{1.5}$$

where

$$d(0) = \sqrt{\sum_{i=1}^{n} \delta x_i^2(0)}$$

Note that we can also define the Lyapunov exponents of the mappings directly. In the case of a one-dimensional map of the form

$$x_{i+1} = f(x_i) \tag{1.6}$$

The tangent map is simply given by

$$\delta_{x_{i+1}} = f'(x_i)\delta x_i = \prod_{j=0}^{i} f'(x_j)\delta x_0 \tag{1.7}$$

where $f'(x_j)$ is the derivative of $f(x)$ evaluated at each point x_j along the given trajectory. Then from (1.5) we can derive the associated Lyapunov exponent

$$\sigma = \lim_{N\to\infty} \frac{1}{N} \ln \left[\prod_{j=0}^{i} f'(x_j) \right]$$

$$= \lim_{N\to\infty} \frac{1}{N} \sum_{j=0}^{N} \ln |f'(x_j)| \tag{1.8}$$

And, in the case of a n-dimensional map, there will be n characteristic exponents corresponding to the n eigenvalues $\lambda_i(N)$ with $i = 1, ..., n$, of the matrix tangent map.

$$\sigma_i = \lim_{N\to\infty} \ln |\lambda_i(N)| \tag{1.9}$$

It can be shown that they can be ordered by size

$$\sigma_1 \geq \sigma_2 \geq ... \geq \sigma_n \tag{1.10}$$

And, the existence of a single $\sigma_i > 0$ is associated with the presence of chaos in the system.

Finally, the last characteristic of classical chaotic systems we examine is ergodicity. The postulate of ergodicity is as follows [25]:

> Let $F = F(q_1, p_1, ..., q_N, p_N)$ be an observable defined in phase space. The average of F along the trajectory is equal to the average of F in the accessible part of phase space, respecting the constant of motion.

Indeed, a system is said to be ergodic when, over a sufficiently long evolution time ($t \to \infty$), it uniformly and randomly traverses its phase space, thus exploring all accessible regions. In other words, ergodicity implies that the system passes through all possible configurations equitably. This implies that it is possible to interchange temporal averages and ensemble averages. Note that ergodicity is not unique to chaotic systems. Although for a system to be chaotic, it must be ergodic, not all ergodic systems are necessarily chaotic.
The concept of ergodicity is also crucial in statistical mechanics as the postulate is used to derive the microcanonical ensemble.

1.1.2 Nonlinear dynamics

A classical system can be classified in two distinct ways, it can either be integrable or non-integrable. A system is considered integrable when the number of degrees of freedom n equals the number of independent constants of motion k [22]. Conversely, a system is labeled non-integrable if it possesses fewer independent constants of motion than degrees of freedom. Non-integrability is an important concept as the emergence of chaos in a system can often be explained by introducing a non-integrable perturbation into an initially integrable system. For instance, in the system studied in this work, we have a Hamiltonian of the form :

$$H(q,p) = \frac{p^2}{2m} - V[1 + \delta \cos(\omega_0 t)] \cos\left(\frac{2\pi q}{L}\right) \tag{1.11}$$

Where V is induced by a potential gradient, m is the mass of the particle, L is the circumference of the ring, δ is the amplitude of the periodic modulation and ω_0 is its frequency. The part $H_0(q,p) = \frac{p^2}{2m} - V\cos\left(\frac{2\pi q}{L}\right)$ corresponds to the equation of a classical pendulum. When neglecting the additional part, the system is integrable, and the equations of motion can be solved analytically. However, the addition of the part $H_1(q,p,t) = V\delta\cos(\omega_0 t)\cos\left(\frac{2\pi q}{L}\right)$ makes the system time-dependent and periodic. Consequently, the system's energy ceases to represents a constant of motion, rendering it non-integrable. The associated equations of motion are non-linear. Depending on the amplitude δ of this perturbation, the system's dynamics will undergo significant changes.

As illustrated in figure 1.4a, the phase space associated with the unperturbed system consists of tori, representing stable periodic orbits. We then have two theorems that tell us how these tori will evolve upon the addition of the perturbation. Two distinct theorems are employed due to the existence of two different kinds of tori [22]. They are distinguished by what is called their winding number $\frac{r}{s}$, with r the frequency associated with the torus under consideration, and s the frequency of the perturbation. Thus :

- Tori with an irrational winding number are preserved, with slight deformations, under the influence of the perturbation, according to the KAM (Kolmogorov-Arnold-Moser) theorem, as long as the perturbation remains within reasonable bounds [26, 27].
  Thus, this theorem ensures the existence of regular structures under small perturbations. It is obtained through an improved perturbation theory called the "*superconvergent perturbation theory*". Indeed, thanks to this theory, Arnold and Moser [26, 27] demonstrate that when the perturbation is taken into account, it is possible to find a new torus that is close to the unperturbed torus and that the transformation from the old to the new one occurs smoothly. This result is only valid for tori with an irrational winding number because for tori with rational winding number, the perturbation theory used diverges.

- With the KAM theorem, we have established that tori with rational winding numbers are destroyed by perturbations. Then, the Poincaré-Birkhoff theorem [17] states that when such a torus is destroyed, it decomposes into an even number of fixed points, with stable and unstable fixed points alternating. And, the stable points are surrounded by elliptic structures, known as resonance islands.
  Every torus with a rational winding number is surrounded by two tori with irrational winding numbers. Thus, the result of this theorem can be found by meticulously studying the deformation of these neighboring tori under the perturbation, one can observe how the fixed points emerge from this dynamics.
  Specifically, we obtain r stable points and r unstable points, where, as the winding number is rational, r/s is the ratio of proportionality between the period of the emerging nonlinear resonances and the period of the system's Hamiltonian. For example, if we consider a torus with a winding number reducible to the fraction $3/2$, this torus will transform into three stable points. A particle on one of these resonance island will make two rotations of our ring trap in three periods of the external driving.

Rigorous explanations of these theorems involve complex concepts beyond the scope of this work and can be found in [22, 17].

Therefore, according to the Poincaré-Birkhoff theorem, a torus with a winding number r/s gives rise to a ring of r periodic orbits, known as resonance islands, separated by r unstable points. This is referred to as an r : s resonance.

Furthermore, as the perturbation amplitude increases, the size of the resonances also grows until resonances from different rings begin to overlap. Chaos emerge from these superpositions [17]. Thus, the regular structures gradually disappear, and chaotic structures appear. And, the addition of a non-integrable periodic perturbation leads to the emergence of chaos in classical dynamics. In some parametric regimes, both types of structures coexist, giving rise to a mixed phase space. It is within such system that we will work, and thus, identifying this particular parametric regime will be the first milestone to the obtaining of our results, as it will be discussed in more details in Chapter 4.

It is also worth noting that, as said earlier, in the remainder of this work, we will focus on the 2:1 resonance, where two regular symmetric islands appear, and where two periods of the movement on one of these islands correspond exactly to one period of the external driving. In the ring trap under consideration, the condensate can rotate clockwise or counterclockwise. In the 2:1 resonance, we will then have two islands for each of these two directions of rotation. We will consider only those which correspond to the clockwise rotation without loss of generality. The figure 1.4 illustrates the successive emergence of these two islands for different values of δ. We observe that for small values of the perturbation, the integrable tori are not altered. Then we see chaotic structures appear and grow with the formation of resonance islands.

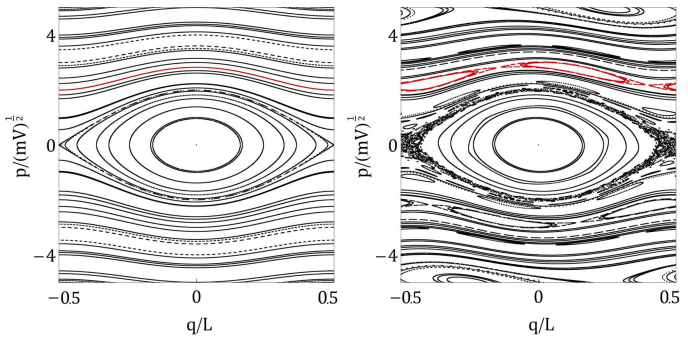

(a) $\delta = 0$ (b) $\delta = 0.2$

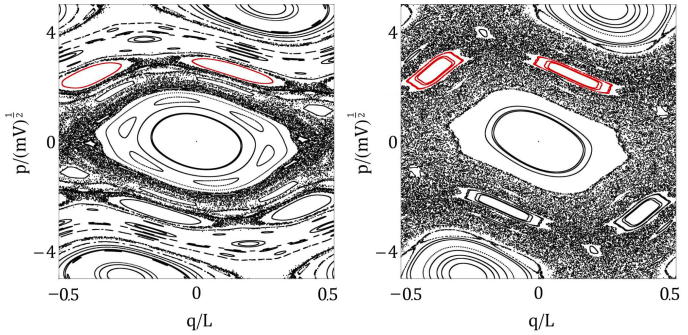

(c) $\delta = 1$ (d) $\delta = 2$

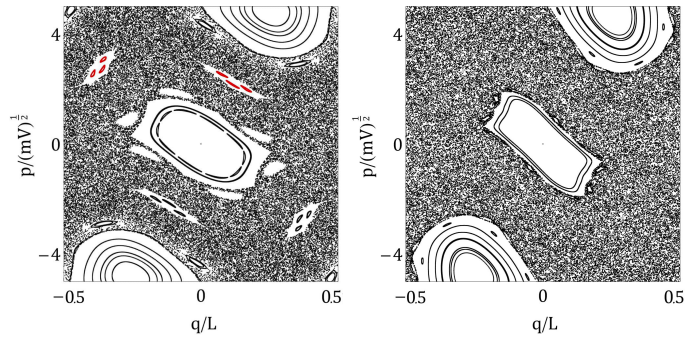

(e) $\delta = 3$ (f) $\delta = 5$

Figure 1.4: Poincaré sections constructed for $\omega_0 t = \pi/2 + 2\pi n$, $\forall n \in \mathbb{Z}$, of the classical dynamics of a particle subject to a perturbation. We have the Hamiltonian $H = p^2/2m - V[1 + \delta\cos(\omega t)]\cos(2\pi q/L)$ with increasing values of δ. Moreover, we have $\hbar\omega = 0.5\ V$, with $\hbar = 0.1\ \sqrt{VmL}/2\pi$. We clearly observe the transition from tori, represented by the Poincaré-Birkhoff theorem, to resonance islands and the emergence of chaos as the amplitude of the perturbation increases, until the perturbation is such that the resonance islands are destroyed, the resonance 2:1 is marked in red. We also see the central island which is a KAM island, we see that it is very little influenced by the disturbance.

1.2 Quantum-classical correspondence

In this section, we introduce two essential tools that will allow us to characterize and study the quantum dynamics of the system, finally enabling us to transition from classical to quantum dynamics.

We begin by introducing the formalism of Floquet theory, used for time-dependent and time-periodic systems, which will enable us to obtain the quantum spectrum of the system. Then, we address the Husimi distributions, which provide a visualization of the various eigenstates of the system in the classical phase space. This visualization will be crucial later on as it will allow us to distinguish the eigensates involved in the tunneling process we wish to study.

1.2.1 Floquet theory

As we have now well established, the system considered in this work shows a temporal dependency in the form of a periodic modulation $\delta\cos(\omega_0 t)$. We will therefore need the formalism of Floquet's theory. This theory was first developed in 1883 by Floquet [28], and is the temporal correspondent of the Bloch theory used in condensed matter physics. It is used to solve the Schrödinger equation with a time-dependent and periodic Hamiltonian.

$$i\hbar\frac{d}{dt}\left|\psi(t)\right\rangle = \hat{H}(t)\left|\psi(t)\right\rangle \tag{1.12}$$

where we consider in our case a Hamiltonian of the form

$$\hat{H}(t) = \hat{H_0}(\hat{q},\hat{p}) + \hat{H_1}(\hat{q},\hat{p})\cos(\omega_0 t) = \hat{H}(t+T) \tag{1.13}$$

with T the period and $\omega_0 = \frac{2\pi}{T}$ the frequency. As we shall see this approach will allow us to restrict the time-dependent problem to a time-independent eigenvalue problem that we will then be able to solve.

Here, we will present the results of this theory from a slightly different perspective. We will focus only on the outcome of the Floquet's theorem, thereby providing an ad hoc explanation that will give us a simpler form of the problem to solve. If the reader seeks a more comprehensive and rigorous demonstration of this theorem, we recommend the following readings [29, 30].
The wave function that describes the temporal evolution of the system can be decomposed as follows :

$$\left|\psi_t\right\rangle = \frac{1}{\sqrt{2\pi}}\int_{-\infty}^{\infty}\left|\widetilde{\psi}_\omega\right\rangle e^{-i\omega t}d\omega \tag{1.14}$$

Which can also be written, assuming $\left|\psi_t\right\rangle$ is integrable, without loss of generality, as :

$$\left|\psi\right\rangle = \frac{1}{\sqrt{2\pi}}\sum_{l=-\infty}^{+\infty}\int_{-\omega_0/2}^{\omega_0/2}d\epsilon\left|\widetilde{\psi}_{l\omega_0+\frac{\epsilon}{\hbar}}\right\rangle e^{-i(l\omega_0+\epsilon/\hbar)t} \tag{1.15}$$

We will note $\left|\widetilde{\psi}_{l\omega_0+\epsilon/\hbar}\right\rangle \equiv \left|\widetilde{\psi}_{l,\epsilon}\right\rangle$. Equivalently, we have the inverse Fourier transform

$$\left|\widetilde{\psi}_\omega\right\rangle = \frac{1}{\sqrt{2\pi}}\int_{-\infty}^{\infty}\left|\psi_t\right\rangle e^{i\omega t}dt \tag{1.16}$$

By injecting this expression into (1.12), the time-dependent Schrödinger equation becomes a time-independent eigenvalue problem.

$$\hbar\omega \left|\widetilde{\psi}_w\right\rangle = \hat{H}_0 \left|\widetilde{\psi}_\omega\right\rangle + \frac{1}{2}\hat{H}_1 \left(\left|\widetilde{\psi}_{\omega+\omega_0}\right\rangle + \left|\widetilde{\psi}_{\omega-\omega_0}\right\rangle\right)$$

Given (1.15) we have,

$$\sum_l \left(\hbar(l\omega_0 + \tfrac{\epsilon}{\hbar}) \left|\widetilde{\psi}_{l,\epsilon}\right\rangle\right) = \sum_l \left(\hat{H}_0 \left|\widetilde{\psi}_{l,\epsilon}\right\rangle + \tfrac{1}{2}\hat{H}_1 \left(\left|\widetilde{\psi}_{l+1,\epsilon}\right\rangle + \left|\widetilde{\psi}_{l-1,\epsilon}\right\rangle\right)\right)$$

$$\Leftrightarrow \sum_l \left((\hat{H}_0 - l\hbar\omega_0) \left|\widetilde{\psi}_{l,\epsilon}\right\rangle + \tfrac{1}{2}\hat{H}_1 \left(\left|\widetilde{\psi}_{l+1,\epsilon}\right\rangle + \left|\widetilde{\psi}_{l-1,\epsilon}\right\rangle\right)\right) = \sum_l \left(\epsilon \left|\widetilde{\psi}_{l,\epsilon}\right\rangle\right)$$

The eigenvalues and eigenvectors are then computed via the diagonalization of the matrix $\mathscr{M}$.

$$\mathscr{M} = \begin{pmatrix} \ddots & \vdots & \vdots & \vdots & \\ \cdots & \hat{H}_0 + \hbar\omega_0 & \frac{1}{2}\hat{H}_1 & \cdots & \cdots \\ \cdots & \frac{1}{2}\hat{H}_1 & \hat{H}_0 & \frac{1}{2}\hat{H}_1 & \cdots \\ \cdots & \cdots & \frac{1}{2}\hat{H}_1 & \hat{H}_0 - \hbar\omega_0 & \cdots \\ & \vdots & \vdots & \vdots & \ddots \end{pmatrix} \tag{1.17}$$

Then, again considering the equality (1.15), we can find the temporal evolution of the system from the solutions of this diagonalization. And we have

$$|\psi(t)\rangle = \frac{1}{\sqrt{2\pi}} \int_{-\omega_0/2}^{\omega_0/2} e^{-i\frac{\epsilon}{\hbar}t} \sum_{l=-\infty}^{+\infty} e^{-il\omega_0 t} \left|\widetilde{\psi}_{l,\epsilon}\right\rangle \tag{1.18}$$

If the Hamiltonian has a discrete spectrum, we can write

$$|\psi(t)\rangle = \sum_{n=1}^{d} c_n e^{-i\frac{\epsilon_n}{\hbar}t} \left|\widetilde{\psi}_{\epsilon_n}(t)\right\rangle \tag{1.19}$$

Here, the summation over n includes all eigenvalues with $d = dim(\hat{H}_0)$, where c_n are coefficients to be determined, dependent on the initial state of the system and

$$\left|\widetilde{\psi}_{\epsilon_n}(t)\right\rangle = \sum_{l=-\infty}^{+\infty} e^{-il\omega_0 t} \left|\widetilde{\psi}_{l,\epsilon_n}(t)\right\rangle \equiv \left|\widetilde{\psi}_n(t)\right\rangle \tag{1.20}$$

These results constitute the Floquet's theorem.

Floquet's theorem

In the case of a time-dependent and periodic Schrödinger equation, the solutions $|\psi_n(t)\rangle$ ($\forall n \in \mathbb{Z}$) of this equation are of the form [28, 30]

$$|\psi_n(t)\rangle = e^{-i\epsilon_n t/\hbar} \left|\widetilde{\psi}_n(t)\right\rangle \tag{1.21}$$

where $\left|\widetilde{\psi}_n(t)\right\rangle$ is a periodic function of the same period as the Hamiltonian. In this case, the ϵ_n are called quasi-energies of the system and $\left|\widetilde{\psi}_n(t)\right\rangle$ are called Floquet states. Thus,

any $|\psi(t)\rangle$ can be decomposed as a linear combination of these Floquet states.

$$|\psi(t)\rangle = \sum_{n=1}^{d} c_n e^{-i\epsilon_n t/\hbar} \left|\widetilde{\psi}_n(t)\right\rangle \tag{1.22}$$

Therefore, the Floquet spectrum is obtained by diagonalizing the matrix (1.17), which can now be referred to as the Floquet matrix. The quasi-energies represent the effective energy levels of the quantum states in our periodic system. They describes the temporal evolution of the energy of the Floquet states in response to the periodicity of the perturbation.
Despite being infinite, the spectrum exhibits a periodicity of $\hbar\omega_0$. We observe intervals of size $\hbar\omega_0$ containing d quasi-energies each, and two quasi-energies separated by this value posses the same Floquet state, with their Fourier coefficients merely shifted.
Indeed, if $\left|\widetilde{\psi}_n(t)\right\rangle$ is a solution with the eigenvalue ϵ_n, $e^{ik\omega_0 t}\left|\widetilde{\psi}_n(t)\right\rangle$ is also a solution with the eigenvalue $\epsilon_n + k\hbar\omega_0$. That is, if

$$\left(\hat{H}(t) - i\frac{d}{dt}\right)\left|\widetilde{\psi}_n(t)\right\rangle = \epsilon_n \left|\widetilde{\psi}_n(t)\right\rangle \tag{1.23}$$

So,

$$\left(\hat{H}(t) - i\frac{d}{dt}\right) e^{ik\omega_0 t}\left|\widetilde{\psi}_n(t)\right\rangle = (\epsilon_n + k\hbar\omega_0)\left|\widetilde{\psi}_n(t)\right\rangle \tag{1.24}$$

And,

$$e^{ik\omega_0 t}\left|\widetilde{\psi}_n(t)\right\rangle = \sum_{l=-\infty}^{+\infty} e^{i(l-k)\omega_0 t}\left|\widetilde{\psi}_{l,\epsilon_n}(t)\right\rangle = \sum_{l=-\infty}^{+\infty} e^{-il\omega_0 t}\left|\widetilde{\psi}_{l,\epsilon_n+k}(t)\right\rangle \tag{1.25}$$

Thanks to this property it will be possible to limit our study to an interval containing d quasi-energies without loss of generality

1.2.2 Husimi representation

Once, we have obtain the Floquet spectrum of our system, we will see later that we will need a tool that enables us to determine the localization of these various Floquet states in phase space.

An intuitive approach would be to represent these different Floquet states in classical phase space, which means representing the wave function in terms of position and momentum variables. However, in quantum mechanics, due to the Heisenberg uncertainty principle

$$\Delta\hat{q}\Delta\hat{p} \geq \frac{\hbar}{2} \tag{1.26}$$

it is not possible to simultaneously specify, for a given wave function, the generalized coordinate and the associated conjugate momentum. This makes the direct representation of a quantum state in phase space impossible. To overcome this limitation, we introduce the Husimi distribution, highlighted by K.Husimi in 1940 [31]. It represents an important tool in quantum mechanics that allows for a more intuitive visualization of a given quantum state by associating a probability of finding that states at each point in phase space.
This approach involves defining, for each quantum state of interest, the corresponding Husimi

function. This function can be defined as the squared projection of this quantum state onto a set of coherent states centered at different points in phase space.

$$\Phi_{|\psi_n\rangle}(Q,P) = |\langle\alpha|\psi_n\rangle|^2 \tag{1.27}$$

With the coherent state which is generally defined as follows in the position representation q.

$$\langle q|\alpha_{Q,P}\rangle = \frac{1}{\sqrt{\sigma_g\sqrt{\pi}}} e^{-(q-Q)^2/2\sigma_g} e^{iP(q-Q)/\hbar} \tag{1.28}$$

Where Q and P are the coordinates of points in phase space and σ_g is the standard deviation of the Gaussian in the direction g.
By performing this calculation at every point in phase space, we evaluate the degree of overlap of the quantum state with the Gaussian wave packet centered at that point, thus giving us the probability of finding that state in that region of phase space. We can then graphically represent the value of this probability in the same phase space, providing a clear visualization of the localization of the different Floquet states, thereby facilitating the identification of those confined to resonance islands. Examples of distributions are illustrated in figure 1.5, displaying Husimi distributions for both the simple pendulum and the pendulum with periodically modulated amplitude. These distributions are presented both individually and superimposed onto the phase spaces, the latter case provides explicit insight into the localization of the concerned eigenstates within this phase space.

Note that to compute the Husimi functions of the different Floquet states, we first need to obtain the Floquet spectrum. However, this step is far from negligible given the complexity that the spectrum can exhibit. In our case, we employ numerical diagonalization of the Floquet matrix, as we have just explain in the previous section.
However, there are also semi-classical analytical approaches that allow for an approximation of the Floquet spectrum within resonance islands.

- EBK semi-classical quantization : The semi-classical EBK quantization, or Einstein-Brillouin-Keller method, is a technique used to extract the eigenergies of quantum mechanics from the classical dynamics of an integrable Hamiltonian system. However, motion within regular islands can be considered integrable under certain approximations. This method relies on associating stable classical orbits with quantum phases according to a rule called the EBK rule. Indeed, when a system is integrable, according to the Liouville-Arnold theorem, it is possible to define canonical action-angle variable (I,θ) such that the Hamiltonian depends only on the action. The definition of action along a periodic orbit is

  $$I = \frac{1}{2\pi}\oint p\ dq \tag{1.29}$$

  Where p is the conjugate momentum of the generalized coordinate q along the trajectory. Then, the EBK method [32] allows for the construction of an approximate solution of the Schrödinger equation in terms of the variables (I,θ) as an integral along the classical trajectory. This construction is possible if and only if

  $$\frac{1}{2\pi}\oint_{\gamma_i} p\ dq = (n_i + \frac{\mu_i}{4})\hbar \tag{1.30}$$

  Where γ_i represents the closed classical orbit, n_i is a quantum number associated with the orbit, and μ_i is a topological index, in our case we always have $\mu_i = 2$ [29].

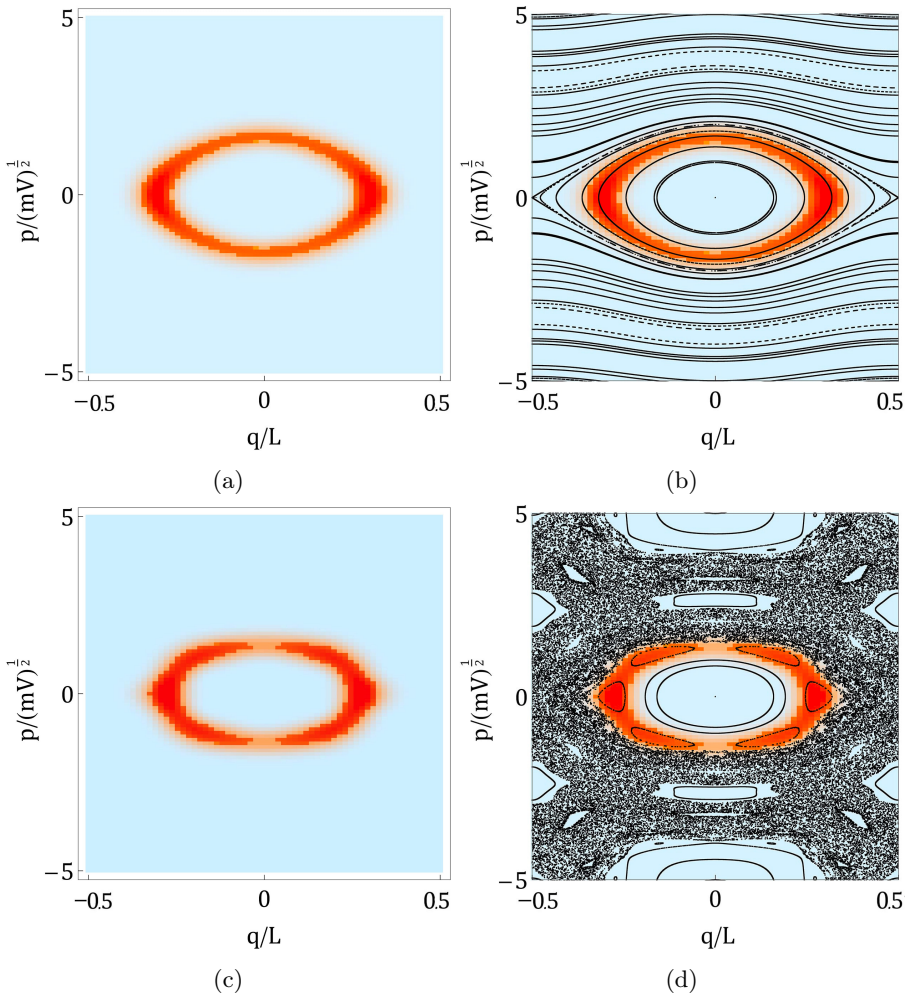

Figure 1.5: Husimi distributions in (a)-(b) for the simple pendulum and (c)-(d) for the periodically modulated pendulum. That is, the two configurations correspond to the Hamiltonian $H = p^2/2m + V[1 + \delta\cos(\omega_0 t)]\cos(2\pi q/L)$ with $\hbar\omega_0 = 0.5\ V$, $\hbar = 0.1\ \sqrt{VmL}/2\pi$, for $\omega_0 t = \pi/2 + 2\pi n$, $\forall n \in \mathbb{Z}$, and where (a)-(b) $\delta = 0$ and the represented eigenstate corresponds to eigenvalue $0.379664\ V$, (c)-(d) $\delta = 2$ and the represented eigenstate corresponds to eigenvalue $3.17474\ V$. In both cases, the distribution was illustrated once alone and then superimposed with the corresponding phase space. Orange indicates a high probability of finding the state of interest in that region of the phase space, while blue corresponds to a zero probability.

Thus by solving this equation, we obtain quantized values of the action that allow, when injected into the classical Hamiltonian, to provide an estimate of the various quantum energy levels with each classical orbit of the resonance islands.

- Mathieu approach : This method relies on Mathieu's equations [33], which are differential equations characterizing the motion of a particle in a periodic potential, often associated

with harmonic oscillators, of the general form

$$\frac{d^2y}{dv^2} + (a - 2q\cos 2v)y = 0 \tag{1.31}$$

The dynamics within resonance islands can be described by these equations given that motion can be considered integrable with certain approximations in the semi-classical limit. The advantage of reducing to such a form is that the solutions of these equations are well known. The coefficients a and q are then defined based on various characteristics of the system, such as the action of the relevant orbit and the frequency. The expression of the coefficient a is also related to the quasi-energies associated with the orbit, but Mathieu's equations only have solutions for a discrete set of values of a. This implies that the quantification of quasi-energy levels can be estimated from the expression of these different a.

Additional details on these methods can be found [22, 29, 12]. They rely on the fact that motion within resonance islands can be approximated by the motion of a harmonic oscillator, thus only giving an approximation of the quasi-energy levels within them. And, by considering a sufficiently large Hilbert space in which we work, numerical diagonalization yields more reliable results.

1.3 Non-dispersive wave packet

We now know that the introduction of the perturbation $\delta\cos(\omega_0 t)$ into our system leads to the emergence of resonance islands. And now that we have the tools to do so, we are going to look at the impacts of this perturbation on the quantum dynamics of the system. We will see that it induces what is known as phase-locked periodic motion of quantum wave packets prepared on one of these two regular islands [34, 29].

The concept of wave packet is closely intertwined to that of localization. We can associate with a classical particle a quantum state $|\psi\rangle$ that is ideally localized around the spatial position of the classical particle at any given time t. However, in quantum mechanics, there exists a limitation on localization imposed by Heisenberg's uncertainty principle (1.26).

Hence, the best we can hope for is a localized quantum state with a finite width $(\Delta\hat{q}, \Delta\hat{p})$, centered around the classical particle's position. Quantum states exhibiting these localization properties in phase space are referred to as wave packets [35]. However, when the Hamiltonian takes a completely general form independent of time, an initially localized wave packet will not maintain its localization as time progresses. In fact, consider such a Hamiltonian

$$\hat{H} = \frac{\hat{p}^2}{2m} + \hat{V} \tag{1.32}$$

with

$$\hat{H}\,|\psi_n\rangle = E_n\,|\psi_n\rangle \tag{1.33}$$

In this case, the time evolution of wave function $|\psi(t)\rangle$ found through the Schrödinger equation $i\hbar\frac{d}{dt}\,|\psi(t)\rangle = \hat{H}\,|\psi(t)\rangle$ will take the form

$$|\psi(t)\rangle = \sum_n c_n e^{-i\frac{E_n t}{\hbar}}\,|\psi_n\rangle \tag{1.34}$$

It can then be observe that if $|\psi(t=0)\rangle$ is initially localized, its localization will degrade as time advances due to the accumulation of relative phases of the different contributions in the

equation (1.34). These contributions interact, creating regions of constructive and destructive interference, resulting in an expanded spatial distribution of the probability of finding the particle associated with the wave function. The wave packet is said to spread. However, to study the phenomenon of dynamic tunneling that we aim to examine in this paper, the wave packet must be able to be confined to a region of phase space. Thus, we inquire about means to counteract the natural dispersion of the wave packet.

Given the form of the wave function (1.34), it becomes apparent that we can recover the initial and localized shape of the wave packet if all phases $e^{-i\frac{E_n t}{\hbar}}$ simultaneously take the same value, meaning if all energy levels E_n are equally spaced [29]. However, this holds true only for harmonic oscillators, which is far too restrictive. It is through classical mechanics that we can find a solution. Indeed, a quantum wave packet propagates like the corresponding classical particles. Consequently, if all classical trajectories in an initial volume of phase space remain well localized during the temporal evolution in this volume, it is reasonable to expect that a wave packet constructed on this initial volume will also not spread. To maintain generality, we can therefore consider quasi-periodic classical trajectories that always remain close to a well-defined periodic orbit [29]. Such trajectories can be easily generated using an external periodic perturbation. Indeed, as we have just seen, the introduction of such a perturbation into our system leads to the appearance of resonance islands via the Poincaré-Birkhoff theorem.
These resonance islands are defined by periodic orbits that form around the corresponding stable points. When a trajectory enters a resonance island, it is influenced by the periodic orbits residing there. These orbits have the particularity of being stable, meaning that slight perturbations of the initial trajectories are gradually corrected, bringing the trajectories back to the corresponding periodic orbit. Consequently, any trajectory started near a stable periodic orbit will remain trapped inside the resonance island, and these islands act as dynamical barriers that confine the trajectories to a specific region of phase space.

Therefore, the distance between the central stable periodic orbit of the island, which has a period equal to a multiple of the period of the external driving $rT = r2\pi/\omega_0$, and a trapped orbit in the same island, will remain limited. Any trajectory in a certain interval around the periodic orbit, cannot drift away from it, this is referred to as the phase-locking phenomenon [34, 29]. Consequently, the resonance island occupies a finite volume of phase space and traps all trajectories in a region where the internal frequencies are close to the excitation frequency ω_0. This characteristic implies that the entire structure, and not just a few trajectories, is phase-locked. Thus, if this resonance island is sufficiently large, it will be possible to construct quantum wave packets locked in phase on the classical orbit and therefore that will not spread. In our system, a wave packet locked on one of the 2:1 resonances thus results in a periodic motion (clockwise) of the condensate in the ring trap as illustrated in Fig. 1.6a. The wave packet prepared on the other island is just delayed by $2\pi/\omega_0$ compared to this first case (Fig. 1.6b).

The quantum objects that naturally correspond to these particular wave packets are Floquet states [29]. Indeed, as we have seen earlier, each Floquet eigenstate is associated with a density of probability in phase space that is strictly periodic in time, with the period of the external driving. Thus, this density of probability changes shape as time elapses, but regains its initial shape after each period, thereby maintaining the localization of the wave packet. This characteristic, combined with the ability to construct Floquet states well localized at specific phases of the excitation field, automatically makes them non-dispersive wave packets.

In summary, creating a non-dispersive wave packet in a time-dependent periodic system amounts

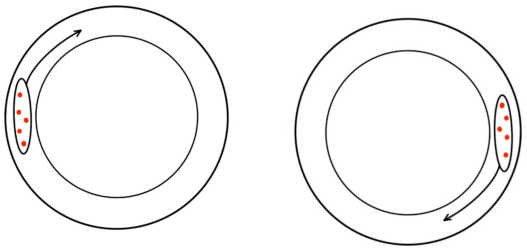

(a) (b)

Figure 1.6: Motion of the condensate in the ring trap when the wave packet is said to be locked on a periodic orbit. Both illustrations show the condensate (the red dots) as it is prepared on each of the resonance islands. In both cases, it will have a regular movement in the trap, and will remain localized without dispersing. The two different solutions are just delayed by a period in their evolution.

to finding a localized Floquet eigenstate. Our objective is therefore to find such localized Floquet states on one of the resonance islands. Thus, we will first have to calculate the Floquet spectrum by diagonalization of the matrix (1.17), then we will be able to identify the resulting Floquet states that are located on the resonance islands, and thus identify the states useful for our study, thanks to their Husimi distributions.

Chapter 2

Time crystals and ultracold atoms

We have now clearly defined the general configuration that our system will adopt. By focusing on the 2:1 resonance, we end up with two perfectly symmetrical regular islands, they are marked in red in the figure 2.1. As a reminder, in this work, we wish to calculate the collective tunneling rate of the atoms of our condensate between these two regular islands. The aim of this chapter is then to study in more detail the intrinsic dynamics of our condensate in such a configuration to understand this phenomenon.

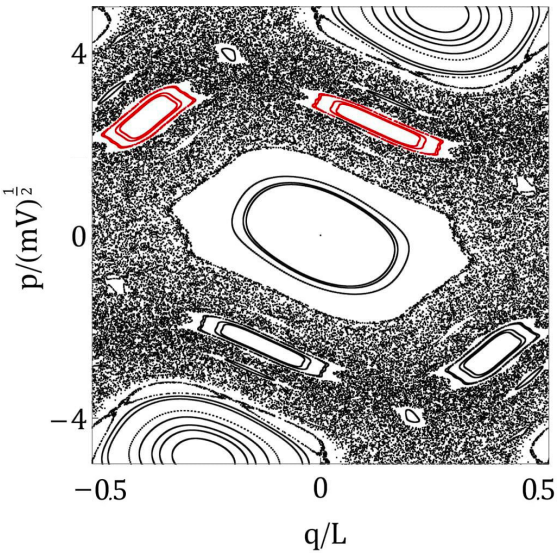

Figure 2.1: Poinacré section constructed for $\omega_0 t = \pi/2 + 2\pi, n \ \forall n \in \mathbb{Z}$, of the classical single-particle dynamics for the model Hamiltonian $H = p^2/2m + V[1 + \delta\cos(\omega_0 t)]\cos(2\pi q/L)$ with $\delta = 2$, $\hbar\omega_0 = 0.5\ V$ and $\hbar = 0.1\ \sqrt{VmL}/2\pi$. The 2:1 resonance islands are marked in red.

Hence, we will introduce the Bose-Hubbard model, one of the simplest model describing ultracold interacting atoms trapped in a periodic potential. It provides expressions for the elements of the effective hopping matrix and the effective atom-atom interaction parameter, which we can calculate. Once these parameters are evaluated, the Bose-Hubbard Hamiltonian allows us to make an initial prediction on the time of the collective tunneling phenomenon of a condensate

of N particles as we will see later.
Then, we will also explain how the consideration of the interaction between particles within the condensate in this particular setup will lead to a breaking of the symmetry of the system, implying that our system is actually what we call a time crystal.

Before presenting the formalism related to the Bose-Hubbard model, it is necessary to revisit the theory of Bose-Einstein condensation. We will thus begin by defining this particular state of matter, the specific properties associated with it, and how we can characterize the dynamics of the atoms constituting it. Then we will define this model and explain how the tunneling rate can be calculated from it. Finally, we will end this chapter by introducing the concept of time crystals and explaining how our system fits into this framework.

2.1 Bose-Einstein condensation

A Bose-Einstein condensate can be seen as a new state of matter that behaves like a coherent wave, emerging when we have a large amount of particles and when the temperature approaches absolute zero. Its origin traces back to Einstein's predictions in 1924-1925 [36, 37], following Bose's work in 1924 [38]. Subsequently, in the 1990s, the first experimental realizations of this phenomenon were achieved by the group of Wieman and Cornell with ^{87}Rb atoms [39] and by Ketterle's group with ^{23}Na [40].
The appearance of Bose-Einstein condensates occurs when the quantum properties of matter must be considered. Indeed, one of the fundamental concepts of quantum physics is the wave-particle duality. This concept states that each particle is characterized by a wavelength

$$\lambda_{dB} = \frac{h}{p} \tag{2.1}$$

where h is Planck's constant and p is the particle's momentum. This wavelength, known as the de Broglie wavelength [41], measures the spatial extension of a particle of mass m at the temperature T. In terms of thermodynamics quantities, we have

$$\lambda_{dB} = \sqrt{\frac{2\pi\hbar^2}{mk_BT}} \tag{2.2}$$

where k_B is the Boltzmann's constant and $\hbar$ is the normalized Planck constant.

We consider a ideal dilute gas ($N \approx 10^5, ..., 10^{10}$) of N indistinguishable particles contained in a volume v, maintained at temperature T and chemical potential μ. At ambient temperature and pressures, the typical distance between particles in such a gas is much greater than λ_{dB} [9]. In this case, the particles can be considered as points, and their energy distribution can be described by the Maxwell-Boltzmann distribution.
However, at lower temperatures, the spatial extensions of the waves associated with the particles begin to overlap, and quantum properties must be taken into account. Now, the quantum properties of a quantum gas of indistinguishable particles differ from the classical case.
Indeed, two types of quantum particles are distinguished : bosons and fermions, which are respectively described by a wave function that is completely symmetric ψ_+ and completely anti-symmetric ψ_-. In other words, the permutation of two identical particles results in a factor $+1$ in the wave function in the symmetric case and a factor -1 in the anti-symmetric case.

$$\psi_\pm(r_1, ..., r_i, ..., r_j, ..., r_N) = \pm\psi_\pm(r_1, ..., r_j, ..., r_i, ..., r_N) \tag{2.3}$$

Considerations of these symmetries lead to the following results [25]

- Two fermions cannot occupy the same quantum state, known as Pauli's exclusion principle.
- In the case of bosons, the probability of finding all particles in the same state is greatly increased, a phenomenon known as Bose enhancement. And this effect becomes more visible as the number of indistinguishable particles in the gas increases.

Thus, when quantum aspects are considered, the Maxwell-Boltzmann distribution must be replaced by the Bose-Einstein distribution for bosons, and by the Fermi-Dirac distribution for fermions.

We are only interested in the case of bosons, for which the Bose-Einstein distribution gives the average occupation number n_k of energy level ϵ_k

$$\langle\ \bar{n}_k\rangle = \frac{1}{\exp\left(\frac{\epsilon_k-\mu}{k_B T}\right)-1} \tag{2.4}$$

which depends only on the temperature T and chemical potential μ. As previously stated, nothing prevents multiple bosons from occupying the same quantum state. Thus, at low temperatures, a significant portion of the particles occupy the ground state ϵ_0.
Furthermore, as the temperature decreases, in order for the average particle density, given by $\frac{\langle\hat{N}\rangle}{v} = \sum_k \langle\ \bar{n}_k\rangle$, to remain constant, μ must adjust itself by approaching ϵ_0.

At a certain temperature T_c, a singular behavior occurs; the occupation of the ground state diverges when $\mu \to \epsilon_0$, and if $\mu > \epsilon_0$ it would correspond to an infinite population of the system, which is not possible. By studying this divergence in more detail, we see that for a temperature $T < T_c$, the chemical potential remains constant at $\mu = \epsilon_0$, and the additional population accumulates in the ground state. This is the signature of Bose-Einstein condensation, and in this case, the particles lose their individuality and condense into the ground state, forming a coherent matter wave. Thus, T_c represents a critical temperature, characterizing a phase transition. This is illustrated in Fig. 2.2.

Note that a Bose-Einstein condensate can also be prepared in an excited state, not necessarily in the ground state, either by applying magnetic fields, lasers, or other means of atom manipulation. In particular, when a condensate is in motion, the atoms composing it are in an excited state.

This state of matter is distinguished by the formation of a coherent matter wave on a large scale. To describe this long-range coherence, we define the one-body density matrix [42]

$$n(\mathbf{r},\mathbf{r'}) = \langle\overline{\hat{\psi}^\dagger(\mathbf{r})\hat{\psi}(\mathbf{r'})}\rangle \tag{2.5}$$

Where $\hat{\psi}(\mathbf{r'})$ is the field operator that destroys a particle at position $\mathbf{r}$, and $\hat{\psi}^\dagger(\mathbf{r})$ creates a particle at position $\mathbf{r}$. If we have $\{(\phi_k)_{k=0,1,\dots}\}$ an orthonormal basis of the one-body Hilbert space, the field operators can be expressed as

$$\hat{\psi}(\mathbf{r}) = \sum_k \phi_k(\mathbf{r})\hat{a}_k\ ,\ \hat{\psi}^\dagger(\mathbf{r}) = \sum_k \phi_k^*(\mathbf{r})\hat{a}_k^\dagger \tag{2.6}$$

with $\hat{a}_k$ the annihilation operator that destroys a particle characterized by the orbital $\phi_k(\mathbf{r})$, and $\hat{a}_k^\dagger$ the creation operator that creates such a particle. So we also have,

$$n_{kk'} = \langle\overline{\hat{a}_k^\dagger\hat{a}_{k'}}\rangle \tag{2.7}$$

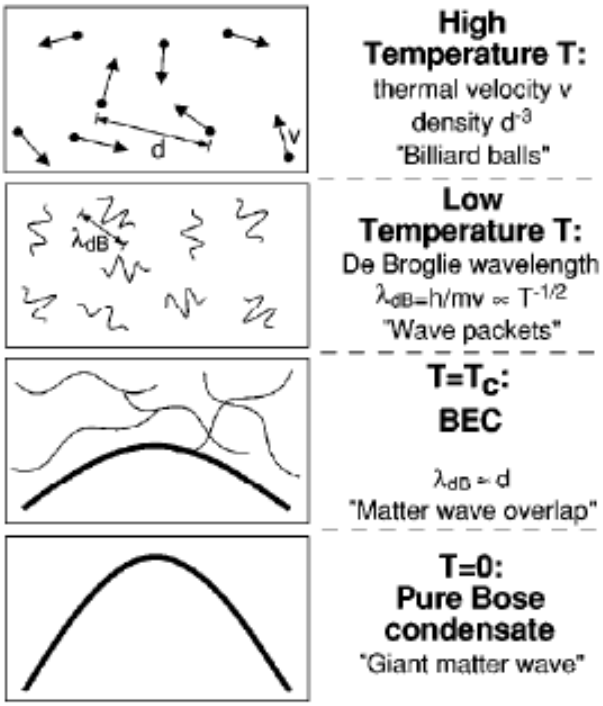

Figure 2.2: Sketch of the Bose-Einstein condensation occurring when the spatial extensions of the bosonic particles sufficiently overlap. We can see the wave behaviour of matter emerging. This image comes from Ref.[42].

This parameter characterizes the long-range coherent behavior, which distinguishes the Bose-Einstein distribution from the Maxwell-Boltzmann distribution and allows condensation. Indeed, if we consider a ideal gas in a normalization volume $v = L^3$, i. e. in a cube with side length L which serves as a reference volume, in this case

$$n_{kk'} = \frac{\delta_{kk'}}{e^{\beta(\epsilon_k - \mu)} - 1}$$

So,

$$n(\mathbf{r}, \mathbf{r'}) = \overline{\langle \hat{\psi}^\dagger(\mathbf{r}) \hat{\psi}(\mathbf{r'}) \rangle} = \sum_{k,k'=0}^{\infty} n_{kk'} \phi_k^*(\mathbf{r}) \phi_{k'}(\mathbf{r'})$$

$$= \sum_{k=0}^{\infty} \frac{\phi_k^*(\mathbf{r}) \phi_{k'}(\mathbf{r'})}{e^{\beta(\epsilon_k - \mu)} - 1} = \frac{1}{V} \sum_{\ell} \frac{e^{i2\pi\ell(\mathbf{r'}-\mathbf{r})/L}}{e^{\beta(\epsilon_\ell - \mu)} - 1}$$

If $V \to \infty$, then $\mathbf{p} = \frac{2\pi\hbar}{L} \to \ell$. And thus, the expression becomes

$$\frac{1}{(2\pi\hbar)^3} \int d^3p \frac{e^{i\mathbf{p}(\mathbf{r'}-\mathbf{r})/\hbar}}{e^{\beta(\mathbf{p}^2/2m - \mu)} - 1} = \frac{1}{v} \int d^3p \; n(\mathbf{p}) e^{\frac{i}{\hbar}\mathbf{p}(\mathbf{r'}-\mathbf{r})}$$

with

$$n(\mathbf{p}) = \begin{cases} \dfrac{v}{(2\pi\hbar)^3} \dfrac{1}{e^{\beta(\mathbf{p}^2/2m-\mu)}-1} & \text{if } T > T_c \\ \dfrac{v}{(2\pi\hbar)^3} \dfrac{1}{e^{\beta(\mathbf{p}^2/2m)}-1} + N_0\delta(\mathbf{p}) & \text{if } T < T_c \end{cases} \tag{2.8}$$

Indeed, we know that for the Bose-Einstein distribution, $n(\mathbf{p})$ is a smooth function above the temperature T_c and thus the one-particle density matrix vanishes for $|\mathbf{r}-\mathbf{r'}| \to \infty$. However, we know that a divergence appears at T_c and below, which results in the presence of a delta function in expression (2.8). Thus,

$$n(\mathbf{r},\mathbf{r'}) \to \begin{cases} 0 & \text{if } T > T_c \\ \dfrac{N_0}{v} & \text{if } T < T_c \end{cases} \tag{2.9}$$

And the long-range behaviour is explicit. It is called "*off-diagonal long-range order*" [43].

These Bose-Einstein condensates are achieved at temperatures scales $\approx 1\mu K$. Several techniques must then be employed to trap and cool atoms. Laser cooling technique traps atoms by using cycles of absorption and spontaneous emission of a photon by an atom, which also allows reaching a temperature of $10\mu K$ but not going below [25]. Then, a second technique, evaporative cooling, is used. This technique removes the most energetic atoms from the trap via radio-frequency radiation. More details can be found in [44]. Alkali atoms are an interesting species of atoms for the experimental construction of such a state of matter; they have a single valence electron whose magnetic moment can interact with an external magnetic field.

Note also that to achieve such a state with a gas of N particles, it is important that this gas be dilute to prevent phase transitions to liquid or solid configurations, even at such low temperatures.

To summarize, in a Bose-Einstein condensate, bosons behave collectively, they are all in the same quantum state. This collective behavior leads to interesting phenomena such as superfluidity, where matter can flow without friction [45].

2.2 Interactions in the condensate

In the condensate, atoms interact not only with external fields used for trapping and cooling, but also with each other. However, atoms are intrinsically neutral, so the interaction is relatively weak, but it cannot be completely neglected in such a configuration where a large fraction of the atoms condense into the same quantum state. Given that the gas of ultracold atoms is dilute, it is reasonable to primarily consider interactions between two atoms, while three-body collisions can be safely ignored.

Therefore, the interaction between atoms in the condensate can be reduced to the collision process between two atoms and can be modeled by a potential of the form $U(\mathbf{r},\mathbf{r'})$ depending on the positions of the two particles $\mathbf{r}$ and $\mathbf{r'}$ considered. In this two-body scenario, it is convenient to study the system in the center-of-mass coordinates defined by $(\mathbf{r}+\mathbf{r'})/2$, and in the relative coordinates $\bar{\mathbf{r}} = |\mathbf{r}-\mathbf{r'}|$. In reality, the interaction depends only on the relative distance between the two particles, thus $U(\mathbf{r},\mathbf{r'}) = U(\bar{\mathbf{r}})$.
In the center-of-mass coordinates, the wave function behaves like a free particle, so it is characterized by plane waves. However, an interesting behavior emerges when considering the relative

coordinates. In this context, the wave function ψ is described by an ordinary Schrödinger equation in which U is treated as an external potential. Essentially we find ourselves in the well-known case of the scattering process of a particle in a central potential U, as schematize in Fig. 2.3.

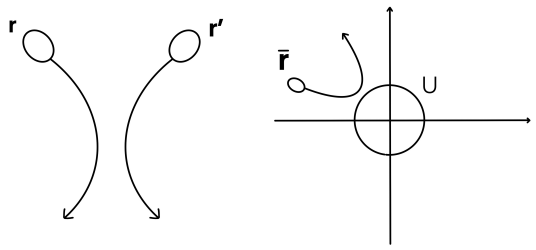

(a) (b)

Figure 2.3: (a) Sketch of the 2-body scattering process. (b) This process can be considered as a one-body scattering process in a central potential U in the relative coordinates $\bar{\mathbf{r}}$.

It is thus possible to write the wave function as a coherent superposition of an incident plane wave (assumed too be oriented along the $\bar{z}$ axis in the relative coordinates) and a scattered part see Fig. 2.4b. By considering that the potential is spherically symmetric, that $U \to 0$ when $\bar{r} \to \infty$ sufficiently rapidly, and that initially, the wave packet is far from the potential, we have [44, 45]

$$\psi(\bar{r}) = e^{ik\bar{z}} + a(\theta)\frac{e^{ik\bar{r}}}{\bar{r}} \tag{2.10}$$

Where $a(\theta)$ is the scattering amplitude that depends only on θ, the scattering angle[1] represented in the figure 2.4a, and where k is the wave vector. This is the angle between the incident motion and the motion after scattering.

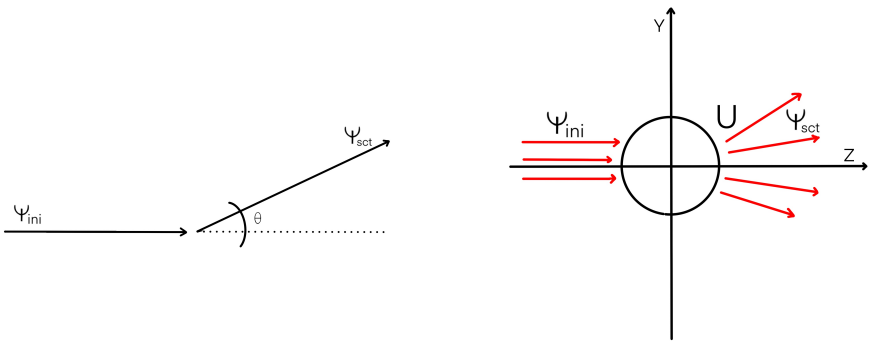

(a) (b)

Figure 2.4: Graph (a) represents the scattering angle θ. Graph (b) is a sketch of the initial incident wave and the wave scattered by the central potential U.

[1]Since we consider a spherically symmetric potential

We would now like to obtain the expression for this scattering amplitude $a(\theta)$, focusing on low energies. Here, we strongly summarize the development to arrive at the desired expression, but more details can be found in [25, 46].
We can observe that this coefficient depends only on δ_l which corresponds to a phase shift of the wave function relative to the potential U. We have $\delta_l = 0$ if $U(\bar{r}) = 0\ \forall \bar{r}$. Then, $\delta_l \to 0$ for $k \to \infty$ because we are in the low energy regime, and so we look at δ_l in the limit $k \to 0$. We examine the behavior of δ_l for different values of l as a function of k [46], if we consider a diffusion potential that decreases in $U \propto -r^{-n}$ with $n > 3$,

$$\delta_l \propto \begin{cases} k^{2l+1} & : \ 2l+1 < n-2 \\ k^{n-2} & : \ 2l+1 \geq n-2 \end{cases} \tag{2.11}$$

And so, we find that δ_0 increases linearly with k and thus the ratio δ_0/k remains constant in the limit $k \to 0$. While for $l > 0$, δ_l increases more rapidly with k, these components then disappear in the limit $k \to 0$. Therefore, $a(\theta)$ can be considered as a constant $a_s = \delta_0/k$. This constant is the scattering length of s-wave and thus fully describes the low-energy collision between two atoms. The scattering wave function then becomes

$$\psi(\bar{r}) = e^{ik\bar{z}} - \frac{a_s}{\bar{r}} e^{ik\bar{r}} \ \overset{k\to 0}{=} \ 1 - \frac{a_s}{\bar{r}} \tag{2.12}$$

Here is a table with typical values of a_s for alkali atoms

	^7Li	^{23}Na	^{87}Rb	^{85}Rb
$a_s[a_B]$	-30	20	100	-370

Table 2.1

Where the values are given in unit of the Bohr radius $a_B = 5.29 \times 10^{-2}$ nm. It is worth noting that a_s can be positive or negative. A negative a_s corresponds to an attractive interaction between atoms and a positive a_s to a repulsive interaction. It is experimentally possible to build a Bose-Einstein condensate in the attractive case, but this situation is more unstable than the repulsive case, as this attraction can lead to the collapse of the condensate onto itself via the appearance of three-body collisions.

Furthermore, the s-wave scattering length therefore represents the typical distance at which atoms interact. With d denoting the typical inter-atomic distance in the ultracold atom gas, the condition of dilute gas is

$$|a_s| << d \tag{2.13}$$

This means that for a typical separation d, atoms do not see each other. It is then convenient to get rid of all the details of the atom-atom interaction, and to model it by a contact potential

$$U(\mathbf{r}, \mathbf{r'}) = g\delta(\mathbf{r} - \mathbf{r'}) \tag{2.14}$$

We can make this replacement as long as this new potential gives us the expected a_s. Then we have the following relation between g and a_s [47]

$$g = \frac{4\pi\hbar^2 a_s}{m} \tag{2.15}$$

where m is the mass of the atomic species considered.

We now seek to obtain the equation governing the dynamics of a Bose-Einstein condensate. Considering the two-body interaction, the Hamiltonian of the system is

$$\hat{H} = \int d^3r\ \hat{\psi}^\dagger(\mathbf{r})(\frac{-\hbar^2}{2m}\Delta + V(\mathbf{r}))\hat{\psi}(\mathbf{r}) + \frac{1}{2}\int d^3r \int d^3r' \hat{\psi}^\dagger(\mathbf{r})\hat{\psi}^\dagger(\mathbf{r'})U(\mathbf{r}-\mathbf{r'})\hat{\psi}(\mathbf{r})\hat{\psi}(\mathbf{r'}) \quad (2.16)$$

where $\hat{\psi}^\dagger(\mathbf{r})$ and $\hat{\psi}(\mathbf{r})$ are the field operators described earlier (2.6) and $V(\mathbf{r})$ represents the trapping potential. We are still in the regime of low temperatures $\approx 1\mu K$, and as we have just shown, for dilute gases $|a_s| << d$, we can approximate the shape of U by (2.14). Moreover we can make the *Hartree* ansatz by assuming that all atoms share the same normalized single-particle orbital $\phi(\mathbf{r})$ [48]. We can then define the condensate wavefunction of a gas of N atoms by

$$\psi(\mathbf{r}) = \sqrt{N}\phi(\mathbf{r}) \quad (2.17)$$

This function represent the collective state in which each particle is located and consequently $|\psi|^2$ would represent the density of condensed atoms [48]. And so, to describe the dynamics of the condensate, all we need to do is describe the time evolution of this particular function. We then have the Gross-Pitaevskii equation for ψ

$$\frac{-\hbar^2}{2m}\Delta\psi(\mathbf{r}) + V(\mathbf{r})\psi(\mathbf{r}) + g|\psi(\mathbf{r})|^2\psi(\mathbf{r}) = \mu\psi(\mathbf{r}) \quad (2.18)$$

where μ is the chemical potential of the condensate. This equation is a nonlinear Schrödinger equation that describes the collective dynamics of the condensate.
It can be obtained by the variational principle for the optimal choice of ψ. We have to minimize the functional $\mathscr{H}[\psi] - \mu\mathscr{N}[\psi]$ with

$$\mathscr{H}[\psi] = \int d^3r\ \left(\frac{\hbar^2}{2m}|\nabla\psi(\mathbf{r})|^2 + V(\mathbf{r})|\psi(\mathbf{r})|^2 + \frac{1}{2}g|\psi(\mathbf{r})|^4\right) \quad (2.19)$$

$$\mathscr{N}[\psi] = \int d^3r\ |\psi(\mathbf{r})|^2 - N \quad (2.20)$$

Where N is the number of particles in the condensate. This approach can be easily generalized to describe time-dependent phenomena, such as the evolution of a condensate in the presence of a time-dependent potential $V(\mathbf{r}, t)$ [49], as discussed in this study. We have the time-dependent Gross-Pitaevskii equation

$$i\hbar\frac{\partial}{\partial t}\psi(\mathbf{r}, t) = \frac{-\hbar^2}{2m}\Delta\psi(\mathbf{r}, t) + V(\mathbf{r}, t)\psi(\mathbf{r}, t) + g|\psi(\mathbf{r}, t)|^2\psi(\mathbf{r}, t) \quad (2.21)$$

Finally, note that when atom-atom interactions are neglected, i.e. for $g = 0$, the Gross-Pitaevskii equation reduces to an ordinary Schrödinger equation. This equation predicts a state of the condensate that adopts a Gaussian shape, when it is confined in a harmonic trap. However, when atom-atom interactions are taken into account, the shape of the condensate can significantly diverge from the Gaussian shape anticipated in the absence of interactions. Thus, the effects of these interactions manifest as alterations to this Gaussian profile. In other words, atom-atom interactions influence the spatial structure of the condensate, giving it a different organization than the one predicted by a model without interactions [47].

2.3 Bose-Einstein condensate in a waveguide

Let's revisit the configuration of our trap. The motion of our condensate within it can be illustrated like in the figure 2.5.

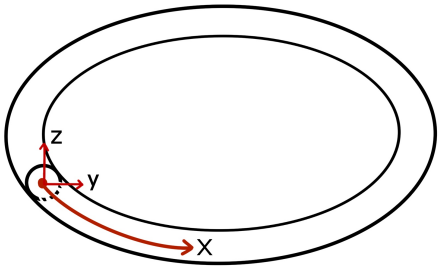

Figure 2.5: Sketch of the ring trap. This clearly shows that the condensate only moves in the direction of the x and remains confined in the two transverse directions y and z.

We immediately notice that the motion can be reduced to one-dimensional motion along the x direction. This means we can approximate the condensate as being subjected to a harmonic trap potential in the transverse directions (along y and z for example). This trap potential is considered isotropic and is associated with a frequency $w_\perp$ in both of these directions. While there is no longitudinal confinement (along x). We also approximate that the curvature of the trap can be ignored along this direction.
Therefore, the condensate wave function $\psi(\mathbf{r})$ can be decomposed as

$$\psi(\mathbf{r}) = \psi_\perp(y,z)\psi(x) \tag{2.22}$$

In this case, we consider that $\psi_\perp(y,z)$ corresponds to the transverse ground state, which is a Gaussian function of the form [50]

$$\psi_{0,\perp} = \frac{1}{\sqrt{\pi}\sigma_\perp} e^{\frac{-y^2}{2\sigma_\perp^2}} e^{\frac{-z^2}{2\sigma_\perp^2}} \tag{2.23}$$

with $\sigma_\perp = \sqrt{\frac{\hbar}{m\omega_\perp}}$, as the transverse trapping potential is assumed to be harmonic.
Then, in order to obtain a one-dimensional Gross-Pitaevskii equation, the three-dimensional equation (2.18) is projected onto the transverse ground state .Note that the potential $V(\mathbf{r})$ can also be decomposed as $V(\mathbf{r}) = V_\perp(y,z)V(x)$, and by projecting onto the transverse part, only the component $V(x)$ remains relevant[2]. We find straightforwardly

$$\frac{-\hbar^2}{2m}\frac{\partial^2}{\partial x^2}\psi(x) + V(x)\psi(x) + g_{1D}|\psi(x)|^2\psi(x) = \mu\psi(x) \tag{2.24}$$

[2]We are restricting ourselves to a one-dimensional Hilbert space

In which only the interaction term undergoes a significant change due to the presence of the modulus square of the wave function $|\psi(\mathbf{r})|^2$ in that term. Thus, the coefficient g characterizing this interaction differs depending on whether one or more dimensions are considered. In the case of the problem reduced to one dimension, we write it g_{1D} to differentiate it from (2.15). We will determine its exact expression in the next section where we will need it to find the form of the effective interaction parameter in the Bose-Hubbard model.

And so, in conclusion, the study of the dynamics of our condensate can be reduced to a one-dimensional problem because of the specific shape of the trap in which it lies.

2.4 Bose-Hubbard model

Historically, the Hubbard model was introduced to study interacting electrons in a solid [51]. However, as we have mentioned before, the system under consideration here is a time crystal. By analogy to solid crystals, this system is defined as one with a periodic potential, but this periodicity is in time rather than in space as we will see in the next section. In this system, it is ultracold atoms, rather than electrons, that are trapped. The Hubbard model can be adapted to describe ultracold bosonic atoms interacting and trapped in a periodic potential, which is referred to as the Bose-Hubbard model [52, 53, 54]. Therefore, it is possible for us to derive this model to describe our system.

Indeed, our condensate is trapped in a ring trap, obtaining such a configuration requires precise steps that we won't detail here, but interested readers can find more information on this topic in [55, 56, 57]. But, as it is now well established, we know that, in addition to the trap potential, we have a periodic modulation of its amplitude, and, in this section, we will simply denote by $V(x,t)$ the potential relative to this trap and its periodic modulation. This potential is thus time-periodic and it can be associated with a double well potential, as we know after Chapter 1 that the presence of the modulation results in the formation of two resonance islands in the case of the 2:1 resonance. In practice, the condensate atoms will only populate the sites corresponding to these wells, i.e., the stable solutions.
So, recalling the conclusion of the previous section, the system's Hamiltonian can be written as

$$\begin{aligned} \hat{H} &= \int dx \hat{\psi}^\dagger(x) \left(\frac{-\hbar^2}{2m} \frac{\partial^2}{\partial x^2} + V(x,t) \right) \hat{\psi}(x) \\ &+ \frac{1}{2} \int dx \int dx' \ \hat{\psi}^\dagger(x) \hat{\psi}^\dagger(x') U(x-x') \hat{\psi}(x) \hat{\psi}(x') \end{aligned} \tag{2.25}$$

And, if we consider a single-particle orthonormal basis $(\phi_k(x))_{k=1,2,\dots}$ in which the two wave functions $\phi_1(x)$ and $\phi_2(x)$ are localized in each of the potential wells. Given what we know about the configuration of the system, we can make a two-mode approximation [48], assuming that the populations of all other orbitals can be neglected. Note that the two modes $\phi_1(x)$ and $\phi_2(x)$ are actually quasimodes, as we will see in the next section. Although we know that in this work we limit ourselves to the case of a 2:1 resonance, we can generalize the following development to the case where we have N_s resonances and N_s quasimodes localized on them. Then, the field operators can be approximately defined as

$$\hat{\psi}(x) = \sum_{j=1}^{N_s} \phi_j(x) \hat{a}_j \tag{2.26}$$

$$\hat{\psi}^\dagger(x) = \sum_{j=1}^{N_s} \phi_j^*(x)\hat{a}_j^\dagger \tag{2.27}$$

Where, therefore, N_s is the number of sites. Then, $\hat{a}_j$ is the operator associated with particle annihilation at site j, and $\hat{a}_j^\dagger$ is the operator associated with particle creation at such a site.
Moreover, as mentioned previously, at low energies, atom-atom collisions are described by the s-wave scattering length a_s.
Thus, the Hamiltonian can now be written as

$$\hat{H} = \sum_{i,j=1}^{N_s} H_{ij}\ \hat{a}_i^\dagger \hat{a}_j + \frac{1}{2} \sum_{i,j,k,l=1}^{N_s} U_{ijkl}\ \hat{a}_i^\dagger \hat{a}_j^\dagger \hat{a}_k \hat{a}_l \tag{2.28}$$

with

$$H_{ij} = \int dx\ \phi_i^*(x) \left(\frac{-\hbar^2}{2m} \frac{\partial^2}{\partial x^2} + V(x,t) \right) \phi_j(x) \tag{2.29}$$

$$U_{ijkl} = g_{1D} \int dx\ \phi_i^*(x)\phi_j^*(x)\phi_k(x)\phi_l(x) \tag{2.30}$$

And in order to obtain the Bose-Hubbard Hamiltonian, we need to make a few more assumptions [9, 58]. First, the different matrix elements considered are assumed to be real. Then, note that the parameter H_{ij} can be divided into two parts. If $j = i$,

$$H_{ii} = \int dx\ \phi_i^*(x) \left(\frac{-\hbar^2}{2m} \frac{\partial^2}{\partial x^2} + V(x,t) \right) \phi_i(x) \tag{2.31}$$

represents the on-site energy of the system, it will be noted $\xi_i = H_{ii}$. Whereas if $j \neq i$, the term represents the hopping parameter. Then we have the second assumption which states that this hopping is restricted to the nearest neighboring sites. Which means that if the lattice is one-dimensional, we have

$$H_{i,i+1} \neq 0\ et\ H_{i,i+l} = 0\ \forall l \geq 2\ \forall i$$

So, we denote

$$-J_i \equiv H_{i,i+1} = \int dx\ \phi_i^*(x) \left(\frac{-\hbar^2}{2m} \frac{\partial^2}{\partial x^2} + V(x,t) \right) \phi_{i+1}(x) \tag{2.32}$$

Next, we assume that the two-body interaction is restricted to particles at the same site. Meaning that non-local interactions are neglected

$$U_{ijkl} \neq 0 \Leftrightarrow i = j = k = l$$

Thus, if we consider a dilute gas of ultracold atoms, then the interaction can be modeled by a contact potential as (2.14), we have

$$U_i \equiv U_{iiii} = g_{1D} \int dx\ |\phi_i(x)|^4 \tag{2.33}$$

Then, we obtain the Bose-Hubbard Hamiltonian

$$\hat{H} = -\sum_{l=1}^{N_s} J_l(\hat{a}_l^\dagger \hat{a}_{l+1} + \hat{a}_{l+1}^\dagger \hat{a}_l) + \frac{1}{2} \sum_{l=1}^{N_s} U_l \hat{a}_l^\dagger \hat{a}_l^\dagger \hat{a}_l \hat{a}_l + \sum_{l=1}^{N_s} \xi_l \hat{a}_l^\dagger \hat{a}_l \tag{2.34}$$

In the case of a periodic boundary conditions, we have $\hat{a}_{N_s+1} = \hat{a}_1$.

In our case, $N_s = 2$, and thus the hopping matrix only have one element, denoted as J. Furthermore, as our system is a time crystal, we have a perfect symmetry of the potential wells, and thus, we can assume $\xi_1 = \xi_2 \equiv \xi$ and $U_1 = U_2 \equiv U$. And then,

$$\hat{H} = -J(\hat{a}_1^\dagger \hat{a}_2 + \hat{a}_2^\dagger \hat{a}_1) + \frac{1}{2}\sum_{l=1}^{2} U \hat{a}_l^\dagger \hat{a}_l^\dagger \hat{a}_l \hat{a}_l + \sum_{l=1}^{2} \xi \hat{a}_l^\dagger \hat{a}_l \tag{2.35}$$

Our goal is to obtain the form of this Hamiltonian, because, as we will see, a straightforward diagonalization of its resulting form yields a first quantitative prediction for the collective tunneling time. We must calculate the effective hopping matrix element and the atom-atom interaction parameter of this model for our two quasimodes.

The hopping between the two potential wells is determined by the splitting of the eigenvalues corresponding to the two states localized on the resonances.

Indeed, as we have seen, the eigenvalues of our system are obtained through Floquet calculations corresponding to the Hamiltonian (1.1), which describes the dynamics of the condensate in the ring. This amounts, in our model (2.35), to diagonalizing the matrix

$$\mathscr{M} = \begin{pmatrix} \xi & -J \\ -J & \xi \end{pmatrix} \tag{2.36}$$

Where, in order to determine the value of J, we assume that the atom-atom interaction U is zero, essentially treating the system as if it contained only a single particle.
The eigenvalues of this matrix are obtained by finding the roots of its characteristic polynomial

$$\det(\mathscr{M} - \lambda I) = 0 \tag{2.37}$$

$$\Leftrightarrow \det \begin{pmatrix} \xi - \lambda & -J \\ -J & \xi - \lambda \end{pmatrix} = 0$$

$$\Leftrightarrow (\xi - \lambda)^2 - J^2 = 0 \;\Leftrightarrow (\xi - \lambda)^2 = J^2$$

$$(\xi - \lambda) = \pm J$$

We then have two distinct solutions, which we denote as λ_1 and λ_2

$$\lambda_1 = \xi + J \;,\; \lambda_2 = \xi - J \tag{2.38}$$

And thus, the splitting between these two eigenvalues is

$$|\lambda_2 - \lambda_1| = |2J| \tag{2.39}$$

Next, we aim to calculate the effective atom-atom interaction parameter. As mentioned earlier, this parameter is equivalent on both sites, so we can calculate it for either one without loss of generality. For instance, let's compute U for the quasimode $\phi_1(x)$. We have,

$$U = g_{1D} \int dx \; |\phi_1(x)|^4 \tag{2.40}$$

with g_{1D} the coefficient that describes the interaction for one dimension. However, we don't know its expression, so we have to determine it. To do this, let's go back to the three-dimensional problem, as we know the form of g in this case, we have

$$U = g \int d^3r \ |\phi_1(\mathbf{r})|^4 \tag{2.41}$$

But, as we have seen in the previous section, $\phi_1(\mathbf{r})$ can be decomposed as $\phi_1(\mathbf{r}) = \phi_{1,\perp}(y,z)\phi_1(x)$ with

$$\phi_{0,\perp} = \frac{1}{\sqrt{\pi}\sigma_\perp} e^{\frac{-y^2}{2\sigma_\perp^2}} e^{\frac{-z^2}{2\sigma_\perp^2}} \tag{2.42}$$

Hence, the interaction parameter is

$$U = g \int dx \ |\phi_1(x)|^4 \int dy \ dz \ |\phi_{0,\perp}(y,z)|^4 \tag{2.43}$$

We can then calculate the second integral of this expression by injecting (2.42) in it. Indeed, this leads us to Poisson integrals for which the solution is well established

$$\int dy \ dz \ |\phi_{0,\perp}(y,z)|^4 = \frac{1}{\pi^2\sigma_\perp^4} \int dy \ e^{\frac{-2y^2}{\sigma_\perp^2}} \int dz \ e^{\frac{-2z^2}{\sigma_\perp^2}} \tag{2.44}$$

$$= \frac{1}{\pi^2\sigma_\perp^4} \frac{\sqrt{\pi}\sigma_\perp}{\sqrt{2}} \frac{\sqrt{\pi}\sigma_\perp}{\sqrt{2}} = \frac{1}{2\pi\sigma_\perp^2} \tag{2.45}$$

Then, remembering the form of g and $\sigma_\perp$, we find the final form of the one-dimensional atom-atom interaction

$$U = \frac{4\pi\hbar^2 a_s}{m} \frac{m\omega_\perp}{2\pi\hbar} \int dx \ |\phi_1(x)|^4 = 2\hbar\omega_\perp a_s \int dx \ |\phi_1(x)|^4 \tag{2.46}$$

And,

$$g_{1D} = 2\hbar\omega_\perp a_s \tag{2.47}$$

Thus, to calculate the effective atom-atom interaction parameter, along with the frequency of the transverse trap potential and the s-wave scattering length of the atomic species considered, we need informations about the spatial localization of one of the state of the single-particle basis corresponding to one of the two resonances.

Let us also note that, as you may have noticed, the computation of these two parameters can be done within the one-particle formalism. Indeed, when computing the hopping, the interaction is considered null, and in the computation of the interaction parameter, we only need the one-particle basis states. And, once these parameters are calculated, we obtain, as wanted, the form of the effective two-sites Bose-Hubbard Hamiltonian. Then, when still considering a single particle, the hopping parameter (2.39) that we have already calculated corresponds to the tunneling rate we are looking for.
However, this scenario changes when dealing with N particles. In this case, we turn to the Fock space where the states are labeled $|n_1, n_2\rangle$ with n_1 and $n_2 = N - n_1$ being the occupation numbers of the quasimodes [59]. The Fock space is then the space whose basis is formed by all these states, so that for N particles, this space has a $N+1$ dimension. Neglecting the on-site energy ξ, the matrix elements of the Bose-Hubbard Hamiltonian, in this basis, are then given by

$$\begin{aligned}\langle n_1, n_2 | \hat{H} | n_1', n_2' \rangle = -J \left[\sqrt{n_2'(n_1'+1)}\delta_{n_1,n_1'+1}\delta_{n_2,n_2'-1} + \sqrt{n_1'(n_2'+1)}\delta_{n_1,n_1'-1}\delta_{n_2,n_2'+1} \right] \\ + \frac{1}{2}U \left[n_1'(n_1'+1)\delta_{n_1,n_1'}\delta_{n_2,n_2'} + n_2'(n_2'+1)\delta_{n_1,n_1'}\delta_{n_2,n_2'} \right]\end{aligned} \tag{2.48}$$

If we assume an even number of particle N, the middle element corresponds to $\langle N/2, N/2| \hat{H} |N/2, N/2\rangle$, and the form of the Bose-Hubbard Hamiltonian in this case is then,

$$\hat{H} = \begin{pmatrix} \ddots & \vdots & \vdots & \vdots & \\ \cdots & \frac{1}{2}U(\frac{N^2}{2}+N+2) & -J\sqrt{\frac{N}{2}(\frac{N}{2}+1)} & \cdots & \cdots \\ \cdots & -J\sqrt{\frac{N}{2}(\frac{N}{2}+1)} & \frac{1}{2}UN(\frac{N}{2}+1) & -J\sqrt{\frac{N}{2}(\frac{N}{2}+1)} & \cdots \\ \cdots & \cdots & -J\sqrt{\frac{N}{2}(\frac{N}{2}+1)} & \frac{1}{2}U(\frac{N^2}{2}+N+2) & \cdots \\ & \vdots & \vdots & \vdots & \ddots \end{pmatrix} \tag{2.49}$$

It is a tridiagonal matrix, with coupling terms that couple the states $|N-n, n\rangle$ and $|N-(n+1), n+1\rangle$, $\forall n \in \{0, ..., N\}$, which is the coupling represented by the hopping parameter calculated earlier (2.39). However, the process of interest in this work is the collective tunneling experienced by the N particles forming the condensate. Therefore, we need the splitting between the energies of the states $|N, 0\rangle$ and $|0, N\rangle$. This is easily obtained from expression (2.49). Indeed, by diagonalizing this matrix, we obtain the eigenvalues and eigenvectors related to the different Fock states, allowing us to directly calculate the difference between the eigenvalues of the two state of interest.

So, in summary, in order to get the tunneling rate we need to calculate these two parameters, (2.39) and (2.40), before diagonalizing the resulting Bose-Hubbard Hamiltonian matrix. It is these calculations that will occupy us in the practical part of this work.

2.5 Time cristals

In the quantum description we know that it will be possible to find localized wave packets moving along one of the periodic orbits of the nonlinear resonances without spreading. We also know that the quantum objects corresponding to this kind of wave packet are Floquet states but, due to the perfect symmetry between our two islands, a single wave packet prepared on one of these cannot form a Floquet state.

To understand this observation, let's consider the absence of interaction between the particles constituting our condensate. In this case, we have a single-particle problem. The invariant tori that appear are distinct duplicates of the same structure, connected by a symmetry relation given the way they are defined by the Poincaré-Birkhoff theorem [12]. Thus, the energy levels corresponding to these islands are quasi-degenerate doublets, separated by a value $\hbar w/2 + J$ where J is the tunneling rate [14]. So, after a time $\hbar/J$, a wave packet prepared on one of the islands will tunnel to the position of the missing wave packet. This situation is therefore not stable, and the periodic solutions in time must be a superposition of the two wave packets propagating along the periodic orbits that exchange their position after a period T. Two wave packets can form two different orthogonal superposition, and thus, we have two such Floquet states.
Another way to understand the existence of solutions in the form of a superposition is that a wave packet prepared along one of the classical resonance orbits with a period twice as long as the period T of the Floquet states, which has the same period as the Hamiltonian by definition. While with a superposition of such two wave packets moving with a period $2T$, we find again the period T of the system. The recovery of this period with the superposition is clearly visible when studying properties of the system such as the temporal evolution of the condensate position in the ring trap or the probability density of measuring a particle as shown in the figures Fig. 2.6

and Fig. 2.7.

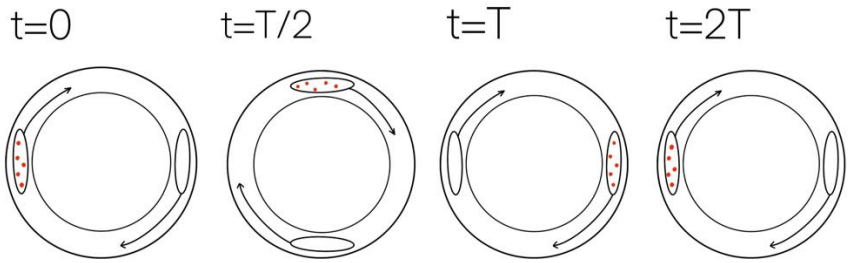

(a)

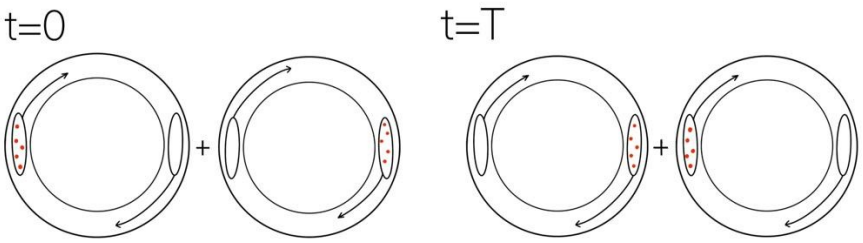

(b)

Figure 2.6: The periodic behaviour over time of the ring trap configurations when we have (a) a wave packet prepared on one of the resonance islands or (b) the superposition. It can be seen that in the latter case, the motion is periodic of period T, whereas a single wave packet prepared on one of the two islands has a periodic motion of double period.

However, interactions between particles cannot be neglected in a Bose-Einstein condensate, and the single-particle problem formalism is not applicable. In the mean-field approximation, all atoms occupy the same single-particle wave function, which is a solution of the Gross-Pitaevskii equation (2.21), as we have just discussed. We then use the Fock formalism [59], which allows us to coherently describe quantum states involving N particles. In this formalism, the states are denoted $|n_1, n_1\rangle$ where n_1 and $n_2 = N - n_1$ are the numbers of particles occupying the states corresponding to the resonance islands.
Considering the two mode approximation made earlier, and that the eigenstates of the Hamiltonian corresponding to the many-body Floquet states must also respect the symmetry of this Hamiltonian, the mean field approximation doesn't accurately describe our situation, and the many-body state is given by the NOON state [8, 61, 5]

$$|\psi\rangle = \frac{|N, 0\rangle + |0, N\rangle}{\sqrt{2}} \tag{2.50}$$

By representing the two resonance islands as a double-well potential, the various possible configurations of our system are depicted in Fig. 2.8. A wave packet prepared on one of the two islands alone is shown in Fig. 2.8a and Fig. 2.8b, while the NOON superposition can be visualized as depicted in Fig. 2.8c.

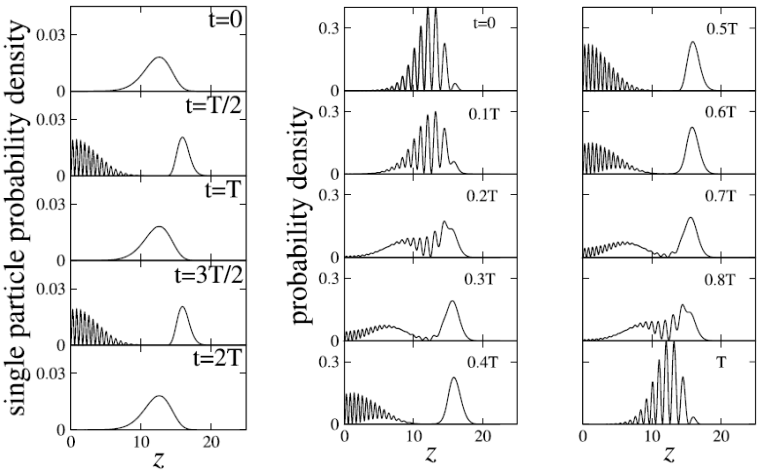

(a) (b)

Figure 2.7: These graphs from ref. [60] show the periodic behaviour of the probability density in the case of (a) a wave packet prepared on one of the resonance islands or (b) the superposition. These measurements are made in the frame of an atom bouncing on an oscillating mirror. In (a) we can clearly see the periodic behaviour of period $2T$ while the behaviour of period T is recover in the case of the superposition (b).

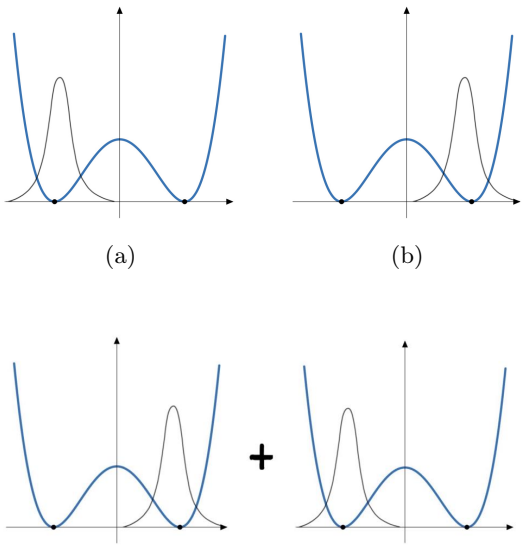

(a) (b)

(c)

Figure 2.8: Visualization in a double-well potential of (a)-(b) a wave packet prepared on one of the resonance islands and (c) of the NOON superposition of two wave packets prepared each on one of the regular islands

However, the experimental preparation of this state that reflects the symmetry of the system is very complicated because it involves preparing a macroscopic superposition of two Bose-Einstein condensates each localized in different potential wells. It requires a perfectly equal distribution of the number of particles between these wells, and the loss of a particle is enough to break the symmetry and for the remaining particles to accumulate in one of the two wells. And thus, for example, the measurement of a particle in one of the two states of the NOON-superposition (2.50) leads to the collapse of the other quantum states into the same state [60][14]. It is then said that the symmetry of the system is broken. More precisely, we speak of spontaneous breaking of temporal translation symmetry τ. Therefore, because of our classical view of things, we actually observe only these states that break this τ symmetry. The system is then what is called a discrete time crystal.

Before explaining what a discrete time crystal is and what is meant by spontaneous symmetry breaking, let us note that after the collapse of the system into one of the two states, $|N,0\rangle$ or $|0,N\rangle$, the system is robust to other measurements and other perturbations. It evolves in time with the period $2T$ [14].
Indeed, taking into account the interaction among the condensate particles, the chemical potential of the well in which all the condensate atoms have collapsed is altered by the value of this interaction. As a result, if the interaction is large enough ($U > J$), the chemical potentials of the two wells are no longer equal and the atoms of the condensate will no longer tunnel individually towards the other resonance. The sequential tunneling observed earlier and occurring at intervals of $\hbar/J$, is suppressed, this is known as quantum self-trapping.
However, in the real many-body dynamics of the system, this trapping phenomenon is "overruled" and the condensate will still tunnel from one resonance to the other, but only if all the particles tunnel together leading to a collective tunnel, and this phenomenon is very slow [48, 9].

2.5.1 Definition and spontaneous symmetry breaking

So, what is a time crystals ? The notion of solid crystal is well known; structures in which constituent atoms follow a regular arrangement in space, due to the mutual interactions between these atoms that then reorganize into a periodic structure. In 2012, F.Wilczek wondered whether a similar structure could exist in the time domain [62]. In other words, is it conceivable to have a structure that exhibits a repetitive pattern not in space, but in time ? However, this notion seems somewhat problematic, as systems with temporal periodicity are not entirely new. We can mention, for example, the Earth, which regains its orientation every 24 hours, pendulum clocks, and many other. It is then necessary to note that in reality, as F.Wilczek says in [63]: "*if it is the symmetries that are at the origin of the aesthetic character of crystals, it is the lack of symmetry in the mathematical sense of these objects that defines them in the eyes of physicists*". Returning to the familiar case of solid crystals, the self-organization of atoms during their formation is a quantum phenomenon tied to the spontaneous breaking of translation symmetry in space [64]. When a liquid or gas cools to form a crystal, the resulting solution, derived from the laws of physics, describe a crystal with less symmetry than the laws themselves. Let's consider the solid state Hamiltonian

$$\hat{H} = \sum_{i=1}^{N} \frac{\hat{\mathbf{p}}_\mathbf{i}^{\,\mathbf{2}}}{2m_i} + \frac{1}{2}\sum_{i\neq j}^{N} U_{ij}(\mathbf{r_i} - \mathbf{r_j}) \tag{2.51}$$

Which describes N particles interacting within a finite volume with periodic boundary conditions. A periodic state in space cannot be the ground state of this many-body system because it

would break the spatial translation symmetry. Indeed, we see that if we shift all atom positions $\mathbf{r_i}$ by the same vector $\mathbf{R}$, the expression (2.51) does not change given that it depends only on the relative distance between these atoms. This indicates that the system possesses a continuous spatial translation symmetry. Formally, a system possesses a symmetry when the operator $\hat{\mathscr{T}}$ associated with this symmetry commutes with the Hamiltonian, $[\hat{H}, \hat{\mathscr{T}}] = 0$, implying that the eigenstates $\psi_n(\mathbf{r_1}, ..., \mathbf{r_N})$ of $\hat{H}$ are also the eigenstates of $\hat{\mathscr{T}}$. Therefore, the eigenstates of the system must reflect the same symmetry as the system itself, or equivalently, the probability density of the measurement of a single particle, ρ_1, must be uniform in space if the system is prepared in the ground state. That is to say, we must have for a crystal of N atoms

$$\begin{aligned}\rho_1(\mathbf{r_1} + \mathbf{R}) &= \int d(\mathbf{r_2} + \mathbf{R})...d(\mathbf{r_N} + \mathbf{R})|\psi_n(\mathbf{r_1} + \mathbf{R}, ..., \mathbf{r_N} + \mathbf{R})|^2 \\ &= \int d\mathbf{r_2}...d\mathbf{r_N}|\psi_n(\mathbf{r_1}, ..., \mathbf{r_N})|^2 = \rho_1(\mathbf{r_1})\end{aligned} \tag{2.52}$$

Nonetheless, when observing the system defined by Hamiltonian (2.51), we see a periodic crystalline structure in space. The states corresponding to this structure no longer possess continuous translation symmetry. To reproduce the same structure, we cannot translate atom positions by any vector $\mathbf{R}$ but only by a vector whose norm is equal to the distance between the atoms $\mathbf{d}$, as illustrated in Fig. 2.9. Consequently, the crystal has a reduced degree of spatial translation symmetry. And if this structure is visible while ρ_1 must be uniform in space, it is because the two-point correlation function,

$$\rho_2(\mathbf{r_1}, \mathbf{r_2}) = \int d\mathbf{r_3}...d\mathbf{r_N}|\psi_n(\mathbf{r_1}, ...\mathbf{r_N})|^2 \tag{2.53}$$

is not necessarily uniform [60]. Moreover, it represents the probability of finding a particle at a position $\mathbf{r_2}$ given that a first particle has been detected at a given position $\mathbf{r_1}$. So, if ρ_2 displays periodic behavior of $\mathbf{r_2}$ for a fixed $\mathbf{r_1}$, it indicates a crystalline structure. Therefore, the measurement of a single particle allows us to detect this periodic organization[3]. That is why we say that the symmetry breaking is spontaneous.

In summary, spontaneous symmetry breaking, characteristic of crystalline structures, occurs when the equations describing a system possess a certain symmetry, yet the system spontaneously chooses a solution that breaks this symmetry. This effect is manifested through a vulnerability of the eigenstates of exact symmetry to weak perturbations, such as measurements or coupling with the environment [64]. Consequently, a time crystal, as conceived by Wilczek, is a time-independent system that spontaneously adopts periodic motion in time, even in its lowest state. That is to say, it is a system in which temporal translation symmetry is broken [62].

Temporal translation symmetry τ is undeniably one of the most fundamental symmetries, as it expresses the principle that a system's physical properties remain unchanged when the direction of time is reversed. Hence, for instance, a many-body time-independent system[4] possesses this continuous symmetry if, when prepared in an eigenstate $|\psi_n\rangle$ of energy E_n, the probability density of detecting particles at a fixed position in configuration space remains constant over time. And, according to Noether's theorem, which states that for every symmetry there corresponds a conserved quantity, τ corresponds to the conservation of energy. So, when this symmetry is broken, energy is no longer conserved and ceases to be a useful characteristic in describing the

[3] Because it provides us with information on the spatial distribution of the other particles in the system

[4] All time-independent systems possess continuous temporal translation symmetry

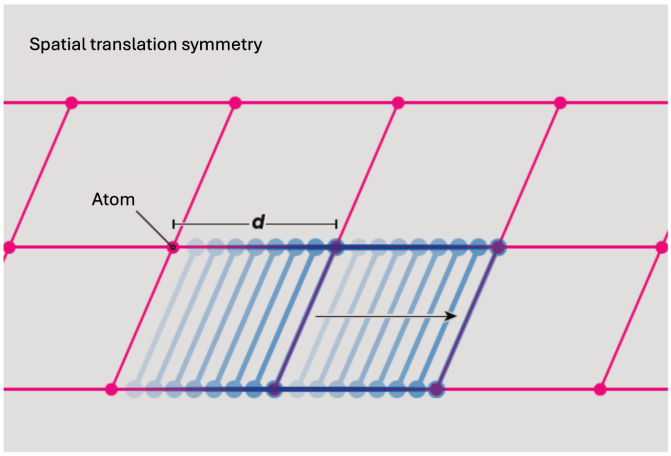

Figure 2.9: Illustration of the spatial translational symmetry of a two-dimensional crystal from the ref [63]. The atoms represented by the pink dots are spaced by a distance d, so if we translate the atoms by a vector other than **d**, we do not find the pink structure but we find ourselves in the situations represented by the blue lines

system.

Thus, the experimental observation of a many-body time-independent system, prepared in its ground state, being able to transition to periodic motion over time under the influence of a weak perturbation, would manifest as periodic behavior in the probability density of measuring the system at a fixed point in configuration space over time. In this case, temporal translation symmetry is said to be discrete. More formal definitions of time crystals can be found in [65] and [66]. The theoretical realization of systems exhibiting this property has been demonstrated in numerous articles. For example, in [16] it is shown that a classical system can reveal periodic motion in the lowest-energy state, while in the article [62] the idea of quantum time crystal is presented. In this latter work, Wilczek considers N bosons interacting attractively in a ring in the presence of a magnetic flux α, called an Aharonov-Bohm ring, whose Hamiltonian thus possesses continuous temporal translation symmetry. He then predicts that for an appropriate value of the flux α, the particle density will exhibit periodic motion along the ring, persisting indefinitely as $N \to \infty$. Other configurations yielding similar results have been considered, such as in [67] where Li and his colleagues propose to examine ions in a ring, under conditions where the ions'kinetic energy is significantly lower than the Coulomb potential energy between them.

Nevertheless, P. Bruno quickly demonstrated that under fairly general conditions, the spontaneous breaking of continuous temporal translation symmetry is not possible in a time-independent system prepared in the ground state [68], a result later reaffirmed in [69]. However, it has been shown that this spontaneous breaking can be observed when a time-independent many-body system is prepared in an excited eigenstate [70]. We will not elaborate on this possibility, as another avenue, inspired by Wilczek's idea, captures our attention.

2.5.2 Discrete Time Crystal

After the realization that the time crystals originally envisioned by Wilczek were not a realistic concept, a revised version of these crystals was proposed by Sacha in 2015 [14], known as discrete

or Floquet time crystals. While it is not possible for a system prepared in its ground state to transition from continuous τ symmetry to discrete τ symmetry, the question arose; would it be possible to transition from a discrete τ symmetry to another discrete τ symmetry with a different period ? The periodically driven systems, which have captivated our interest since the beginning of this work, are systems possessing a discrete τ symmetry. Sacha then posed the question of whether a periodically driven many-body system, prepared in a Floquet state, could spontaneously reorganize over time and evolve with a period distinct from that of the driving. He then demonstrated, using a setup involving ultra-cold atoms bouncing off an oscillating mirror in the presence of the gravitational field, that such a transition is indeed possible [14]. Other methods for creating these discrete temporal crystals have been proposed in driven spin systems [71], and the existence of this crystallization phenomenon in the time domain has been experimentally validated in [72] where researchers succeeded in creating one in their laboratory[5]. The three different types of temporal translation symmetry that we consider are shown in Fig 2.10.

Therefore, despite the expectation that a periodically driven system in its steady state would synchronize with the external driving, it turns out that, owing to the mutual interactions among particles, the system prefers to follow a periodic motion with a period different from that of the driving. This phenomena defines discrete temporal crystals and corresponds to the situation of our system described earlier.

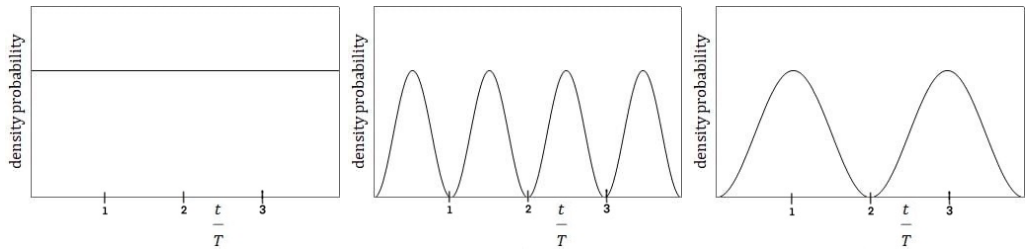

(a) (b) (c)

Figure 2.10: Probability density plot as a function of time t/T, where T is the period of the driving, to represent the temporal translation symmetry τ in three cases: (a) continuous, (b) discrete with the period of the driving T, and (c) discrete with a different period than that of the driving.

As a result, we observe a broken symmetry state $|N, 0\rangle$ moving periodically along a 2:1 resonance orbit. This state will still be able to tunnel to the other resonance island, but at a significantly slower pace as we explained earlier. This process constitutes the focus of our investigation and is the subject of the next Chapter. Hence, more than generating chaos in our system as we have seen in the first Chapter, the periodic perturbation $\delta \cos \omega_0 t$ allows the formation of a discrete temporal crystal. Although it is similar to a static double-well potential configuration, it provides an optimal arrangement for studying the dynamic tunneling effect of our Bose-Einstein condensate. The perfect symmetry of the regular islands is an intrinsic property of such a system, and its maintenance is essential for studying this phenomenon, which is not trivial in the case of the static double-well.

[5]Such systems can also exhibit solid-state phenomena in the time domain[60]

Chapter 3

Dynamical tunneling

As a reminder, the objective of this work is to calculate the tunneling rate of our condensate when it is prepared on one of the resonance islands. In this case, as we have explained earlier, due to the interactions between the particles of this condensate, we are in a self-trapping regime where the sequential tunneling of individual atoms is suppressed. However, the entire condensate can undergo what is called collective tunneling to the other island. This chapter therefore focuses in more detail on the study of this collective tunneling. We have already explained in Section 2.4 how we will practically be able to calculate the corresponding tunneling rate for this phenomenon, the purpose of this chapter is not to provide another explanation but rather to give a theoretical view of what happens concretely during this phenomenon.

Tunneling is one of the most remarkable implications of quantum theory. It is often introduced as the ability of a quantum particle to penetrate an energy barrier, whereas such penetration is completely prohibited classically. In other words, in quantum theory, there is a nonzero probability of detecting the quantum particle on the other side of a classical barrier, owing to the evanescent components of its wave function. However, this concept can be generalized to all sorts of transitions that are classically forbidden in phase space, not only through static potential barriers, but also through dynamic barriers formed by other constraints of the underlying classical dynamics. This is what is then referred to as "*dynamical tunneling*" [73, 74]. This generalization allows for a deeper understanding of this process, enabling its extension to multi-dimensional cases, in which the presence of a potential barrier to separate phase space is not particularly evident. For example, in our case, it is the resonance islands that play the role of the dynamical barriers. As we have seen in the previous chapters, these resonances represent regular motion, and therefore, classically speaking, a trajectory starting in their vicinity will remain confined nearby.

Thus, tunneling refers to the quantum processes that are classically forbidden, and two types can be distinguished, barrier tunneling and dynamical tunneling. Despite its fundamentally quantum nature, this concept is characterized in a semiclassical framework, as the quantum system behaves according to quantum theory, and labeling what occurs as tunneling can only be done in comparison to the classical counterpart. Furthermore, it will be seen that again despite its purely quantum nature, tunneling is also strongly affected by the structure of the phase space of the underlying classical dynamics [75]. For example, the presence of chaos and nonlinear resonances in this space can significantly increase the tunneling rate. This is exactly what will happen in our case.

Indeed, due to interactions between the condensate particles, the tunneling we want to observe is actually very slow, even too slow compared to the lifetime of a Bose-Einstein condensate in such a situation. Fortunately for us, the presence of nonlinear resonances and chaotic sea among them will significantly accelerate this phenomenon. The mechanisms associated with these accelerations are respectively called resonance-assisted tunneling [76] and chaos-assisted tunneling [13]. And so, their study will be the subject of this chapter.
Before delving into the explanations related to these processes, we need to introduce the tool of random matrix ensembles that we will need in the formalism of chaos-assisted tunneling. Then, we will also take the time to quickly examine the tunneling rate in integrable systems to understand well the change that will be brought about by the presence of chaos and nonlinear resonances.

3.1 Random matrices ensemble

In Section 1.1, it was explained that one of the distinctive features of quantum chaos is the fluctuation of levels in the system's spectrum, and in 1984, Bohigas, Giannoni, and Schmidt claimed that the energy level fluctuations of a quantum system whose classical counterpart is entirely chaotic correspond to the fluctuations predicted by the theory of random matrix ensembles [21]. This theory aims to study the statistics of energy levels, particularly focusing on the fluctuations in distances between these levels.

In contrast to integrable systems, where energy levels are ordered and predictable, chaotic systems exhibit random fluctuations in their spectral levels. Nevertheless, numerous numerical and empirical observations suggest a universality of these local fluctuations for systems exhibiting global chaos in their classical phase space [77]. Indeed, it has been observed that all Hamiltonian matrices corresponding to such situations, and of sufficiently large dimension, produce the same spectral fluctuations, provided they have the same group of canonical transformations. In particular, the distribution of splittings between levels generally takes on a characteristic from depending on the canonical group.
It is this universality that forms the basis of random matrix theory. It postulates that Hamiltonian matrices of chaotic systems can be modeled by ensembles of random matrices, characterized by specific distributions of resulting energy levels, which are then determined by the properties and symmetries of the system. Furthermore, the conjecture by Bohigas, Giannoni, and Schmidt suggests that all such matrices follow Gaussian distributions. Moreover, symmetries further constrain the ensembles that model them, without needing to know too much about the system. Thus, there exist three universality classes of random matrix ensembles :

- Gaussian Orthogonal Ensembles (GOE), if the system is invariant under time reversal, represented by the time reversal operator $\hat{T}$. This means that the Hamiltonian commutes with $\hat{T}$ and so, that it is a real symmetric matrix. Therefore, it is invariant under orthogonal transformation.

- Gaussian Unitary Ensembles (GUE), if the system is not invariant under a time reversal transformation $\hat{T}$. In this case, $\hat{H}$ corresponds to a complex Hermitian matrix and thus is invariant under all unitary basis transformations.

- Gaussian Symplectic Ensembles (GSE), if the system is again invariant under a time reversal transformation $\hat{T}$, but specifically with $\hat{T} = -1$. In this case, all levels are doubly

degenerate, and $\hat{H}$ is invariant under basis transformations represented by unitary simplectic matrices.

One important result of this theory is that each of these universality classes exhibits a specific distribution of the distance between neighboring energy levels s, and these three distributions are quite distinct from the integrable case, which by analogy is often described by *Poissonian* matrix ensembles [22].

$$P(s) = \begin{cases} e^{-s} & integrable \\ s\frac{\pi}{2}e^{-s^2\frac{\pi}{4}} & GOE \\ s^2\frac{32}{\pi}e^{-s^2\frac{4}{\pi}} & GUE \\ s^3\frac{2^18}{3^6\pi^3}e^{-s^2\frac{64}{9\pi}} & GSE \end{cases} \tag{3.1}$$

In summary, random matrix ensemble theory amounts to representing the system by matrices whose elements are randomly chosen while preserving the symmetric structure of the said system. Moreover, it is then convenient to perform what is called a random matrix average on the eigenvectors and eigenvalues of all the matrices of the ensemble chosen to model the system, for example, in order to study the overall statistical properties of the spectrum. That is, statistical averages of results are calculated for all matrices in the ensemble to capture general trends and obtain meaningful values to work with.

This conjecture will then be useful in the case of our mixed system to model the chaotic sea surrounding our regular islands. Here, we have simply introduced the tool represented by this theory, but more information can be found in [22, 19, 20].

3.2 Tunneling rate in integrable systems

Here, we will quickly examine the form taken by the tunneling rate when the system under consideration is integrable. Indeed, this tangent seems interesting as it will allow us to clearly see the change in behavior of this tunneling rate when the non-integrable perturbation is added to the system. Note then that we will not detail the calculations since only the results interests us, we will follow the same reasoning as in references [76, 78].

Thus, in the integrable case, we know that the phase space is formed by tori. Two of these tori symmetrically related are not necessarily connected in phase space. And so, if the initial conditions are chosen on one of the tori, the time evolution will never reach the other torus. However, to solve this problem one can perform an analytical continuation of the canonical variables in the complex plane. Indeed, if we represent the tori with the action-angle coordinates (I, θ), then the tori corresponding to the action I_n are described by $(q_L(I_n, \theta), p_L(I_n, \theta))$ and $(q_R(I_n, \theta), p_R(I_n, \theta))$, where p and q are the position and momentum variables, and the indices L and R distinguish the two tori. Then in this case, it is possible to show that the analytical continuations of these tori are indeed the same manifold when θ can take complex values. We thus have an imaginary path connecting the two symmetrically connected tori, and we can therefore calculate the tunneling rate between them. The energy splitting is given by

$$\Delta E = \frac{\hbar}{T}\exp\Big(-\frac{\sigma}{\hbar}\Big) \tag{3.2}$$

Where T is the classical period of the torus and σ is the action integral of the analytical continuation

$$\sigma = \mathrm{Im}\left[\int_{\Gamma_k \to \Gamma_k'} p\ dq\right] \tag{3.3}$$

We then observe that, in an integrable system, the tunneling rate exhibits an exponentially decreasing behavior in $1/\hbar$. This also implies that in the classical limit, this tunneling effect disappears.

This approach of analytical continuation no longer work as soon as a non-integrable perturbation is added, even if it is relatively weak. Indeed, as we saw in the previous chapter, in this case, invariant tori still exist by virtue of KAM's theorem, but their analytical continuations in the complex plane will not intersect. And, numerous numerical calculations in the early 90s [13, 79] showed that the tunneling splitting in non-integrable systems is greatly increased compared to the integrable case. The smooth exponential behavior in $1/\hbar$ is no longer visible, the splitting ΔE in this case has a very different $\hbar$ dependence. This difference can then be explained by the presence of nonlinear resonances and/or chaos, for higher perturbation amplitudes, in these systems, which we will explore in the following sections.

3.3 Chaos-assisted tunneling

We start by examining how chaos impacts the tunneling rate. In our system, this mechanism will be dominant and will have the most influence on the tunneling rate, compared to the resonance-assisted tunneling mechanism, which will be the subject of the next section.

At the core of this mechanism is the fact that in mixed systems like the one we're studying in this work, the doublet of localized quasimodes involved in tunneling is no longer isolated in the spectrum. It resonantly interacts with states belonging to the chaotic sea.
Indeed, due to their delocalized nature in phase space, chaotic states typically exhibit significant overlap with the boundaries of regular regions, such as resonance islands. Thus, it's easy to understand that these states can provide a coupling mechanism between the quasimodes localized on the islands. The increase in the tunneling rate in such systems has been understood, by Bohigas *et al.* [12] and Tomsovic *et al.* [13], in terms of an *avoided crossing* between the tunneling pair and a third state associated with the chaotic region. We will see that this three-level model is a simplified representation of the phenomenon, but it's still interesting to begin with its explanation as it provides an initial understanding of the mechanism behind this enhancement.

Therefore, we consider a pair of tunneling states, each localized on one of the regular islands, with respective quasi-energies, which we can denote, for example, as E_r and $E_r + \delta$, where with this notation δ represents the regular tunneling rate. These two states have opposite parity, subsequently, we will assume that E_r is even without any loss of generality. Next, we must also consider a third state in the chaotic region whose associated quasi-energy can be denoted as $E_r + \Delta_c$, where Δ_c is the difference between the regular state and the considered chaotic state of same parity. Indeed, this state also has a parity, an even parity for example. In this configuration, the chaotic state does not interact with the odd-parity quasimode but rather with the even one. It's important that this chaotic state does not have a corresponding state of opposite parity, which can generally be assumed since chaotic states typically do not appear in closely spaced doublets [73].

The Hamiltonian of this simplified situation can be written as

$$H_{\text{eff}} = \begin{pmatrix} E_r + \delta & 0 & 0 \\ 0 & E_r & \beta/2 \\ 0 & \beta/2 & E_r + \Delta_c \end{pmatrix} \tag{3.4}$$

where β represents the coupling between the chaotic state and the regular state of the same parity. Then, these two states undergo an avoided crossing, modifying the effective energy associated with the even-parity regular state. Depending on this modification, the tunneling rate can be increased or decreased. Indeed, if this coupling modifies the effective energy of the regular state so that it exactly matches the energy of the other regular state, the two states of complementary parity involved in the tunneling process will perfectly *cross*, thus completely suppressing the process. Conversely, if the modification increases the energy difference between the regular state coupled to the chaotic state and the energy of the other regular state involved in the process, the tunneling rate between these two states will also increase. There's a strong dependence of the tunneling rate on a parameter.

Another way to visualize this mechanism is to imagine that at each moment, a small part of the condensate localized on one of the quasimodes breaks off and is transferred to the chaotic state. It is then transferred back to the other quasimode, and so on until all the condensate ends up in this other quasimode. This corresponds to an indirect path with multiple steps traversing the chaotic region, in contrast to regular tunneling, which corresponds to a direct path in a single step.

We mentioned earlier that this three-level mechanism is simplified. Indeed, in reality, no chaotic state plays a predominant role over the others. Instead of a three-level mechanism, we have a multilevel mechanism in which multiple chaotic states will couple to regular states. In this case, H_{eff} (3.4) must be modified. The chaotic sea is now modeled by a block in this matrix [75, 80, 81, 82]

$$H_{\text{eff}} = \begin{pmatrix} E^+ & V_{\text{eff}} & & \\ \mathrm{V}_{\text{eff}} & \boxed{\text{chaos}} & & \\ & & & \mathrm{V}_{\text{eff}} \\ & & V_{\text{eff}} & E^- \end{pmatrix} \tag{3.5}$$

where $E^{\pm}$ represents the energy corresponding to regular states and V_{eff} is the effective coupling to the chaotic sea.
Next, since we know that chaotic states interact exclusively with the regular state of the same parity as them, the matrix (3.5) can be separated into its symmetric and antisymmetric parts.

$$H^{\pm}_{\text{eff}} = \begin{pmatrix} E^{\pm} & V_{\text{eff}} & \\ \mathrm{V}_{\text{eff}} & \boxed{\text{chaos}^{\pm}} & \\ & & \end{pmatrix} \tag{3.6}$$

The chaotic blocks can then be adequately modeled by a random matrix from the Gaussian Orthogonal Ensemble (GOE).

$$\boxed{H^{\pm}_{\text{chaos}}} \rightarrow \boxed{GOE}^{\pm} \tag{3.7}$$

Note that the random matrices chosen to model these chaotic blocks of different parity are completely independent. Also, note that the situation where the chaotic sea can be described by a single[1] of these matrices is an idealized situation in which the presence of partial barriers in the chaotic region is neglected. We will remain in this approximation until the end of our explanations, in line with what is done in [13, 83]. However, it seemed important to clarify that in reality, it's not that simple. Generally, the chaotic part of phase space is subdivided into several subregions that are weakly coupled to each other. The partial barriers separating these regions are formed by other resonances. Further details on the role of these barriers can be found in [75].

Returning now to the case where the presence of these barriers is neglected, we have (3.7), and in this case, after a prediagonalization of H_{chaos} giving us the eigenvectors $\phi^{\pm}_j$ and the eigenvalues $\epsilon^{\pm}_j$, the shifts of the energies of the symmetric and antisymmetric states can be found with a first-order perturbative approach

$$E^{\pm} = E_0 + \sum_{j=1}^{N_c} \frac{|v^j_{\text{eff}\pm}|^2}{E_0 - \epsilon^{\pm}_j} \tag{3.8}$$

with $v^j_{\text{eff}\ \pm} = V_{\text{eff}} \left\langle n|\phi^{\pm}_j\right\rangle$, $|n\rangle$ being the regular state.
Then, by taking the random matrix average for the eigenvectors, we obtain $\overline{|\left\langle n|\phi^{\pm}_j\right\rangle|^2} \approx 1/N_c$, $\forall j = 1, ..., N_c$. This demonstrates that none of the chaotic eigenstates is distinguished from the others. Consequently, V_{eff} is independent of j and $v^2_{\text{eff}} = V^2_{\text{eff}}/N_c$. This implies that the chaotic eigenstates are all coupled in the same way on average to $|n\rangle$.
Furthermore, the random matrix average over the eigenvalues ϵ_j gives a Cauchy distribution for the energy shifts, and therefore, also for the splitting $\Delta E_0 = |E^+ - E^-|$, as proven in [83]. We have the probability distribution

$$P(\Delta E_0) = \frac{2}{\pi} \frac{\Delta\overline{E_0}}{(\Delta E_0)^2 + (\Delta\overline{E_0})^2} \tag{3.9}$$

with

$$\Delta\overline{E_0} = \frac{2\pi v^2_{\text{eff}}}{\Delta_c} \tag{3.10}$$

where Δ_c represents the mean level spacing in the chaos at energy E. This distribution is valid for $\Delta E_0 << v_{\text{eff}}$ and presents a cutoff at $\Delta E_0 \approx 2v_{\text{eff}}$ to avoid divergences.

Moreover, tunneling rates are usually studied on a logarithmic scale. Thus, we define our "*mean*" splitting $\langle\Delta E_0\rangle_g$ as the geometric mean of ΔE_0.

$$\langle\Delta E_0\rangle_g = \exp(\langle\ln \Delta E_0\rangle) \tag{3.11}$$

And we obtain [75, 80, 82]

$$\langle\Delta E_0\rangle_g = \Delta\overline{E_0} \tag{3.12}$$

[1] two counting both parities

We can further simplify this expression in our case. Indeed, in periodically driven, the chaotic eigenvalues are distributed over a Floquet block, $\xi < \epsilon_j^{\pm} \leq \hbar\omega + \xi$, with level repulsion related to GOE modeling [22]. Hence, we have

$$\Delta_c = \frac{\hbar\omega}{N_c} \tag{3.13}$$

This yields

$$\langle \Delta E_0 \rangle_g = \frac{2\pi V_{\text{eff}}^2}{N_c} \frac{N_c}{\hbar\omega} = \frac{2\pi V_{\text{eff}}^2}{\hbar\omega} \tag{3.14}$$

Thus, we have the modified expression for the tunneling rate compared to the integrable case (3.2). However, we still lack the form of the effective coupling element V_{eff}, which is necessary to calculate the tunneling rate. It is through the process of resonance-assisted tunneling that we will be able to accomplish this step.

3.4 Resonance-assisted tunneling

We have just seen how the presence of chaos in a system can affect the tunneling rate. However, even in nearly integrable systems, where the non-integrable perturbation isn't strong enough for chaos to emerge, a change in the tunneling rate can be observed [84].

Indeed, the presence of nonlinear resonances alone will lead to an increase in the tunneling rate. We will see that their presence will couple the regular ground states of the islands to excited states within these same islands, a coupling that will increase the tunneling rate to the other island [75].
To understand what happens in this process, Brodier *et al.* [84, 76] developed a quantitative semiclassical theory of near-integrable tunneling with which they succeeded to reproduce the exact quantum splittings. In the context of this work, as this mechanism plays a secondary role in the increase of the tunneling rate, we will not detail all the theoretical steps, but we will summarize the important results. An interested reader can find complete developments of this theory in [76, 75, 80].

Different approximations to describe the dynamics of the system in the resonant islands are made, for example, the first step is to assume that the Hamiltonian can be decompose into an integrable part $H_0(I, \theta)$ and a perturbation $V(I, \theta, t)$, in terms of action-angle variables (I, θ). We won't detail all the other approximations made in this theory, but, they are made to finally find that, in such dynamics, chain-like substructures appear in the resonance islands. And, if we consider the case where our two resonance islands exhibit a predominant resonance r:s, it is then directly possible to find that the perturbation induces a coupling $V_k = \langle n + kr | \hat{H}_{res} | n \rangle$ between the states $|n\rangle$ and $|n + kr\rangle$. The perturbation is decomposed into a Fourier series and V_k are the Fourier components of this series. In this configuration, $|n\rangle$ represents the ground state of the regular island, $|n + kr\rangle$ represents an excited state of this same island with k a positive integer, and $\hat{H}_{res}$ denotes the approximate form of the Hamiltonian. So, in a regular island, the true eigenstate is given by the state $|n\rangle$ plus all the admixtures of this state with the other quasimodes $|n'\rangle$ that satisfy the selection rule $|n' - n| = kr$.
Then, assuming that the perturbation is weak, it is possible, in quantum perturbation theory, to derive the form of the modification of the tunneling rate by the presence of this resonance r:s.

$$\Delta E_n = \sum_{k=0}^{k_c} |\mathscr{A}_{n,n+kr}^{(r:s)}|^2 \Delta E_{n+kr}^{(0)} \tag{3.15}$$

with

$$\mathscr{A}_{n,n+kr}^{(r:s)} = \prod_{j=k}^{k} \frac{\langle n+jr| \hat{H}_{res}^{(r:s)} |n+jr\rangle}{E_n^{(0)} - E_{n+jr}^{(0)} + js\hbar\omega} \tag{3.16}$$

which represents the admixture of the *kr-th* excited state with the unperturbed ground state $|n\rangle$. And in these two expressions, the indicators $^{(0)}$ mean that the unperturbed values of the energies are considered. And finally, k_c is the maximum number of coupled states due to the finite size of the islands. We have

$$k_c = \left[\frac{1}{2}\left(\frac{\text{area of the island}}{2\pi\hbar} - \frac{1}{2}\right)\right] \tag{3.17}$$

where [ ] means that we consider the integer part of this expression. Then, it can be shown that the admixture between the states $|n\rangle$ and $|n'\rangle$ is particularly strong if the resonance r:s is symmetrically located between the two tori associated with the action I_n and $I_{n'}$ of these two involved states, $I_n + I_{n'} \approx 2I_{r:s}$. That is, the unperturbed ground state $|n\rangle$ located at the center of the island will be significantly coupled with an excited state at the border of the regular island. And thus, the coupling will modify the energy associated with state $|n\rangle$ and increase the tunneling rate to the other island.

Now that we have explained in summary the mechanism of tunneling rate enhancement via an r:s resonance, we will see how it can be combined with the chaos-assisted tunneling mechanism. But, before, note that in the semiclassical limit $\hbar \to 0$, this process often involves more than one resonance. We then speak of a multiresonances process, and in this case, the expression for the tunneling rate (3.15) is modified with additional terms. However, we do not consider this case further in the following.

As we have just stated, the two mechanisms that we introduced in these last two sections can be combined [75, 80]. The effective coupling element V_{eff} of expression (3.14) can be calculated using resonance-assisted tunneling. Indeed, we consider that the effective model found to describe this latter process in the vicinity of the resonances can also be extended to the chaotic sea in the near vicinity of the regular islands.
Near the regular-chaotic boundary, the transition between the quasimodes inside and outside the regular region is still dominated by an r:s resonance inside the regular island. Consequently, the "*true*" structure of the effective Hamiltonian that describes the coupling of the ground state $E_0^{\pm}$ to the chaotic sea is given by

$$H_{\text{eff}}^{\pm} = \begin{pmatrix} E_0^{\pm} & V_{r:s}^{(r)} & & & \\ V_{r:s}^{(r)} & \ddots & \ddots & & \\ & \ddots & E_{k_c r}^{\pm} & V_{r:s}^{[(k_c+1)r]} & \\ & & \mathrm{V}_{r:s}^{[(k_c+1)r]} & & \\ & & & \boxed{\text{chaos}^{\pm}} & \end{pmatrix} \tag{3.18}$$

If we assume that the couplings induced by the resonance r:s are mostly described by the lowest non-vanishing Fourier component V_1 of the perturbation, denoted as $V_{r:s}^{(n+r)} = \langle n+r| \hat{H}_{\text{eff}} |n\rangle$.

And where the E_{kr} are the unperturbed eigenenergies of the regular region, and the chaotic block is modeled by a random matrix from the Gaussian orthogonal ensemble (GOE) as explained in the previous section. In this situation, k_{cr} is the last state in the island, the highest unperturbed state that is connected by the resonance r:s to the ground state localized in this island. And then, the effective coupling element V_{eff} between this state and the ground state and the chaotic block of the expression (3.14) is given by

$$V_{\text{eff}} = V_{r:s}^{(k_c+1)r} \prod_{k=1}^{k_c} \frac{V_{r:s}^{(kr)}}{E_0 - E_{kr} + ks\hbar\omega} \tag{3.19}$$

The form of this expression allows us to see that the behavior in $\hbar$ is quite different from (3.2). In general, the tunneling do no longer follow a smooth exponential scaling with $1/\hbar$ as in (3.2), but displays huge fluctuations [80].

Chapter 4

Results

We now have all the necessary keys to study the collective tunneling rate of the Bose-Einstein condensate between the two sites of our time crystal.

Indeed, we have seen that it was possible to obtain it by diagonalizing the Bose-Hubbard Hamiltonian matrix. This matrix has, for a gas of N ultracold atoms, a dimension $N+1$, and its elements in the Fock basis are given by

$$\begin{aligned}\langle n_1, n_2 | \hat{H} | n_1', n_2' \rangle = -J \left[\sqrt{n_2'(n_1'+1)}\delta_{n_1,n_1'+1}\delta_{n_2,n_2'-1} + \sqrt{n_1'(n_2'+1)}\delta_{n_1,n_1'-1}\delta_{n_2,n_2'+1} \right] \\ + \frac{1}{2}U \left[n_1'(n_1'+1)\delta_{n_1,n_1'}\delta_{n_2,n_2'} + n_2'(n_2'+1)\delta_{n_1,n_1'}\delta_{n_2,n_2'} \right]\end{aligned} \tag{4.1}$$

where J is the effective hopping parameter and U is the effective interaction parameter. They are respectively given by

$$J = \frac{|\lambda_2 - \lambda_1|}{2} \tag{4.2}$$

$$U = g_{1D} \int dx \, |\phi_i(x)|^4 \ , \ i = 1, 2 \tag{4.3}$$

where, λ_1 and λ_2 are the quasi-energies associated to the one-particle Floquet states, $\phi_1(x)$ and $\phi_2(x)$, localized on our two resonance island of interest, and g_{1D} is the coefficient that characterizes the interaction (2.47).

So in order to obtain the form of this matrix, we need to calculate these two parameters, and to calculate these two parameters we only have to diagonalize the Floquet matrix corresponding to our system when considering only one particle. Indeed, this diagonalization provides us with all the necessary elements we need to then compute the two parameters of interest, namely the single-particle Floquet states $\{\phi_i(x)\}_{i=1,2}$ localized on resonance islands and the associated quasi-energies, λ_1 and λ_2.

4.1 Phase space parametrization

The first step, before going into these calculations, is to determine the optimal settings of the parameters characterizing this said time crystal, including V which is included by a potential gradient, as well as the amplitude δ and the frequency ω_0 of its periodic modulation. To do this,

we undertake an analysis through stroboscopic Poincaré sections of the classical phase space associated with the motion of a particle in the ring trap subject to a periodic modulation. The corresponding classical Hamiltonian, as we have seen before, is as follows :

$$H(q,p) = \frac{p^2}{2m} - V[1 + \delta\cos(\omega_0 t)]\cos\left(\frac{2\pi q}{L}\right) \tag{4.4}$$

Where q is the position of the particle, p is its momentum, m, the mass of the atomic species concerned, is considered equal to 1 and L is the circumference of the ring which is considered equal to 2π.

Although this step may seem somewhat obsolete, it is of major importance for the continuation of the protocol. Indeed, specific conditions must be met for the tunneling phenomenon to occur as desired in our system. Thus, the optimal parameters should lead us to a mixed regular-chaotic phase space, in which the 2:1 resonance is clearly manifested through a pair of sufficiently large regular islands represented in red in the figure 4.1. Indeed, if the resonance islands are too small, as explained in Section 1.3, it will not be possible thereafter to find in the quantum description a Floquet state localized on them. Another important point is the presence of residual dynamic barriers, or partial barriers. These barriers, which we neglected in the previous chapter, are in fact necessary because they prevent tunneling transitions of the particle between clockwise and counterclockwise rotations, which could lead to atom-atom collisions [85, 12]. We know that these barriers are induced by the presence of additional resonance islands, in our case it is the 3:1 resonances shown in blue in the figure 4.1 that are important and prevent the phenomenon of unwanted tunneling from top to bottom and vice versa.
The appropriate phase space is obtained for the following numerical values of the various parameters :

- $m = 1$
- $V = 1$
- $L = 2\pi$
- $\delta = 2$
- $\hbar\omega = 0.5\ V$ with $\hbar = 0.1\ \sqrt{Vm}L/2\pi$

Note that, for aesthetic reasons, we construct the stroboscopic Poincaré section for times $\omega_0 t = \pi/2 + 2\pi n$, $\forall n \in \mathbb{Z}$, thus making the two islands of the 2:1 resonance more visible in the window of positions ranging from -0.5 to 0.5. It is represented in figure 4.1.

4.2 Floquet matrix and Husimi distributions

Next, we aim to diagonalize the Floquet matrix corresponding to our situation in order to obtain the quasi-energies and Floquet states of the system needed to calculate our parameters J and U. Indeed, we saw in Section 1.2 that this method was more effective than the analytical approaches presented in the same Section. Therefore, as a reminder, the matrix we want to diagonalize takes

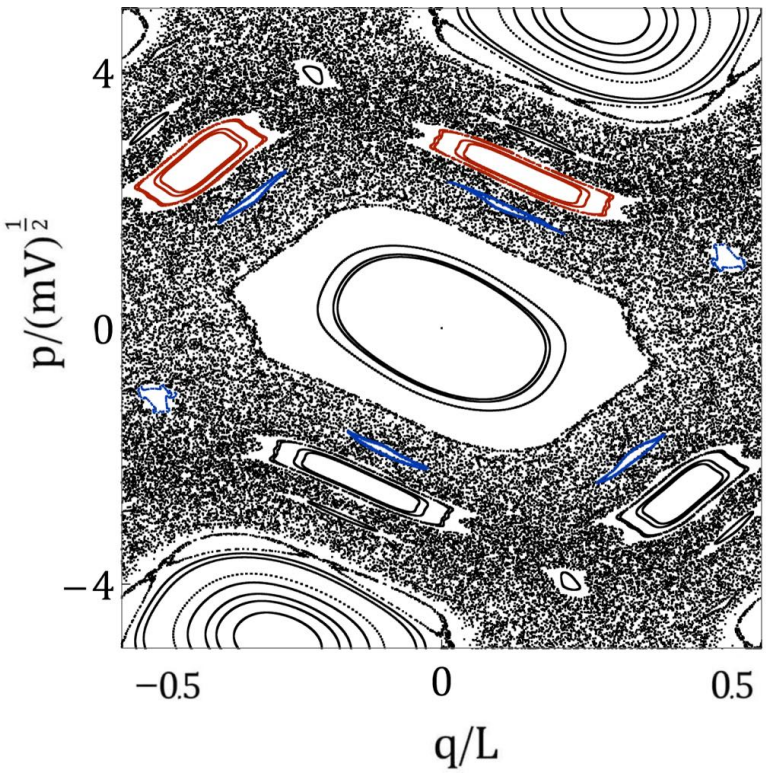

Figure 4.1: Poinacré section for $\omega_0 t = \pi/2 + 2\pi n$, $\forall n \in \mathbb{Z}$, of the classical single-particle dynamics for a promising parameter configuration. Plotted are the position and momentum coordinates q and p, for the model Hamiltonian (4.4) with $\delta = 2$, $\hbar\omega_0 = 0.5\ V$ and $\hbar = 0.1\ \sqrt{VmL}/2\pi$. The 2:1 resonance islands are marked in red. The additional resonance islands that give rise to the necessary residual barriers are the 3:1 resonance islands marked in blue.

the form :

$$\mathscr{M} = \begin{pmatrix} \ddots & \vdots & \vdots & \vdots & \\ \cdots & \hat{H}_0 + \hbar\omega_0 & \frac{1}{2}\hat{H}_1 & \cdots & \cdots \\ \cdots & \frac{1}{2}\hat{H}_1 & \hat{H}_0 & \frac{1}{2}\hat{H}_1 & \cdots \\ \cdots & \cdots & \frac{1}{2}\hat{H}_1 & \hat{H}_0 - \hbar\omega_0 & \cdots \\ & \vdots & \vdots & \vdots & \ddots \end{pmatrix} \tag{4.5}$$

Where, $\hat{H}_0 = \hat{p}^2/2m - V\cos(2\pi\hat{q}/L)$ and $\hat{H}_1 = V\delta\cos(2\pi\hat{q}/L)$. In our case, we perform this diagonalization for 50 Floquet blocks and 100×100 matrix elements in the momentum basis within these blocks. We thus have a 5000×5000 matrix elements and in the following, we note $d = \dim \hat{H}_0 = 100$ and f the number of Floquet blocks, $f = 50$. The details of this method have been extensively discussed in the Section 1.2.1.
At the end of this operation, we obtain the quasi-energies and Floquet states of the system. To be precise, at the end of this diagonalization, we obtain eigenvectors of 5000 elements, and we

must then calculate the Floquet states $|\psi_n(t)\rangle$ corresponding to these eigenvectors. We have

$$|\psi_n(t)\rangle = \sum_{l=-25}^{24} \left|\widetilde{\psi}_{n,l}\right\rangle e^{-il\omega_0 t} \tag{4.6}$$

Note that, given the periodicity of the Floquet spectrum, it is not necessary to perform these calculations for all the eigenvectors of the matrix (4.5). Indeed, it is sufficient to choose a suitable interval and to restrict the study to the d states within this interval. To choose this interval we directly look at the classical phase space, we calculate the average momentum of the unperturbed torus, which will transform into these two resonance islands, and then calculate the energy associated with this momentum. By looking at the mixed phase space in Fig. 4.2, constructed for $\omega_0 t = 0 + 2\pi n$, $\forall n \in \mathbb{Z}$, we can see that the two regular islands of interest seem to correspond to a momentum $p = 2.4$. We then average the momenta of the unperturbed torus that seems to correspond, the torus marked in red in the figure 4.2, yielding to $\overline{p} = 2.45$ and thus, the associated energy is $\overline{p}^2/2m \approx 3\ V$. Thus we will only consider the eigenstates whose associated quasi-energies lie within the interval $[3\ V - \hbar\omega_0/2\ ;\ 3\ V + \hbar\omega_0/2]$.

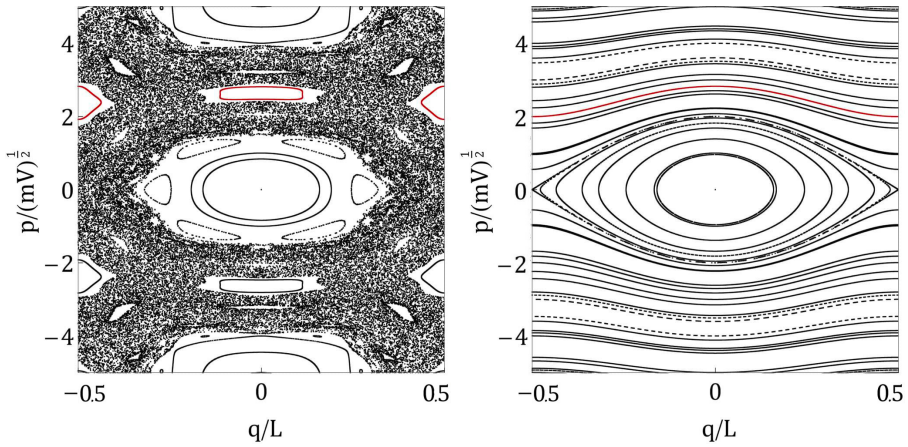

(a) (b)

Figure 4.2: Poincaré sections for $\omega_0 t = 0 + 2\pi n$, $\forall n \in \mathbb{Z}$, of the classical single-particle dynamics corresponding to the Hamiltonian $H = p^2/2m + V[1 + \delta\cos(\omega_0 t)]\cos(2\pi q/L)$. The figure on the left represents the optimal configuration we just found. The figure on the right represents the same unperturbed system with $\delta = 0$, represents a quantum pendulum. In both figures, the 2:1 resonance islands and the unperturbed torus, which appears to correspond to the same momentum, are marked in red.

The choice of our interval is approximate, but once again, due to the periodicity of the spectrum, we do not need to be more precise.

Now that we have the quasi-energies and associated Floquet states, we will calculate the Husimi distributions of these states to find which ones are localized on the resonance islands. This tool was presented earlier in the Section 1.2.3, thus we won't dwell on the formalism associated with it, but we will simply specify the form of the Gaussian wave packet onto which we project our eigenfunctions in our specific case.

We have

$$|\alpha_{Q,P}(q)\rangle = \frac{1}{(\pi\hbar)^4}\ \exp\left(\frac{-1}{2\hbar}(q-Q)^2 + \frac{i}{\hbar}P(q-Q)\right) \tag{4.7}$$

where in our case we consider $\hbar = 0.1\ \sqrt{Vm}L/2\pi$. And before we can calculate the scalar product (1.27), we must also express the eigenvector of interest $|\psi_n\rangle$ in the representation of positions q.

$$|\psi_n(q)\rangle = \sum_k \psi_{k,n}\frac{e^{ikq}}{\sqrt{2\pi}} \tag{4.8}$$

Then,

$$|\ \langle\alpha_{Q,P}|\psi_n\rangle\ |^2 = |\int dq\ \alpha^*_{Q,P}(q)\ \psi_n(q)|^2$$

$$= \Big|\frac{1}{\sqrt{2\pi}}\sum_k\ |\psi_{k,n}\rangle\ \int_{-\infty}^{\infty}\ e^{-\frac{1}{2\hbar}(q-Q)^2}e^{\frac{-i}{\hbar}(P-\hbar k)(q-Q)}\ e^{ikQ}\ dq\Big|^2$$

$$= \Big|\frac{1}{\sqrt{2\pi}}\sum_k\ |\psi_{k,n}\rangle\ e^{ikQ}\ \int_{-\infty}^{\infty}\ e^{-\frac{1}{2\hbar}(q-Q)^2}e^{\frac{-i}{\hbar}(P-\hbar k)(q-Q)}\ dq\Big|^2$$

We can make a variable change in the integral $u = q - Q$ and so $du = dq$. So we have

$$\mathscr{I} = \int_{-\infty}^{\infty} e^{\frac{1}{2\hbar}u^2}e^{\frac{-i}{\hbar}(P-\hbar k)u}du$$

Which corresponds to the Fourier transform of a Gaussian. Thus,

$$\mathscr{I} = e^{\frac{-(P-\hbar k)^2}{\hbar^2}\frac{2\hbar}{4}} = e^{\frac{-(P-\hbar k)^2}{2\hbar}}\sqrt{2\pi\hbar}$$

And finally we have

$$\Phi_{|\psi_n\rangle}(Q,P) = \left(\frac{\hbar}{\pi}\right)^{1/4}\sum_k |\psi_{k,n}\rangle\, e^{\frac{-(P-\hbar k)^2}{2\hbar}}e^{ikQ} \tag{4.9}$$

As the diagonalization of the matrix (4.5) may actually prove to be a challenge in itself, to refine the calculation of the Husimi distribution, we start by examining the problem without the periodic excitation, i.e., the problem corresponding to a simple quantum pendulum. In this scenario, for eigenstates such as $|\psi_0\rangle$ and $|\psi_4\rangle$, for example, we obtain the distributions depicted in the figure 4.3 superimposed on the classical phase space.
Subsequently, for the Floquet states, we obtain for example the distributions shown in the figure 4.4, still superimposed on the corresponding classical phase space for enhanced clarity.
These examples correspond to the parameters obtained for the optimal configuration, and the corresponding Poincaré sections are constructed for $\omega_0 t = 0 + 2\pi n$, $\forall n \in \mathbb{Z}$. On the left, we have the Husimi distribution of a regular state localized on the 3:1 resonance, in the middle, we have a regular state, localized on a KAM torus this time, at the center of the phase space, and on the right, we have a chaotic state, clearly showing the delocalization of this state in the phase space.

Thus, we find the Floquet states localized on the 2:1 resonance islands and their associated quasi-energies. We find four such states corresponding to the following quasi-energies:

- $\epsilon_{4462} = 2.9087025\ V$
- $\epsilon_{4463} = 2.9087765\ V$

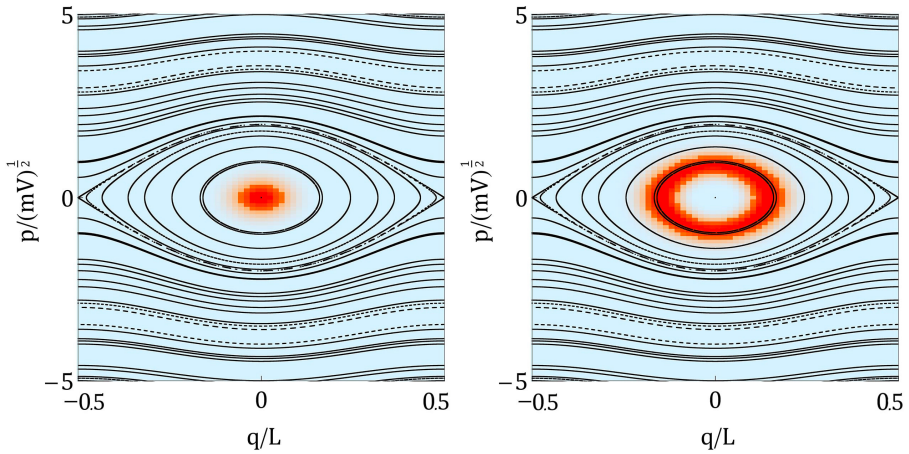

(a) $|\psi_0\rangle$ (b) $|\psi_4\rangle$

Figure 4.3: Husimi distributions of the regular states $|\psi_0\rangle$ and $|\psi_4\rangle$ of the quantum pendulum corresponding to the Hamiltonian $\hat{H} = \hat{p}^2/2m + V\cos(2\pi\hat{q}/L)$, where $\hbar = 0.1\sqrt{VmL}/2\pi$. These distributions are superimposed on the corresponding classical phase space, thus allowing a clear visualization of the localization of these eigenstates within it. Orange indicates a high probability of finding the state of interest in that region of the phase space, while blue corresponds to a zero probability.

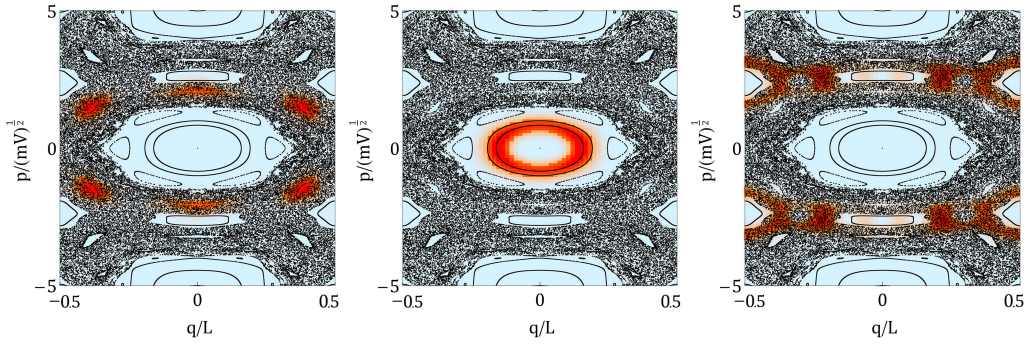

(a) (b) (c)

Figure 4.4: Husimi distributions of three different Floquet states of the system with the periodic modulation, they are superimposed on the corresponding classical phase space with $H = p^2/2m + V[1 + \delta\cos(\omega_0 t)]\cos(2\pi q/L)$ for $\delta = 2$, $\hbar\omega_0 = 0.5\ V$, $\hbar = 0.1\sqrt{VmL}/2\pi$ and for $\omega_0 t = 0 + 2\pi n$, $\forall n \in \mathbb{Z}$. Graph (a) represents a regular state localized on the 3:1 resonance islands, (b) represents a regular state localized on a KAM torus and (c) represents a chaotic state. This later is delocalized into phase space as expected. Orange indicates a high probability of finding the state of interest in that region of the phase space, while blue corresponds to a zero probability.

- $\epsilon_{4571} = 3.1587729\ V$
- $\epsilon_{4572} = 3.1587878\ V$

They all have the same Husimi distribution, so we only show the distribution of one of these

states in Fig. 4.5, the state $|\psi_{4572}\rangle$ for example, and we show it superimposed on the associated classical phase space. We show the situation for two different times.

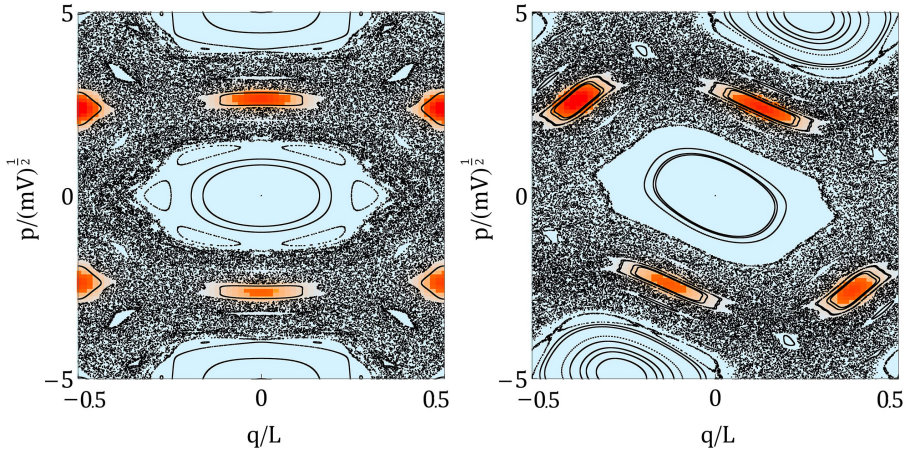

(a) (b)

Figure 4.5: Husimi distributions of one of the Floquet states localized on the 2:1 resonance islands. More specifically, it is the Husimi distribution of the state $|\psi_{4572}\rangle$ associated with the quasi-energy $\epsilon_{4572} = 3.1587878\ V$. The distribution is superimposed on the corresponding classical phase space with $H = p^2/2m + V[1 + \delta\cos(\omega_0 t)]\cos(2\pi q/L)$. $\delta = 2$, $\hbar\omega_0 = 0.5\ V$ and $\hbar = 0.1\ \sqrt{Vm}L/2\pi$. The difference between figures (a) and (b) is that they are both plotted for different times. The stroboscopic Poincaré section in (a) is constructed for $\omega_0 t = 0 + 2\pi n$ and the one in (b) for $\omega_0 t = \pi/2 + 2\pi n$, $\forall n \in \mathbb{Z}$. Orange indicates a high probability of finding the state of interest in that region of the phase space, while blue corresponds to a zero probability.

4.3 Effective hopping parameter

The effective hopping parameter is given, up to a factor two, by the splitting between the quasi-energies of the Floquet states localized on the resonance islands (4.2). However, at the end of the previous step, we end up with four such states, grouped into two pairs, and not just two states. Furthermore, their Husimi distributions (Fig. 4.5) show us states localized on the four 2:1 resonance islands, corresponding to the two islands with a clockwise rotation and the two islands with a counterclockwise rotation.

It is therefore easy to understand that we have these two pairs of states because there are these two directions of rotation. Thus, in reality, we distinguish two different hopping parameters, the hopping between islands of different rotation directions and the hopping between the two islands of the same rotation direction. As we have now well established, within the scope of this work, it is the tunneling phenomenon between the two islands propagating in the clockwise direction that interest us. So, in order to identify which of the four states are involved in this process and from which splitting the hopping parameter related to this phenomenon can be calculated, we compute the Husimi distributions of the different superpositions of these four states. These different superpositions are shown in figure 4.6.

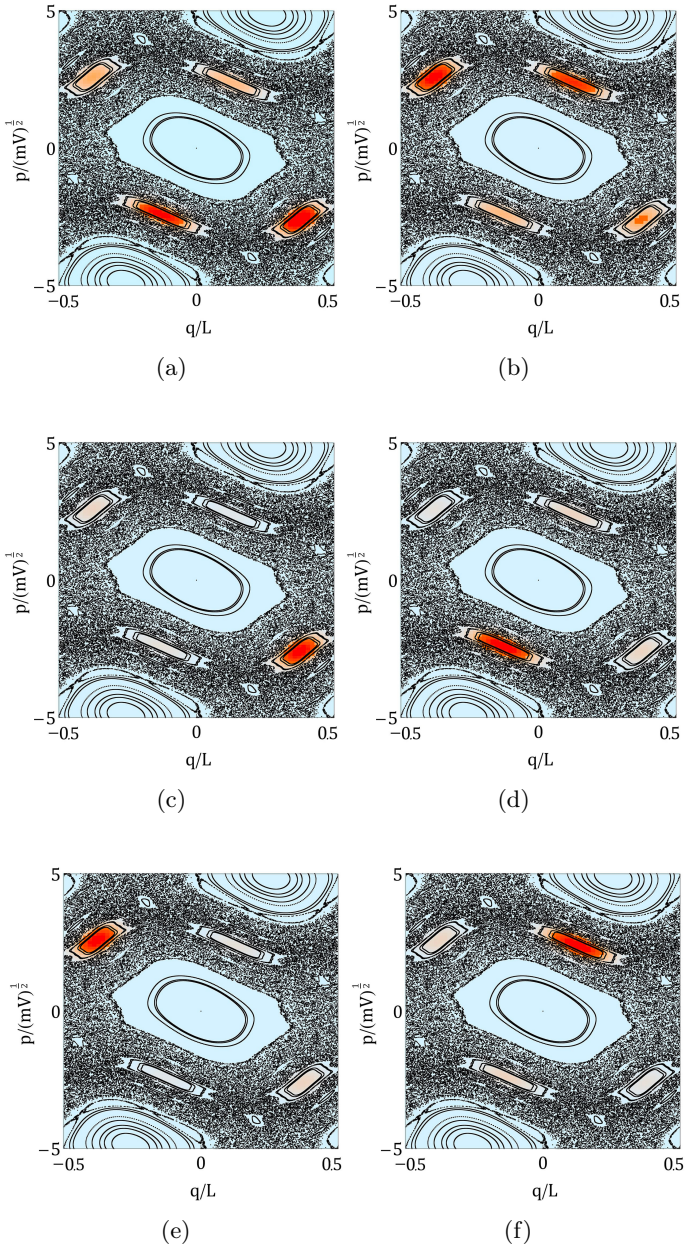

Figure 4.6: Husimi distributions of the different superpositions of the four Floquet states localized on the 2:1 resonance islands. These distributions are superimposed on the corresponding classical phase space, this phase space is model by the Hamiltonian $H = p^2/2m + V[1 + \delta\cos(\omega_0 t)]\cos(2\pi q/L)$ with $\delta = 2$, $\hbar\omega_0 = 0.5\ V$ and $\hbar = 0.1\ \sqrt{VmL}/2\pi$, for $\omega_0 t = \pi/2 + 2\pi n$, $\forall n \in \mathbb{Z}$. The figure (a) and (b) respectively represent the symmetric and antisymmetric superpositions of the states $|\psi_{4462}\rangle$ and $|\psi_{4463}\rangle$, (c) and (d) represent the symmetric and antisymmetric superpositions of the states $|\psi_{4462}\rangle$ and $|\psi_{4571}\rangle$, and finally, (e) and (f) represent the symmetric and antisymmetric superpositions of the states $|\psi_{4463}\rangle$ and $|\psi_{4572}\rangle$.

The figure 4.6a corresponds to the symmetric superposition of the states $|\psi_{4462}\rangle$ and $|\psi_{4463}\rangle$, while figure 4.6b corresponds to the antisymmetric superposition of these states. We obtain similar results with states $|\psi_{4571}\rangle$ and $|\psi_{4572}\rangle$. We see that the splittings between these two pairs of states actually represent the tunneling phenomenon between the different directions of rotation. Then, figures 4.6c and 4.6d represent the symmetric and antisymmetric superpositions of states $|\psi_{4462}\rangle$ and $|\psi_{4571}\rangle$, these are therefore the states involved in the tunneling between the two islands moving in the counterclockwise direction. Hence, it is the states $|\psi_{4463}\rangle$ and $|\psi_{4572}\rangle$, whose superpositions are represented in figure 4.6e and 4.6f, that interest us in this work.

We then obtain

$$J = 0.1250056\ V \tag{4.10}$$

Subsequently, in the Floquet theory presented in Section 1.2.1, the calculations are done with an infinite-dimensional matrix, but in practice, we have done the calculation for a 5000×5000 matrix. Therefore, we will now conduct a convergence study of the parameter J for different dimensions of this matrix to determine if the chosen dimension is sufficient.

- For 50 Floquet blocks but with only 50×50 elements per block : The results are more ambiguous, instead of observing two quasi-energy doublets, we end up with four different values. Namely; 2.7682151 V , 2.9742364 V, 3.0208845 V and 3.2276796 V. Furthermore, the Husimi distributions of these states are not as well localized as our previous results, as shown in Fig. 4.7a. We conclude that this configuration lacks sufficient precision.

- For 20 Floquet blocks with 100×100 elements per block : In this case, we already recover the two pairs of quasi-energies; 2.9081489 V, 2.9081700 V, 3.158310 V and 3.1583097 V. We can see that the values of these quasi-energies differ slightly from what we find with 50 Floquet blocks, and we obtain a hopping parameter equal to 0.1250698 V. Furthermore, the Husimi distributions are well localized on the islands, Fig. 4.7b. Thus this configuration might already be sufficient, but we will see that the results really converge starting from 50 blocks.

- For 50 Floquet blocks with 200×200 elements per block : We find almost exactly the same quasi-energies as in the case with 100 elements per block, namely 2.9087042 V, 2.9087283 V, 3.1587877 V and 3.1587878 V. Therefore the associated hopping is $J = 0.1250297\ V$. And the Husimi distributions associated with these quasi-energies are very well localized, Fig. 4.7c.

We can see that the results are well converged in our configuration and we conclude that 50 Floquet blocks with 100×100 elements per block are sufficient, and we will use the value (4.10) in the rest of the calculations.

Next, still to verify if our approximation is indeed sufficient, we check if the periodicity of the spectrum is preserved. We calculate the splitting in an interval centered at 11.1550137 V, and we find that the two Floquet states corresponding to our phenomenon have the quasi-energies 10.9087839 V and 11.1587985 V. Therefore, we obtain $J = 0.1250073\ V$, which is quite close to the value (4.10).

Finally, we will study the behavior of this parameter for different values of $\hbar$. We keep all other parameters fixed, including the dimension, and calculate the splitting ΔE between the two Floquet states localized on the 2:1 resonance island concerned in our process. We do this calculation for seven different values of $\hbar$: 0.05, 1/18, 1/15, 1/12, 0.1, 1/7, 0.3, 0.4, 0.5 and 1.

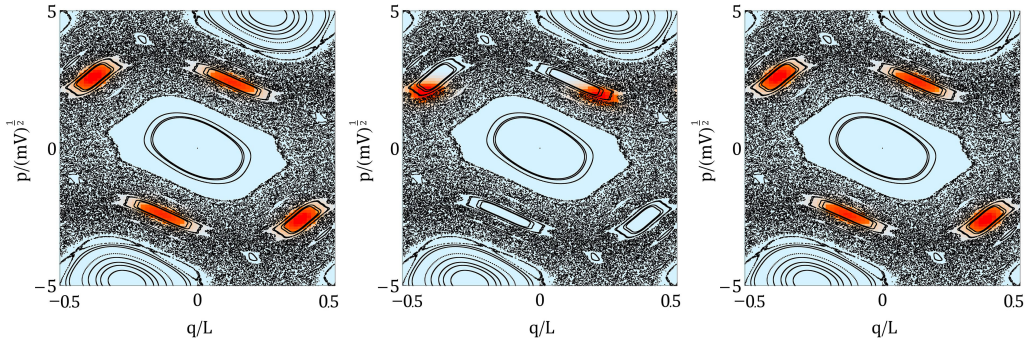

(a) (b) (c)

Figure 4.7: Husimi distributions of one of the Floquet states localized on the 2:1 resonance islands, superimposed on the corresponding classical phase space that is, the space modeled by $H = p^2/2m + V[1 + \delta\cos(\omega_0 t)]\cos(2\pi q/L)$ with $\delta = 2$, $\hbar\omega_0 = 0.5\ V$, $\hbar = 0.1\ \sqrt{Vm}L/2\pi$ and for $\omega_0 t = \pi/2 + 2\pi n$, $\forall n \in \mathbb{Z}$. The three figures correspond to three different dimensions of the space in which the calculations are performed. (a) 50 Floquet blocks but with only 50×50 elements per block, (b) 20 Floquet blocks with 100×100 elements per block and (c) 50 Floquet blocks with 200×200 elements per block.

We represent the results in a graph of the logarithm of the splittings found as a function of $1/\hbar$, Fig. 4.8.

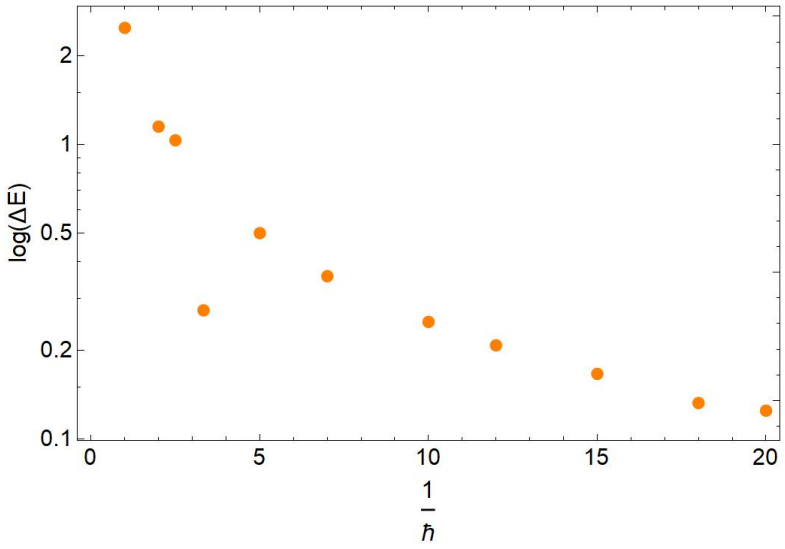

Figure 4.8: Graph of the logarithm of the splittings as a function of $1/\hbar$. The points correspond to the different values we have compute for seven different values of $\hbar$: 0.05, 1/18, 1/15, 1/12, 0.1, 1/7, 0.3, 0.4, 0.5 and 1. All the others parameters are fixed, so we have $\delta = 2$ and we consider 50 Floquet blocks with 100×100 elements per block.

We clearly see the decay predicted by the theory of chaos- and resonance-assisted tunnel-

ing [12, 13, 75, 84], and we also see a peak for $\hbar = 0.3$, representing one of the characteristic fluctuations of these phenomena.

4.4 Effective interaction parameter

Now that we have the effective hopping parameter, we want to calculate the effective interaction parameter. This is obtained through an analysis of the spatial localization properties of the Floquet states localized on the resonance islands.

$$U = g_{1D} \int |\phi_i(x)|^4 \, dx \ , \ i = 1 \text{ or } 2 \tag{4.11}$$

$\phi_1(x)$ and $\phi_2(x)$ are the two single-particle states respectively localized on one of the two resonance islands.
We know that the Floquet states obtained after diagonalizing the Floquet matrix (4.5) are localized on the four islands. However, we need a state localized on one of the islands that rotates clockwise. In the previous section, we found that such situations are given by the symmetric and antisymmetric superpositions of states $|\psi_{4463}\rangle$ and $|\psi_{4572}\rangle$, see figure 4.6. We choose to work with the antisymmetric superposition of these states. For simplicity and consistency with (4.11), we will denote this state as ϕ_1.

The first step is to normalize this vector. We must have

$$\int |\phi_1(x)|^2 \, dx = 1 \tag{4.12}$$

This integral should theoretically be performed from $-\infty$ to $+\infty$, but in practice, we restrict our calculations to an interval of size L, and we always consider a Floquet matrix composed of 50 blocks with 100×100 elements per block. So, we have

$$\int_{-L/2}^{L/2} |\phi_1(x)|^2 \, dx = 1 \tag{4.13}$$

Since $\phi_1(x)$ is a Floquet state, for recall by definition we have

$$\phi_1(x) = \sum_{k=1}^{d} \phi_k e^{\frac{2i\pi}{L} kx} \tag{4.14}$$

where the $\{\phi_k\}_{k=1,..,d}$ are the Floquet components which we have access to numerically. We have

$$\begin{aligned} &\int_{-L/2}^{L/2} |\sum_{k_1=1}^{d} \phi_{k_1} e^{\frac{2i\pi}{L} k_1 x}|^* |\sum_{k_2=1}^{d} \phi_{k_2} e^{\frac{2i\pi}{L} k_2 x}| \, dx \\ &= \int_{-L/2}^{L/2} \sum_{k_1,k_2=1}^{d} \phi_{k_1}^* \phi_{k_2} e^{\frac{2i\pi}{L}(k_2-k_1)x} \, dx \qquad (4.15) \\ &= \sum_{k_1,k_2=1}^{d} \phi_{k_1}^* \phi_{k_2} \int_{-L/2}^{L/2} e^{\frac{2i\pi}{L}(k_2-k_1)x} \, dx \qquad (4.16) \end{aligned}$$

This integral is easily calculated, and we obtain

$$\int |\phi_1(x)|^4 \, dx = L \sum_{k=1}^{d} |\phi_k|^2 = 1 \Leftrightarrow \sum_{k=1}^{d} |\phi_k|^2 = 1/L \tag{4.17}$$

With $L = 2\pi$. Thus, we need to calculate this sum and normalize correctly the vector.

We can now calculate the integral in (4.11). Since our system is time-dependent, the nonlinear resonances move in the Poincaré section as time progresses. Since the integral to be calculated depends on the localization of the considered Floquet state on this island, to be complete, we need to calculate the time average of this integral. In practice, this can be done in two different ways.

The first method involves calculating it for X different time values and then averaging the X results obtained.
In this case, we start with the superposition of the two eigenvectors of interest of the matrix (4.5) before calculating the corresponding Floquet state. Indeed, as seen in the previous Section, the Floquet state depends on time, so it must be calculated for each considered time.
Next, we can calculate

$$\int_{-L/2}^{L/2} |\phi_1(x)|^4 \, dx \tag{4.18}$$

We proceed as in the normalization calculation, and we have

$$\int_{-L/2}^{L/2} \sum_{k_1,k_2,k_3,k_4=1}^{d} \phi_{k_1}^* \phi_{k_2}^* \phi_{k_3} \phi_{k_4} e^{\frac{2i\pi}{L}(k_3+k_4-k_2-k_1)x} \, dx$$

$$= \sum_{k_1,k_2,k_3,k_4=1}^{d} \phi_{k_1}^* \phi_{k_2}^* \phi_{k_3} \phi_{k_4} \int_{-L/2}^{L/2} e^{\frac{2i\pi}{L}(k_3+k_4-k_1-k_2)x} \, dx \tag{4.19}$$

$$= L \sum_{k_1,k_2,k_3,k_4=1}^{d} \phi_{k_1}^* \phi_{k_2}^* \phi_{k_3} \phi_{k_4} \delta_{k_1+k_2,k_3+k_4} \tag{4.20}$$

Furthermore, the $\{\phi_k\}_{k=1,\dots,d}$ are the components of the Floquet state that we have calculated. Thus, if we have normalized correctly, it is sufficient to make the appropriate sum of these components to obtain the value of this integral in units of $1/L$.
Using this method, for 100 different times (from $t = 0$ to $t = 1.24407$), we obtain

$$0.0704833 \; 1/L \tag{4.21}$$

The second technique involves directly calculating this average analytically, which means we want to calculate

$$\frac{1}{T} \int_0^T \int_{-L/2}^{L/2} |\phi_1(x)|^4 \, dx \, dt \tag{4.22}$$

We have just calculated the first integral of this expression, we have

$$\frac{1}{T} \int_0^T \sum_{k_1,k_2,k_3,k_4=1}^{d} L \phi_{k_1}^* \phi_{k_2}^* \phi_{k_3} \phi_{k_4} \delta_{k_1+k_2,k_3+k_4} \, dt \tag{4.23}$$

In order to continue, we need to recall the decomposition of the Floquet components, we have

$$\phi_k = \sum_{l=1}^{f} \phi_{k,l} e^{il\omega_0 t} \tag{4.24}$$

where the $\{\phi_{k,l}\}_{l=1,\dots,f}$ correspond to the components of the "rough" eigenvectors obtained directly after diagonalizing the Floquet matrix. Then,

$$\begin{aligned}
&\frac{L}{T}\int_0^T \sum_{k_1,k_2,k_3,k_4=1}^{d} \sum_{l_1,l_2,l_3,l_4=1}^{f} \phi^*_{k_1,l_1}\phi^*_{k_2,l_2}\phi_{k_3,l_3}\phi_{k_4,l_4} e^{i\omega_0 t(l_3+l_4-l_2-l_1)}\delta_{k_1+k_2,k_3+k_4}\, dt \\
&= \frac{L}{T} \sum_{k_1,k_2,k_3,k_4=1}^{d} \sum_{l_1,l_2,l_3,l_4=1}^{f} \phi^*_{k_1,l_1}\phi^*_{k_2,l_2}\phi_{k_3,l_3}\phi_{k_4,l_4}\delta_{k_1+k_2,k_3+k_4} \int_0^T e^{i\omega_0 t(l_3+l_4-l_2-l_1)}\, dt \qquad (4.25) \\
&= L \sum_{k_1,k_2,k_3,k_4=1}^{d} \sum_{l_1,l_2,l_3,l_4=1}^{f} \phi^*_{k_1,l_1}\phi^*_{k_2,l_2}\phi_{k_3,l_3}\phi_{k_4,l_4}\delta_{k_1+k_2,k_3+k_4}\delta_{l_1+l_2,l_3+l_4} \qquad (4.26)
\end{aligned}$$

Again, the $\{\phi_{k,l}\}$ are the components of the superposition of the eigenvectors that we can access numerically. Thus, if we have normalized correctly, it is again sufficient to make the appropriate sum of the components, this time of the eigenvector and not the Floquet state, in order to obtain the time average of the integral in units of $1/L$.
Using this method, we obtain

$$0.0704833\ 1/L \tag{4.27}$$

We see that both techniques provide the same results. Although in the second method there is only one calculation to be made, compared to X calculations for the first method, the sum in this calculation is much larger. To the point that, for the dimensions considered in this work (5000×5000), the second method takes much longer than the first.

To obtain the final expression of the interaction parameter, we now need to multiply (4.27) by g_{1D}. We have

$$U = g_{1D} \times 0.0704833/L \tag{4.28}$$

with

$$g_{1D} = 2\hbar\omega_\perp a_s \tag{4.29}$$

Therefore, we actually need to calculate g_{1D}/L. To do this, we need to set the real parameters of our system. Indeed, so far, we have been working in numerical units. We have expressed the different values in terms of V, L and m. If we denote the associated numerical units as $V^{(0)}$, $L^{(0)}$ and $m^{(0)}$, we have

$$\begin{cases}
m = m^{(0)} \\
L = 2\pi\ L^{(0)} \\
\hbar = 0.1\ \sqrt{V^{(0)}m^{(0)}}L^{(0)} \\
V = V^{(0)} \\
\omega_0 = 5\ \omega_0^{(0)} = 5\ \sqrt{\dfrac{V^{(0)}}{m^{(0)}}}\dfrac{1}{L^{(0)}}
\end{cases} \tag{4.30}$$

But, in reality, if we consider that our condensate is made of ^{87}Rubidium atoms, we have

$$\begin{cases} m = 1.4192261 \times 10^{-25} \text{ kg} \\ a_s = 5 \times 10^{-9} \text{ m} \end{cases} \tag{4.31}$$

We know that $\hbar = 1.05457 \times 10^{-34}$ Js and L and $\omega_\perp$ are the trap parameters, these parameters can be controlled and we decide to set them to the following values

$$\begin{cases} L = 10^{-5} \text{ m} \\ \omega_\perp = 2\pi \times 10 \text{ kHz} \end{cases} \tag{4.32}$$

So, we can calculate

$$\begin{aligned} g_{1D} &= 6.62606 \times 10^{-38} \text{ J m} \\ \Leftrightarrow g_{1D}/L &= 6.62606 \times 10^{-33} \text{ J} \end{aligned} \tag{4.33}$$

This value is expressed in SI units. However, we must re-express it in units of V to find an effective interaction parameter also in units of V. Indeed, to use the value of this parameter for the numerical diagonalization of the Bose-Hubbard matrix in the next step, it must be expressed in numerical units, just like the effective hopping parameter. To do this, we need the value of the potential V in SI units, but we do not know it, we must calculate it.
Since the value of $\hbar$ is known, we re-express our parameter again, this time in terms of $\hbar^{(0)}$, $L^{(0)}$ and $m^{(0)}$, with $\hbar = 0.1\hbar^{(0)}$. Thus, using the equalities in (4.30), we find

$$V^{(0)} = \frac{\hbar^{(0)2}}{m^{(0)}L^{(0)2}} \tag{4.34}$$

Using the equalities (4.30), (4.31) and (4.32), we can find the values of $\hbar^{(0)}$, $L^{(0)}$ and $m^{(0)}$ in SI units. We have

- $\hbar = 1.05457 \times 10^{-34}$ Js $= 0.1\ \hbar^{(0)}$. So, $\hbar^{(0)} = 1.05457 \times 10^{-33}$ Js
- $L = 10^{-5}$ m $= 2\pi\ L^{(0)}$. So, $L^{(0)} = 10^{-5}/2\pi$ m
- $m = 1.4192261 \times 10^{-25}$ kg $= 1\ m^{(0)}$. So, $m^{(0)} = 1.4192261 \times 10^{-25}$ kg

Thus,

$$V = V^{(0)} = \frac{\hbar^{(0)2}}{m^{(0)}L^{(0)2}} = 3.09356 \times 10^{-30} \text{ J} = 29334.8 \text{ Hz} \tag{4.35}$$

Dividing (4.33) by (4.35), we get the value of g_{1D}/L in units of V

$$g_{1D}/L = 0.002142\ V \tag{4.36}$$

And thus,

$$U = 0.00015098\ V \tag{4.37}$$

4.5 Computation of the collective tunneling rate

We have thus calculated the two effective parameters needed to obtain the Bose-Hubbard matrix, using only the eigenvalues and eigenvectors of the Floquet matrix of the single-particle problem. With this, we can now consider the case of a gas of N ultracold atoms. Then, we have to

express the Bose-Hubbard matrix in the corresponding Fock space, where only the quasimodes associated with the two islands will be populated and therefore taken into account. The matrix is of dimension $N+1$ and, as a reminder, its elements are given by

$$\begin{aligned}\langle n_1, n_2|\,\hat{H}\,|n_1', n_2'\rangle = -J\left[\sqrt{n_2'(n_1'+1)}\delta_{n_1,n_1'+1}\delta_{n_2,n_2'-1} + \sqrt{n_1'(n_2'+1)}\delta_{n_1,n_1'-1}\delta_{n_2,n_2'+1}\right] \\ +\frac{1}{2}U\left[n_1'(n_1'+1)\delta_{n_1,n_1'}\delta_{n_2,n_2'} + n_2'(n_2'+1)\delta_{n_1,n_1'}\delta_{n_2,n_2'}\right]\end{aligned} \tag{4.38}$$

We know that if the condensate is prepared on one of our two resonance islands, due to the presence of interaction between the N atoms in the condensate, if $U > J$ we are in the self-trapping regime, and the particles cannot tunnel individually to the other resonance island. However, they can tunnel all together, which is referred to as collective tunneling. In other words, in the Fock basis, the state of the system can transition from state $|N,0\rangle$ to the state $|0,N\rangle$. It is this collective tunneling that we have been aiming to characterize from the beginning of this work.

If we consider $N = 5$, the associated Fock space is of dimension 6, and the Bose-Hubbard matrix in this space is given by

$$\hat{H} = \begin{pmatrix} 15U & -\sqrt{5}J & 0 & \cdots & \cdots & 0 \\ -\sqrt{5}J & 11U & -\sqrt{8}J & \ddots & & \vdots \\ 0 & -\sqrt{8}J & 9U & -3J & \ddots & \vdots \\ \vdots & \ddots & -3J & 9U & -\sqrt{8}J & 0 \\ \vdots & & \ddots & -\sqrt{8}J & 11U & -\sqrt{5}J \\ 0 & \cdots & \cdots & 0 & -\sqrt{5}J & 15U \end{pmatrix} \tag{4.39}$$

Here, the parameter J represents the coupling between the states $|N-n, n\rangle$ and $|N-(n+1), n+1\rangle$, $\forall n = 0, ..., N$. It corresponds to the tunneling rate of the non-interacting system, i.e., the single-particle system. This is the tunneling rate of the sequential process, which is suppressed when we are in the self-trapping regime.

The collective tunneling rate is then simply given by the splitting between the energies associated with states $|N,0\rangle$ and $|0,N\rangle$.

After diagonalizing the matrix (4.39), we find that the eigenvalues associated with these states are the two largest eigenvalues. Indeed, $|N,0\rangle$ and $|0,N\rangle$ are the two states at the ends of the diagonal of the matrix, and as can be observed, they have the highest coefficients, making them the largest elements of this matrix. Additionally, by examining the coefficients of this matrix, we can observe that the tridiagonal elements are much smaller than the diagonal elements. Thus, the eigenvalues obtained after diagonalization are not significantly altered compared to these diagonal elements, confirming that the two largest eigenvalues are indeed the eigenvalues of interest.

As mentioned in the previous Section, the parameter $\omega_\perp$ is a trap parameter that we can adjust. We have just calculated the value of the effective parameter U for $\omega_\perp = 2\pi \times 10$ kHz. Here, we will perform the diagonalization of the matrix (4.39) for two different values of this frequency, and thus two different values of U, to highlight the two different regimes that can be encountered depending on the value of this interaction parameter. If $U > J$, we are in the self-trapping regime where collective tunneling can be observed, otherwise, we are in a regime where sequential tunneling of the condensate atoms is observed. We will consider $\omega_{\perp,1} = 2\pi \times 10$ kHz and

$\omega_{\perp,2} = 2\pi \times 50000$ kHz. Additionally, it is known that $J = 0.1250056\ V$, a value that does not change regardless of the transverse confinement frequency.

Let us start with $\omega_{\perp,1} = 2\pi \times 10$ kHz. In this case, we already know the value of the effective interaction parameter, $U_1 = 0.00015098\ V$. By inserting the values of U_1 and J into the Bose-Hubbard matrix (4.39) and after diagonalization, we obtain the eigenvalues

$$\lambda_1 = 0.3768288\ V \tag{4.40}$$

$$\lambda_2 = 0.6265380\ V \tag{4.41}$$

Therefore, the corresponding tunneling rate is given by

$$J_{\text{col},1} = 0.2497092\ V \tag{4.42}$$

We see that $J_{\text{col},1}$ is of the same order of magnitude as J, which is not what is expected for the collective tunneling rate. Indeed, as we have already stated, J represents the tunneling rate in our time crystal when there is only one particle. Therefore, it should be much greater than $J_{\text{col},1}$, the tunneling rate of N particles. Indeed, sequential tunneling is much faster than collective tunneling. Additionally, $U_1 \ll J$, thus, with this transverse confinement frequency, we are not in the self-trapping regime. To be in such a regime, the effective interaction between particles must be greater than the effective hopping between our two islands. Therefore, $J_{\text{col},1}$ does not represent the collective tunneling rate of our N particles we are looking for.

Another way to determine whether or not we are in the self-trapping regime is to examine the eigenvectors associated with our two eigenvalues of interest. In the self-trapping regime, these eigenvectors should have a structure resembling $(1/\sqrt{2}, 0, 0, 0, 0, 1/\sqrt{2})$, indicating a NOON superposition of these states. In our case we have

$$|\psi_1\rangle = (-0.39564, 0.53017, -0.24977, -0.24977, 0.53017, -0.39564) \tag{4.43}$$

$$|\psi_2\rangle = (0.17704, -0.39540, 0.55885, -0.55885, 0.39540, -0.17704) \tag{4.44}$$

We clearly see that they do not correspond to vectors indicating a NOON superposition.

Now, let us look for $\omega_{\perp,2} = 2\pi \times 50000$ kHz. In this case, we need to recalculate g_{1D}/L. We have

$$g_{1D}/L = 3.31303 \times 10^{-29}\text{J} \tag{4.45}$$

$$= 10.7094\ V \tag{4.46}$$

Therefore,

$$U_2 = 0.7548338\ V \tag{4.47}$$

And this time, we obtain the two eigenvalues

$$\lambda_1 = 11.3483794\ V \tag{4.48}$$

$$\lambda_2 = 11.3484181\ V \tag{4.49}$$

The associated eigenvectors are

$$|\psi_1\rangle = (0.70408, -0.06517, 0.00467, 0.00467, -0.06517, 0.70408) \tag{4.50}$$

$$|\psi_2\rangle = (0.70407, -0.06527, 0.00552, -0.00552, 0.06527, -0.70407) \tag{4.51}$$

We observe that in this case, they possess the structure indicating a NOON superposition. This means that with this value of the transverse confinement frequency, we are in the self-trapping regime. Thus, the splitting between these two eigenvalues indeed represents the collective tunneling rate of the N condensate atoms between the two sites of our time crystal that we have been seeking since the beginning of this work. We obtain

$$J_{\mathrm{col},2} = 0.0000387\ V \tag{4.52}$$

To better understand this result, we can calculate the times associated with the tunneling rates found

$$t_{\mathrm{seq}} = \frac{\hbar}{J} \tag{4.53}$$

$$t_{\mathrm{col},2} = \frac{\hbar}{J_{\mathrm{col},2}} \tag{4.54}$$

To obtain a time in seconds, we must first re-express J and $J_{\mathrm{col},2}$ in SI units, we have

$$J = 3.86713 \times 10^{-31}\ \mathrm{J} \tag{4.55}$$

$$J_{\mathrm{col},2} = 1.19721 \times 10^{-34}\ \mathrm{J} \tag{4.56}$$

Therefore,

$$t_{\mathrm{seq}} = 0.000273\ \mathrm{s} \tag{4.57}$$

$$t_{\mathrm{col},2} = 0.880856\ \mathrm{s} \tag{4.58}$$

The time t_{seq} represents the interval after which an atom tunnels from one of our resonance islands to the other, and then back to the initial island, and so on, when the interaction between particles is not taken into account. The time $t_{\mathrm{col},2}$ represents the interval after which the entire condensate, prepared on one of the resonance island, tunnels to the other resonance when the interaction between particles is considered.
As expected, we have $t_{\mathrm{seq}} << t_{\mathrm{col},2}$. Furthermore, we can see that $t_{\mathrm{col},2} < 1$s, which seems to be a reasonable time and proves that the collective tunneling process is significantly accelerated by the presence of chaos in the system. Indeed, it was mentioned earlier that without assistance, the collective tunneling is extremely slow. In reality, it can be so slow that it is never observed because the condensate's lifetime is shorter. However, it is known that the average lifetime of a condensate can range from a few seconds to several minutes, $t_{\mathrm{col},2}$ is much smaller, which clearly shows that the tunneling process between the two sites of the time crystal is accelerated.

Note that, although these results are theoretically correct, in practice, achieving a transverse confinement frequency of $2\pi \times 50000$ kHz would be difficult. This means that, for the parameters we have chosen, the self-trapping regime is not easily reached. This is not a problem in itself for our results, but we could improve them in different ways to obtain a smaller $\omega_{\perp,2}$ value where the self-trapping regime appears. We could reduce L to 5×10^{-6} m, but again, going below this value seems too challenging experimentally. We could also increase the number of atoms considered. Another approach would be to consider a smaller value of $\hbar$, which would enhance the spatial localization on the islands.

Conclusion

The aim of this Master's thesis was to study the collective tunneling of a Bose-Einstein condensate prepared on one of the two sites of a time crystal. More specifically, the main objective was to calculate a first prediction of the time associated with this process for a given population value N of the sites, using Floquet theory an the two-site Bose-Hubbard model.

To achieve this, we began by studying the classical dynamics associated with the Hamiltonian of our system. We observed that the introduction of a non-integrable perturbation $\delta \cos \omega_0 t$ to the potential led to the emergence of chaos in the classical system, and more importantly, to the formation of nonlinear resonances according to the Poincaré-Birkhoff theorem. We focused more specifically on the 2:1 resonance where two symmetric islands appear. We found that this specific configuration of the classical phase space strongly influences the underlying quantum dynamics and allows the observation of a tunneling effect between these two islands, by confining the wave packets to specific regions of the phase space, which are these resonance islands. Therefore, the first thing we needed to do was to find the optimal values of the parameters δ and ω_0 to obtain the optimal phase space configuration for the study of our phenomenon.
We then found that the quantum objects corresponding to these localized wave packets are the Floquet states, and thus we introduced the Floquet theory.
Until then, we had neglected the interaction between the particles of our condensate, which was equivalent to considering a single-particle system. However, by introducing the theory of Bose-Einstein condensates, we saw that this interaction could not be neglected and its consideration has significant consequences. The first of these consequences is that we only observed symmetry-broken states, making our system a discrete time crystal. The second one is that taking this interaction into account also defined a self-trapping regime in which the sequential tunneling of atoms constituting the condensate from one to the other is suppressed, "trapping" the condensate particles in the symmetry-broken state they are prepared into. Only a collective tunneling of the whole condensate can be observed in this regime. However, we saw that this phenomenon is normally very slow but can be accelerated by the presence of chaos and resonance in our system.

Then, to study this collective tunneling in practice, we introduced the two-site Bose-Hubbard model. We saw that in this model, the tunneling rate of the collective tunneling phenomenon, for a condensate composed of N particles, could be simply obtained by diagonalizing the Bose-Hubbard matrix in the associated Fock space of dimension $N+1$. We also saw that the elements of this matrix depended only on the parameters U and J, where U is the effective interaction parameter and J is the effective hopping parameter. In the Bose-Hubbard model, these parameters can be computed simply from the one-particle Floquet states localized on our resonance islands, and the associated quasi-energies. Therefore, we only need the single-particle Floquet spectrum to obtain the form of our Bose-Hubbard matrix and then calculate the collective tunneling rate.

We thus had to calculate this Floquet spectrum of our system when neglecting the interaction between the condensate particles. To do this, we performed a numerical diagonalization of the corresponding Floquet matrix for 50 Floquet blocks, each consisting of 100×100 elements. This diagonalization, combined with the calculation of the Husimi distributions of the obtained Floquet states, allowed us to identify the states of the single-particle Floquet spectrum localized on our resonance islands and the quasi-energies associated with them. We were then able to directly obtain the value of the effective hopping parameter, $J = 0.1250056\ V$. We also conducted some analysis to verify if the obtained value was well converged and if J had the expected behavior as a function of $\hbar$ according to the theory of chaos- and resonance-assisted tunneling. We then observed that J decreased with $1/\hbar$ while showing random fluctuations in this decrease, exactly as predicted by these theories.
Next, thanks to the results of this diagonalization, we were also able to directly calculate the value of the effective interaction parameter. We performed a numerical calculation of the integral in the expression of U from the components of one of the Floquet states localized on one of the two islands, and we calculated the coefficient g_{1D} by fixing the real parameters of our system. Assuming that our condensate was composed of Rubidium atoms, we tried for two values of $\omega_\perp$. For, $\omega_{\perp,1} = 2\pi \times 10$ kHZ, we obtained $U_1 = 0.00015098\ V$ and for $\omega_{\perp,2} = 2\pi \times 50000$ kHZ, we obtained $U_2 = 0.7548338\ V$. Going back to the N-particles problem and numerically diagonalizing the Bose-Hubbard matrix in the associated Fock space, we obtained $J_{\text{col},1} = 0.2497092\ V$ and $J_{\text{col},2} = 0.0000387\ V$. We then noticed that for the first value we were not in the self-trapping regime in which we need to be to observe the collective tunneling of our condensate. Indeed, the value of the collective tunneling rate is too close to the value of J, which represents the tunneling rate of a single particle when the interaction is not taken into account. The second value, however, correspond to the self-trapping regime.

As expected, $J_{\text{col},2} \ll J$, the sequential tunneling phenomenon of an atom described by the rate J is much faster than the collective tunneling phenomenon of the entire condensate described by $J_{\text{col},2}$. We then calculated the characteristic times associated with these phenomena, we obtained $t_{\text{seq}} = 0.000273$ s and $t_{\text{col},2} = 0.880856$ s. The second time thus being the time we were looking for. Finally, we note that although it is much larger than t_{seq}, this time remains quite small, which proves that the collective tunneling phenomenon in our system has indeed been accelerated by the presence of chaos, given that collective tunneling times without assistance are often too long to even be observed within the typical lifetime of a condensate. We have also discussed the practical feasibility of the obtained results.

Perspectives

As we have now already mentioned plenty of times, the deliverable of this work is the value of the collective tunneling time between the two sites of a time crystal for different values of the population N of the sites. However, there is another way to view this Master's thesis. It can be considered as the first step of a theoretical elaboration of a protocol for creating NOON states with ultracold bosonic atoms and for predicting the time scale of this creation, as we explained in the introduction.
As a reminder, it has already been demonstrated [9] that such states can be created through the collective tunneling process in a self-trapping regime of an atomic gas between the two wells of a symmetric double-well potential. Our system is equivalent to this configuration. Thus, at half of the collective tunneling time t_{col} that we have calculated, the NOON state is obtained. However, the value of this time obtained at the end of this work is only a first prediction and can be improved to better represent reality, which is why we refer to it as a first step.

We have already discussed how to achieve results that are more achievable in practice.
To go further, we could start by studying how our parameters δ and ω_0, which characterize the periodic modulation, can be tuned as a function of the mode population N to achieve an optimal tunneling rate, i.e., to have optimally fast tunneling, even for large values of N.
Additionally, the Bose-Hubbard model we use in this work is actually too simple, as it does not account for certain complications that may arise. For example, the parameters U and J can depend on the population N of a given site. Indeed, as N increases, the single-particle wave function describing these sites extends if the interaction is repulsive and contracts if the interaction is attractive. Moreover, the two-mode approximation we use to develop the Bose-Hubbard model is actually too simple. To address these issues, more sophisticated numerical calculations of this collective tunneling effect are required, such as many-body simulations in the tilted ring configuration for a limited number of atoms. This step provides us with a more reliable quantitative prediction of the desired tunneling rate, allowing us to recalibrate the Bose-Hubbard model used in this work. Specifically, by considering more single-particle modes and making the interaction and hopping parameters population-dependent, which can be done by including higher-order terms in the effective many-body Hamiltonian. This will yield a model that is as reliable as possible while maintaining reasonable numerical complexity. This model will then serve as a versatile tool for calculating the chaos-assisted tunneling rate, even for larger atomic populations.
We could go even further. For example, we could also investigate how an additional periodic modulation might further boost the tunneling rate. We could also examine how this collective tunneling process behaves in other resonance chains, such as the 3:1 resonances, and between the 1:1 resonance and its mirror counterpart rotating in the opposite direction, where, in this case, collisions between atoms must be taken into account.

Bibliography

[1] M.-A. Nielsen and I.-L. Chuang, *Quantum Computation and Quantum Information: 10th Anniversary Edition* (Cambridge University Press, 2010).

[2] L. Pezzè, A. Smerzi, M.-K. Oberthaler, R. Schmied, and P. Treutlein, Rev.Mod.Phys. **90** (2018).

[3] I. Afek, O. Ambar, and Y. Silberberg, Science **328** (2010).

[4] J. Z. et al., Phys. Rev. Lett. **121** (2018).

[5] J.-I. Cirac, M. Lewenstein, K. Molmer, and P. Zoller, Phys. Rev. A **57** (1998).

[6] D. Gordon and C.-M. Savage, Phys. Rev. Lett. **59** (1999).

[7] K.-W. Mahmud, H. Perry, and W.-P. Reinhardt, J. Phys. B: At. Mol. Opt. Phys. **36** (2003).

[8] L.-D. Carr, D.-R. Dounas-Frazer, and M.-A. Garcia-March, Europhysics Letters **90** (2010).

[9] G. Vanhaele, *Creating highly entangled states with ultracold bosonic atoms through resonance- and chaos-assisted tunneling*, Ph.D. thesis, Université de Liège (2021).

[10] A. Smerzi, S. Fantoni, S. Giovanazzi, and S.-R. Shenoy, Phys. Rev. Lett **79** (1997).

[11] M. A. et al., Phys. Rev. Lett. **95** (2005), 10.1103/PhysRevLett.95.010402.

[12] O. Bohigas, S. Tomsovic, and D. Ullmo, Physics Reports **223** (1993).

[13] S. Tomsovic and D. Ullmo, Phys. Rev. E **50** (1994).

[14] K. Sacha, Phys. Rev. A **91** (2015), 10.1103/PhysRevA.91.033617.

[15] F. Wilczek, Phys. Rev. Lett. **111** (2013), https://doi.org/10.48550/arXiv.1308.5949.

[16] A. Shapere and F. Wilczek, Phys. Rev. Lett. **109** (2012), https://doi.org/10.1103/PhysRevLett.109.160402.

[17] M. Tabor, *Chaos and Integrability in Nonlinear Dynamics, an introduction* (John Wiley Sons, 1989).

[18] M. Berry, Physica Scripta **40** (1989), http://iopscience.iop.org/1402-4896/40/3/013.

[19] H.-J. Stöckmann, *Quantum chaos, an introduction* (Cambridge University Press, 1999).

[20] F. Haake, *Quantum Signatures of Chaos* (Springer, 1991).

[21] O. Bohigas, M.-J. Giannoni, and C. Schmit, Phys. Rev. Lett. **52** (1984).

[22] S. Wimberger, *Nonlinear Dynamics and Quantum Chaos* (Springer, 2014).

[23] G. Vanhaele, A. Bäcker, R. Ketzmerick, and P. Schlagheck, Phys. Rev. A **106** (2022), https://doi.org/10.1103/PhysRevA.106.L011301.

[24] M. Richter, S. Lange, A. Bäcker, and R. Ketzmerick, Phys. Rev. E **89** (2014).

[25] P. Schlagheck, "Atomes ultrafroids et condensats de bose-einstein," (2023), pHYS2027-2.

[26] V.-I. Arnold, Russ. Math. Surv. **18** (1963), 10.1070/RM1963v018n05ABEH004130.

[27] J. Moser, Nachr. Akad. Wiss. Göttingen Math.-Phys. Kl. II (1962).

[28] G. Floquet, Ann. Sci. de l'Ecole Norm. Supérieure **2** (1883).

[29] A. Buchleitner, D. Delande, and J. Zakrzewski, Phys. Rep. **368**, 409 (2002).

[30] J.-H. Shirley, Phys. Rev. **138** (1965).

[31] K. Husimi, Proc. Phys. Math. Soc. Japan **22** (1940), https://doi.org/10.11429/ppmsj1919.22.4$_2$64.

[32] A. Einstein, Verh. d. Dtsch. Phys. Gen. **82** (1917).

[33] in *Handbook of Mathematical Functions*, edited by M. Abrammowitz and I. A. Stegun (Dover, 1972).

[34] A. Buchleitner and D. Delande, Phys. Rev. Lett. **75**, 1487 (1995).

[35] E. Schrödinger, Die Naturwissenschaften (1926).

[36] A. Einstein, Sitzber. Kgl. Preuss. Akad. Wiss. **261** (1924).

[37] A. Einstein, Sitzber. Kgl. Preuss. Akad. Wiss. **3** (1925).

[38] S.-N. Bose, Z. Phys. **26** (1924).

[39] M.-H. Anderson, J.-R. Ensher, M.-R. Matthews, C.-E. Wieman, and E.-A. Cornell, Science **269** (1995).

[40] K.-B. Davis, M.-O. Mewes, M.-R. Andrews, N.-J. van Druten, D.-S. Durfee, D.-M. Kurn, and W. Ketterle, Phys. Rev. Lett. **75** (1995).

[41] L. de Broglie, *Recherche sur la théorie des quanta*, Ph.D. thesis, Paris (1924).

[42] W. Ketterle, Phys. Rev. Lett. **74** (2002).

[43] O. Penrose and L. Onsager, Phys. Rev. **104** (1956).

[44] C.-J. Pethick and H. Smith, *Bose-Einstein Condensation in Dilute Gases* (Cambridge University Press, 2008).

[45] L. Pitaevskii and S. Stringari, *Bose-Einstein condensation and superfluidity* (Oxford University Press, 2016).

[46] L. Landau and E. Lifshitz, *Mécanique quantique (Volume 3)* (Mir, 1971).

[47] F. Dalfovo, S. Giorgini, L. P. Pitaevskii, and S. Stringari, Rev. Mod. Phys. **71**, 463 (1999).

[48] P. Schlagheck, *Tunneling in Presence of Chaos and Interactions*, Ph.D. thesis, Universität Regensburg (2006).

[49] A.-D. Jackson, G.-M. Kavoulakis, and C.-J. Pethick, Phys. Rev. **71** (1999).

[50] I. Bloch, J. Dalibard, and W. Zwerger, Review of Modern Physics **80** (2007), 10.1103/RevModPhys.80.885.

[51] J. Hubbard, Proc. R. Soc. A **129** (1963).

[52] M.-P.-A. Fisher, P.-B. Weichmann, G. Grinstein, and D.-S. Fisher, Phys. Rev. B **40** (1989).

[53] M. Greiner, O. Mandel, T. Esslinger, T.-W. Hänsch, and I. Bloch, Nature **415** (2002).

[54] D. Jaksch, C. Bruder, J.-I. Cirac, C.-W. Gardiner, and P. Zoller, Phys. Rev. Lett. **81** (1998).

[55] A. Ramanathan, K.-C. Wright, S.-R. Muniz, M. Zelan, W.-T. Hill, C.-J. Lobb, K. Helmerson, W.-D. Phillips, and G.-K. Campbell, Phys. Rev. Lett. **106** (2011).

[56] O. Zobay and B.-M. Garraway, Phys. Rev. Lett. **86** (2001).

[57] F. Damon, G. Condon, P. Cheiney, A. Fortun, B. Georgeot, J. Billy, and D. Guéry-Odelin, Phys. Rev. A **92** (2015).

[58] O. Morsch and M. Oberthaler, Reviews of Modern Physics **78** (2006), 10.1103/RevModPhys.78.179.

[59] P. Schlagheck, T. Bastin, and J. Martin, "Mécanique quantique avancée," (2022), pHYS3021-1.

[60] K. Sacha and J. Zakrzewski, Rep. Prog. Phys. **81**, 016401 (2017).

[61] G. Vanhale and P. Schlagheck, Phys. Rev. A **103** (2021).

[62] F. Wilczek, Phys. Rev. Lett. **109** (2012), https://doi.org/10.1103/PhysRevLett.109.160401.

[63] F. Wilczek, Pour La Science **507** (2020).

[64] F. Strocchi, *Symmetry Breaking (The Lecture Notes in Physics)* (Springer, 2005).

[65] D.-V. Else, B. Bauer, and C. Nayak, Phys. Rev. Lett. **117** (2016).

[66] V. Khemani, C.-W. von Keyserlingk, and S.-L. Sondhi, Phys. Rev. B **96** (2017), https://doi.org/10.1103/PhysRevB.96.115127.

[67] T. Li, Z.-X. Gong, Z.-Q. Yin, H.-T. Quan, X. Yin, P. Zhang, L.-M. Duan, and X. Zhang, Phys. Rev. Lett. **109** (2012).

[68] P. Bruno, Phys. Rev. Lett. **111** (2013).

[69] H. Watanabe and M. Oshikawa, Phys. Rev. Lett. **114** (2015).

[70] A. Syrwid, J. Zakrzewski, and K. Sacha, Phys. Rev. Lett. **119** (2017), https://doi.org/10.1103/PhysRevLett.119.250602.

[71] V. Khemani, A. Lazarides, R. Moessner, and S.-L. Sondhi, Phys. Rev. Lett. **116** (2016).

[72] J. Zhang, P.-W. Hess, P. Kyprianidis, A Becker, A. Lee, J. Smith, G. Pagano, I.-D. Potirniche, A.-C. Potter, A. Vishwanath, N.-Y. Yao, and C. Monroe, Nature **543** (2017).

[73] D. Steck and M. Raizen, in *Dynamical Tunneling: Theory and Experiment* (S. Keshavamurthy and P. Schlagheck, 2011).

[74] M.-J. Davis and E.-J. Heller, J. Chem. Phys. **75** (1981).

[75] P. Schlagheck, A. Mouchet, and D. Ullmo, in *Dynamical Tunneling: Theory and Experiment* (S. Keshavamurthy and P. Schlagheck, 2011).

[76] O. Brodier, P. Schlagheck, and D. Ullmo, Annals of Physics **300** (2002), 10.1006/aphy.2002.6281.

[77] M.-L. Mehta, *Random Matrices* (Academic, New York, 1967).

[78] S.-C. Creagh, J. Phys. A: Math. Gen. **27** (1994).

[79] W.-A. Lin and L.-E. Ballentine, Phys. Rev. Lett. **65** (1990).

[80] P. Schlagheck, C. Eltschka, and D. Ullmo, in *Progress in Ultrafast Intense Laser Science I*, edited by K. Yamanouchi, S. L. Chin, P. Agostini, and G. Ferrante (Springer, 2006) pp. 107–131.

[81] A. Mouchet, C. Eltschka, and P. Schlagheck, Phys. Rev. E **74** (2006).

[82] C. Eltschka and P. Schlagheck, Phys. Rev. Lett. **94**, 014101 (2005).

[83] F. Leyvratz and D. Ullmo, J. Phys. A: Math. Gen. **29** (1996).

[84] O. Brodier, P. Schlagheck, and D. Ullmo, Phys. Rev. Lett. **87** (2001).

[85] M. Michler, A. Bäcker, R. Ketzmerick, H.-J. Stöckmann, and S. Tomsovic, Phys. Rev. Lett. **109** (2012), 10.1103/PhysRevLett.109.234101.